

16–21 July 2012

НОЦ



Computer simulation of advanced materials

International School of the
European University network

**MSU Nanotechnology
Education and Research Center**



Materials in extreme states:
from WARM DENSE MATTER to
laser induced surface nanostructuring

Norman G.E.

JOINT INSTITUTE for
HIGH TEMPERATURES RAS

MOSCOW INSTITUTE of
PHYSICS and TECHNOLOGY



Coauthors from MIPT/JIHT RAS



V.V. Stegailov
Dr.Habil. 2012
JIHT laboratory head
MIPT assistant professor
born 1981



S.V. Starikov
Ph.D. 2010
JIHT senior researcher
MIPT assistant
born 1984



I.M. Saitov
MIPT PhD student
JIHT junior researcher
born 1987



P.A. Zhilyaev
MIPT PhD student
JIHT junior researcher
born 1988

Contents

Warm dense matter (WDM), examples

Two temperature WDM. *Exotic properties*

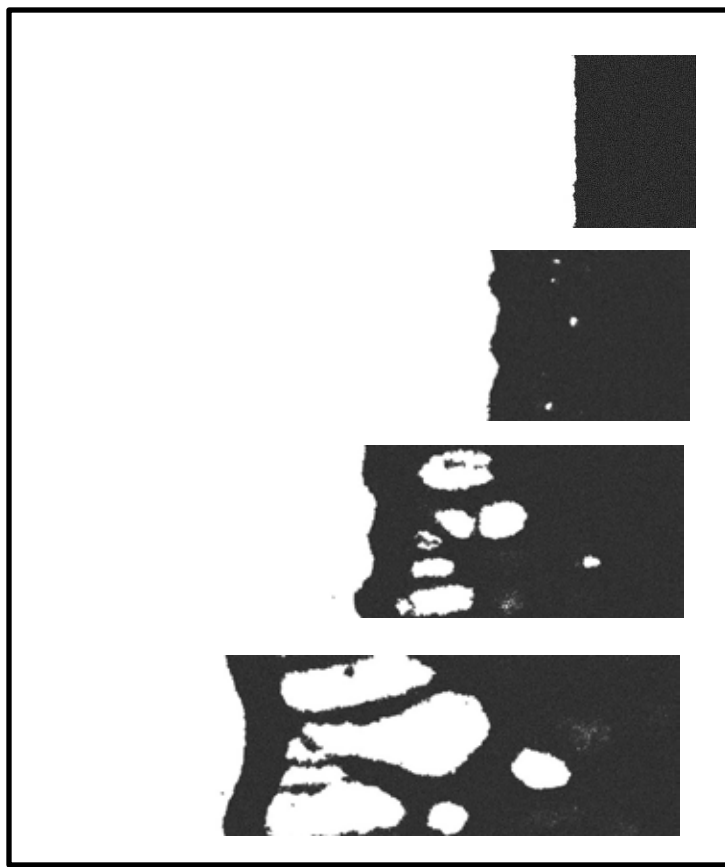
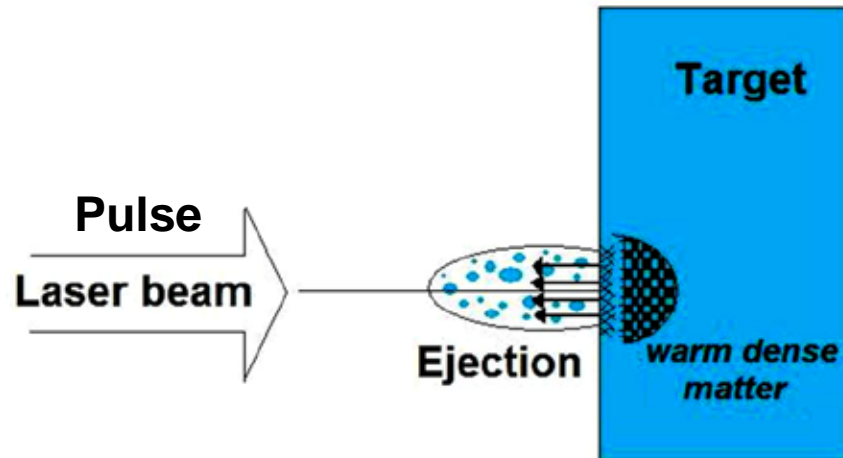
Basic equations for WDM relaxation

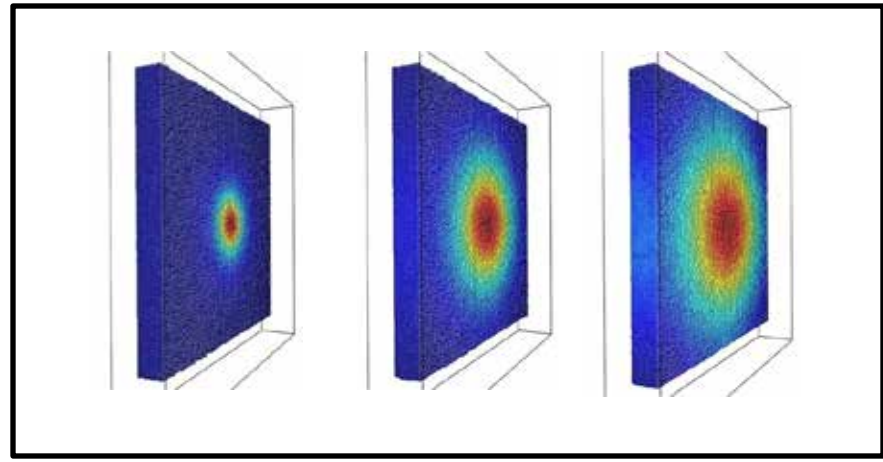
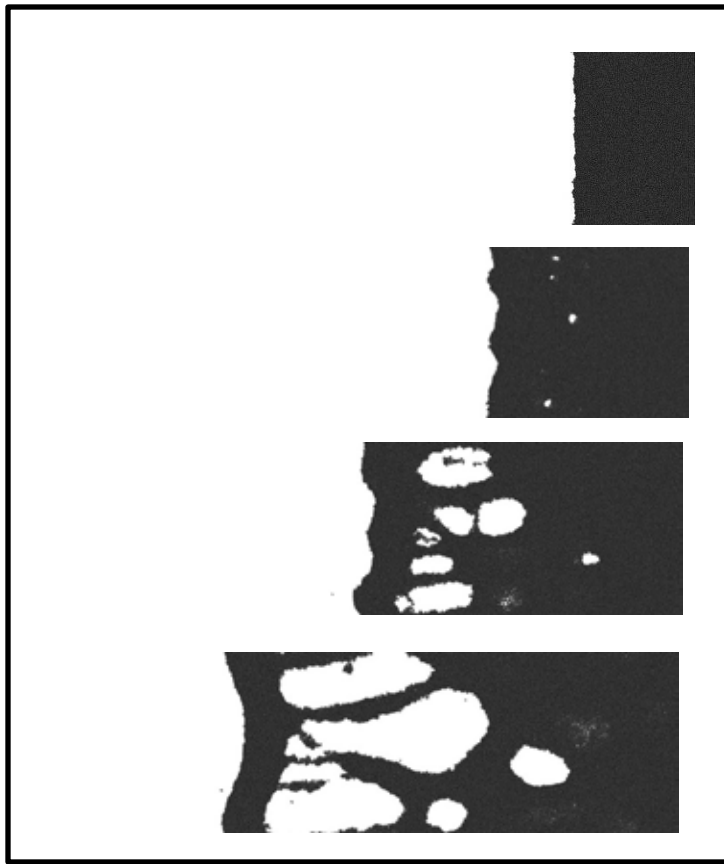
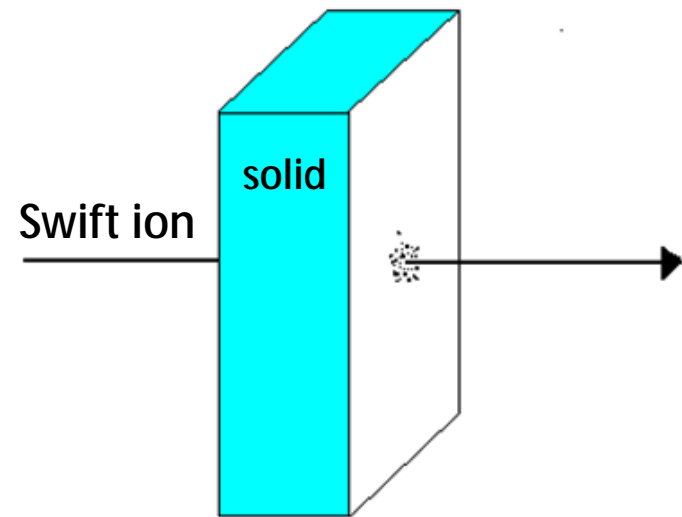
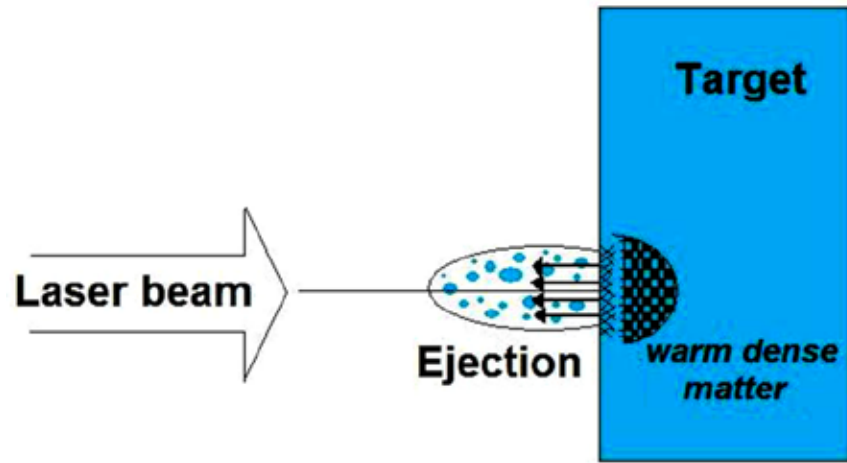
Electron-temperature dependent
interionic potential

Example 1: Laser ablation of gold

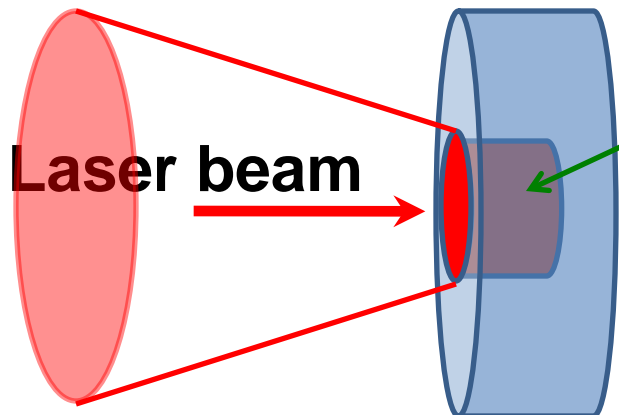
Example 2: Tracks formation in metals

Warm dense matter Examples



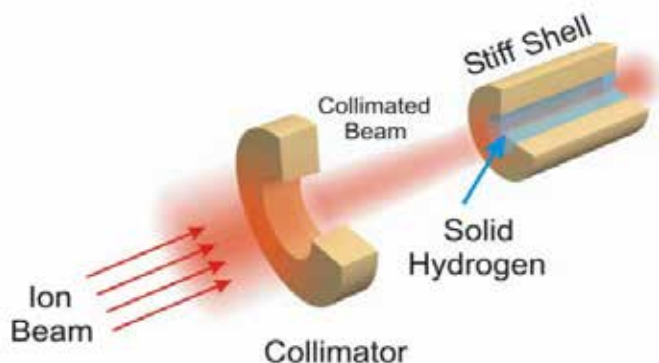


Diverse sources of generation:



WDM *IR, visible, UV, XUV lasers*

- A. Saemann, K. Eidmann, I. E. Golovkin, et al, PRL 82, 4843 (1999)
K. Widmann, T. Ao, M. E. Foord, et al, PRL 92, 125002 (2004)
S. B. Hansen, K. B. Fournier, A.Ya. Faenov, et al, PRE 72, 036408 (2005)
Y. Ping, D. Hanson, I. Koslow, et al, PRL 96, 255003 (2006)
U. Zastrau, C. Fortmann, R. R. Fäustlin, et al, PRE 78, 066406 (2008)



***fast single ions, ion beams
in condensed matter***

- A.V.Larkin, I.V.Morozov, G.E.Norman, S.A. Pikuz Jr.,
I.Yu.Skobelev Phys. Rev. E 79, 036407 (2009)

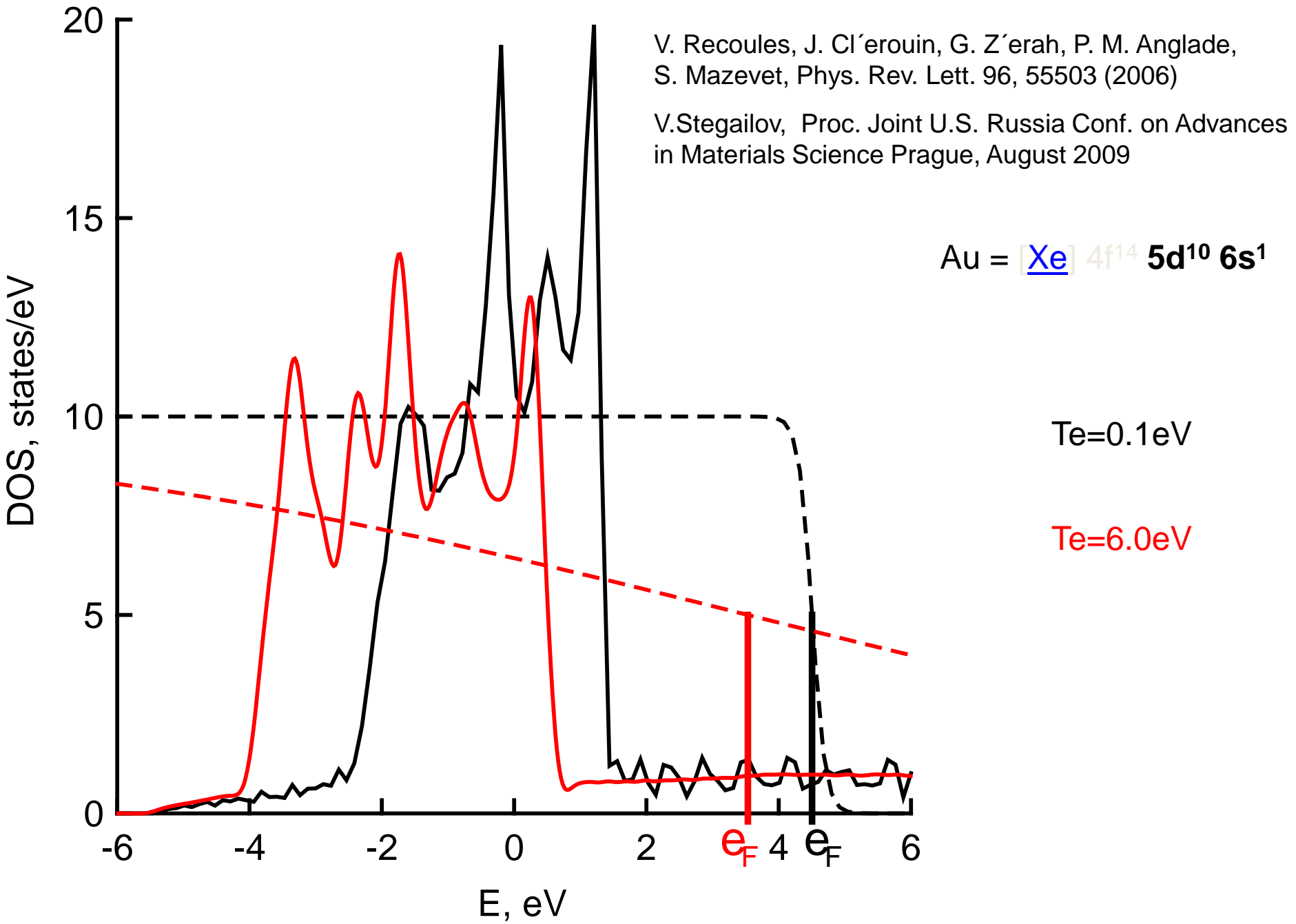
***Nanosecond Electric
Explosion of Wires***

- G.E. Norman, V.V. Stegailov, A.A. Valuev.
Contrib. Plasma Phys. 43, 384 (2003)

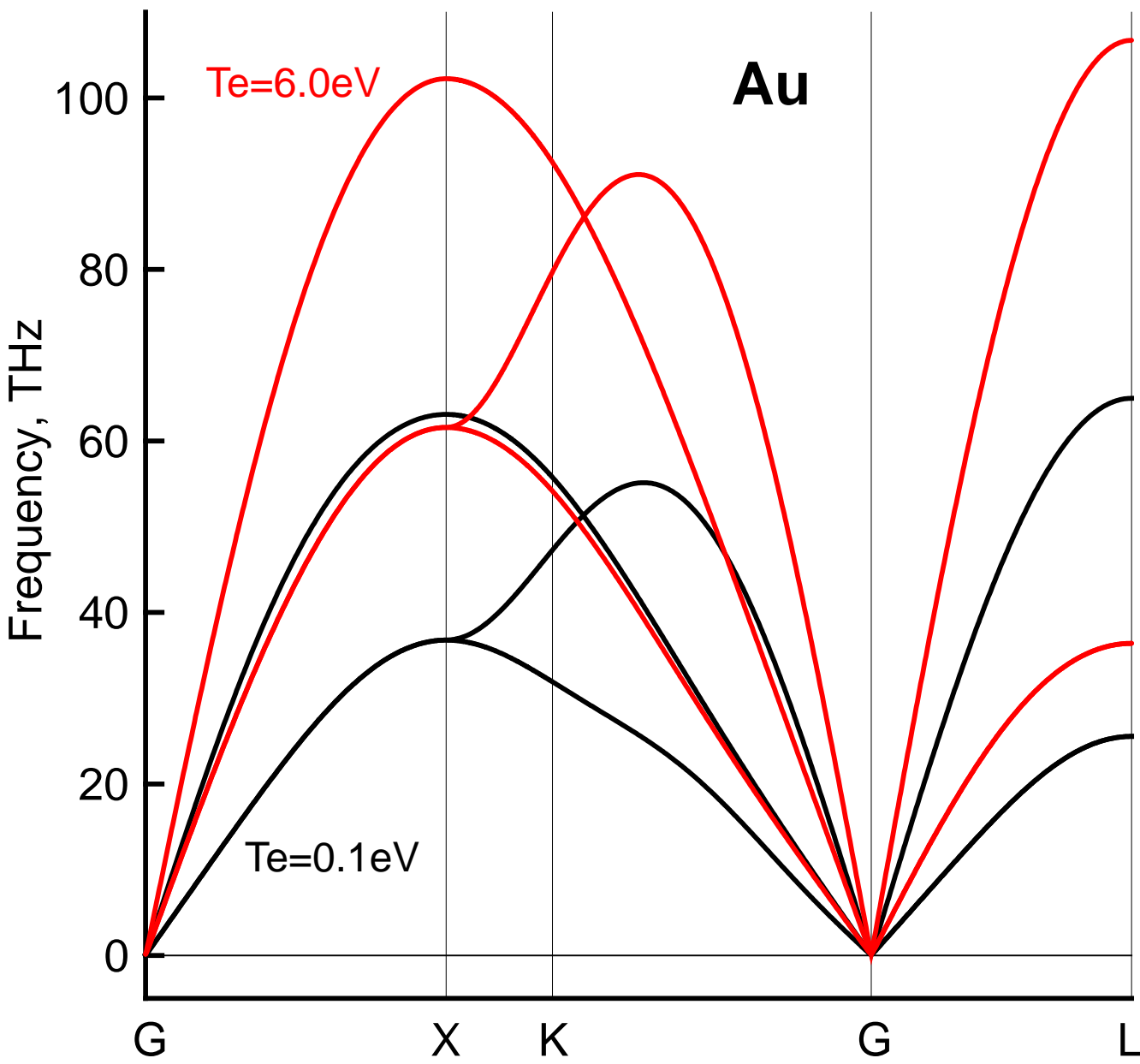
***Explosions of tips
(protrusion, whisker)
on cathode surface***

Two temperature
warm dense matter.
Exotic properties

Gold: electron DOS (d- and s-electrons)



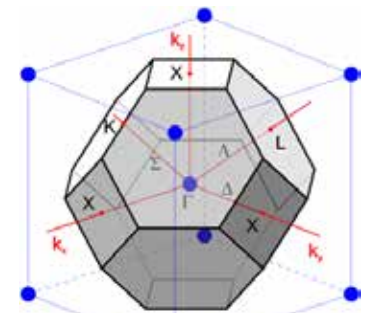
FCC gold phonon spectrum after pulse irradiation



Au

$T_e = 6.0 \text{ eV}$

$T_e = 0.1 \text{ eV}$

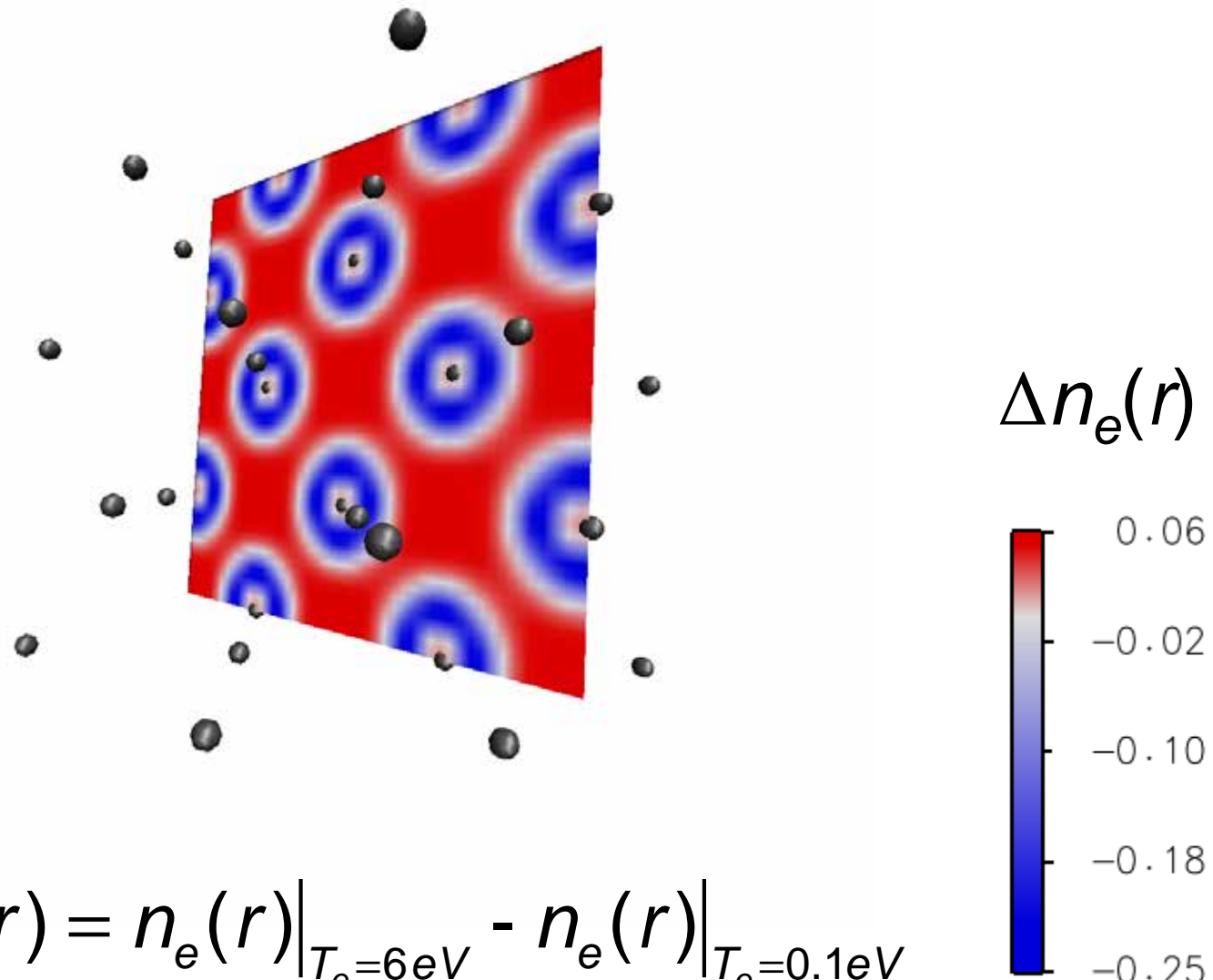


V. Recoules, J. Cl'erouin, G. Z'erah,
P. Anglade, S. Mazevet,
Phys. Rev. Lett. 96, 55503 (2006)

V. Stegailov, Proc. Joint
U.S. Russia Conf. on
Advances in Materials Science,
Prague, August 2009

Spatial redistribution of the electron density after the electron temperature increase

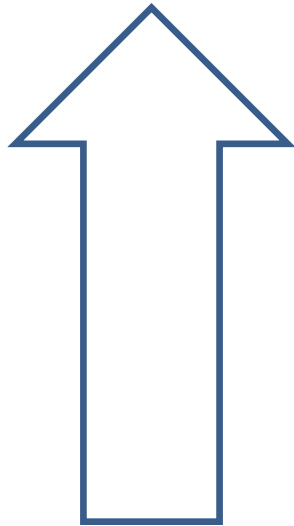
f.c.c. Au



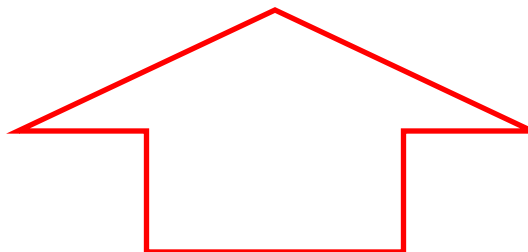
Basic equations for WDM relaxation

MD simulation for IONS : ETD-potential + Langevin thermostat + P_e

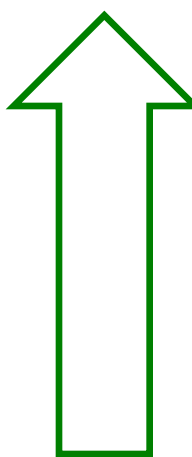
$$m \frac{d\vec{v}_i}{dt} = \vec{F}_i(T_e) - b\vec{v}_i + \vec{x}(T_e) - \frac{\tilde{N}P_e^{deloc}}{r_{ion}}$$



Electron-temperature dependent
interionic potential



Electron-ion relaxation
Langevin thermostat



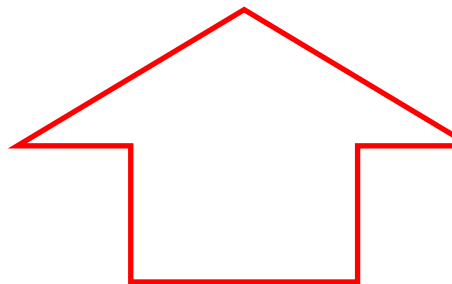
Electronic pressure
(delocalized electron energy)

Thermal conductivity equation for *ELECTRONS* at continuum media approximation

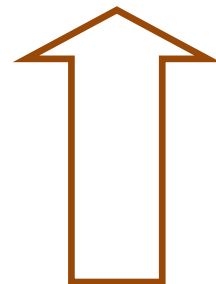
$$C_e \frac{\nabla T_e}{\nabla t} = \tilde{N} (K_e \tilde{N} T_e) - g_p (T_e - T_i) + \tilde{N} Q$$



Electron thermal conductivity



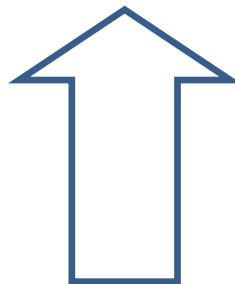
Electron-ion relaxation



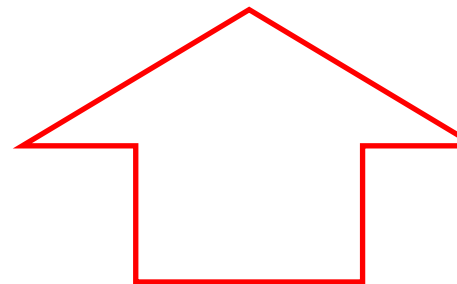
Source of
heating
at ablation

Thermal conductivity equation for *ELECTRONS* at continuum media approximation

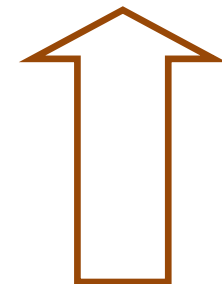
$$C_e \frac{\nabla T_e}{\nabla t} = \tilde{N} (K_e \tilde{N} T_e) - g_p (T_e - T_i) + \tilde{N} Q$$



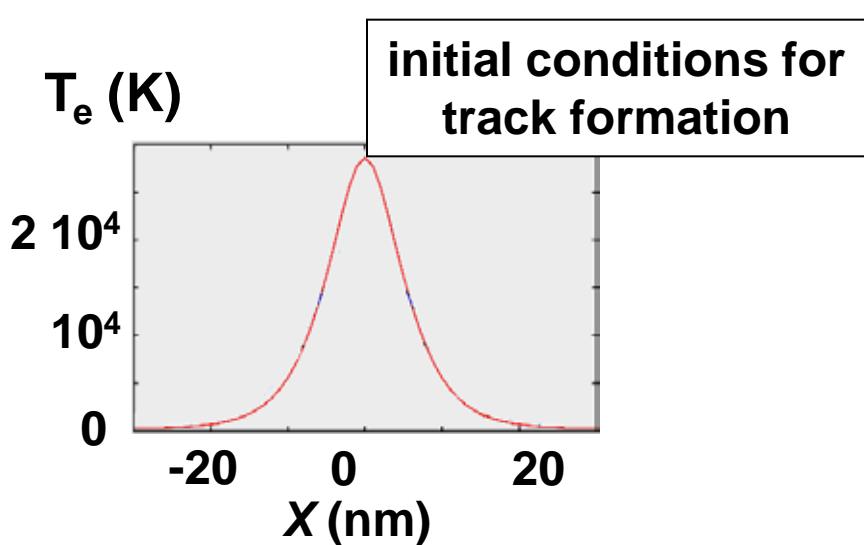
Electron thermal conductivity



Electron-ion relaxation



Source of
heating
at ablation



$Q = I_0 \exp[-x/d]$	$t < \text{pulse width}$
$Q = 0$	$t \geq \text{pulse width}$

laser ablation

Complete model

{ ELECTRONS: thermal conductivity equation at continuum media
 MD simulation for IONS: ETD-potential + Langevin thermostat + P_e
 modification of LAMMPS

$$C_e \frac{\nabla T_e}{\nabla t} = \tilde{N} (K_e \tilde{N} T_e) - g_p (T_e - T_i) + \tilde{N} Q$$

$$m \frac{d\nu_i}{dt} = F_i(T_e) - b\nu_i + x(T_e) - \frac{\tilde{N} P_e^{deloc}}{r_{ion}}$$

$$Q = I_0 \exp[-x/d] \quad t < \text{pulse width}$$

$$Q = 0 \quad t \geq \text{pulse width}$$

laser ablation

initial distribution of T_e

track formation

g_p – factor of electron-ion relaxation

C_e – electron heat capacity

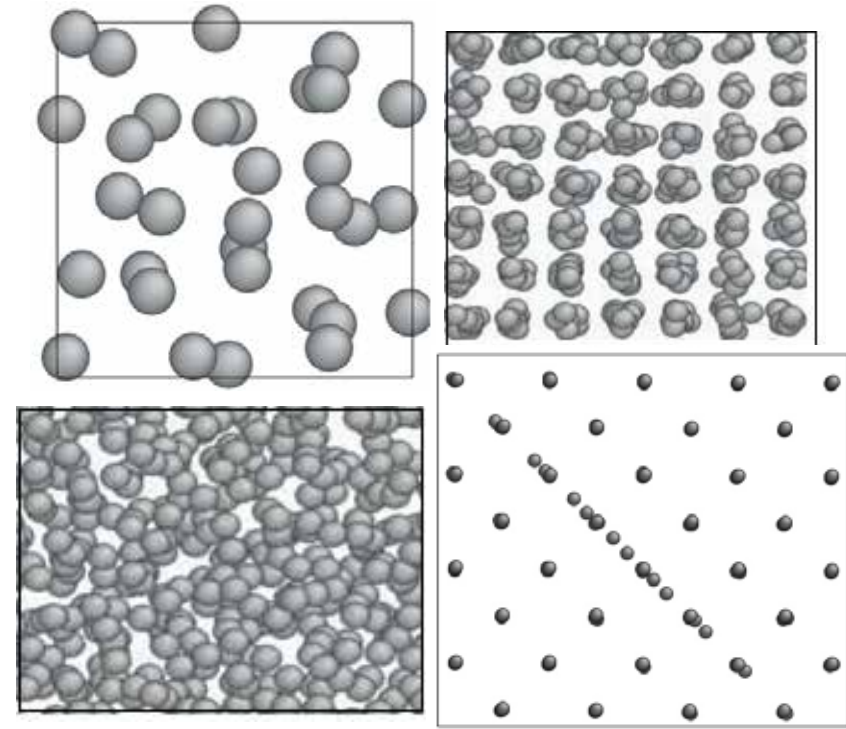
K_e – electron heat conductivity

$$\beta = \beta(g_p, C_e) \quad \xi \sim T_e^{1/2}$$

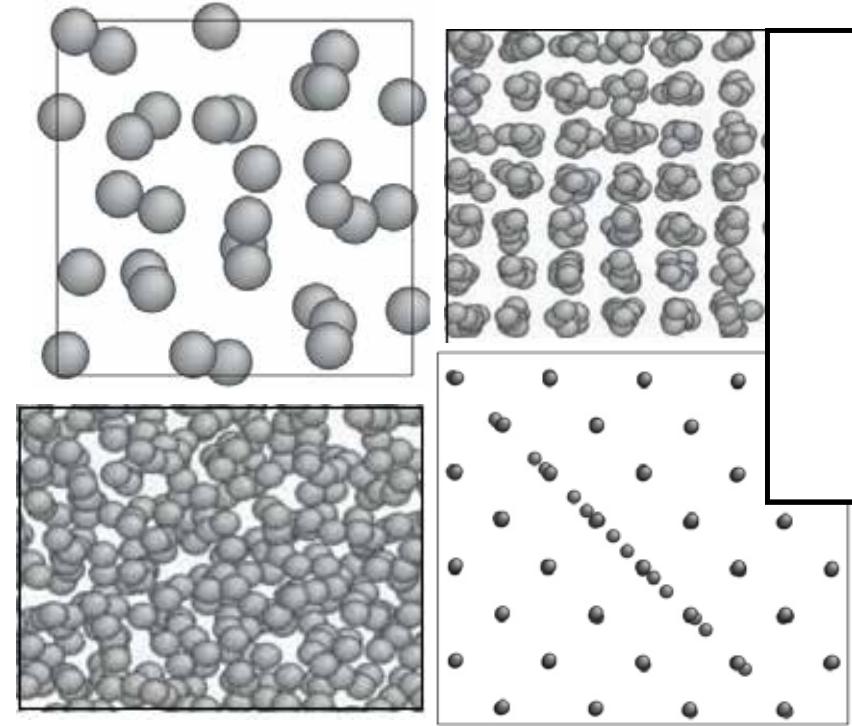
$$t = \frac{m}{b} \quad \tau \sim 20 \text{ ps}$$

Electron-temperature dependent interionic potential

Force matching method for development of potential



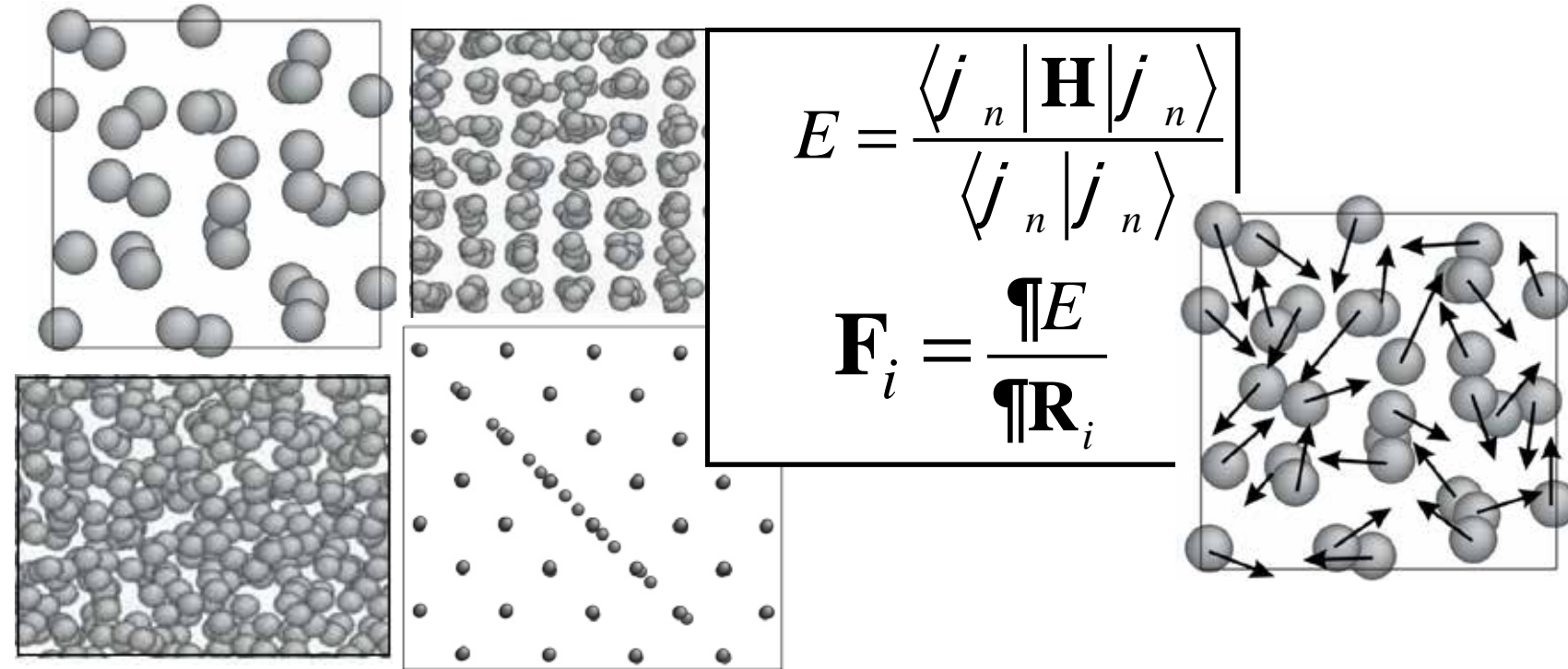
Force matching method for development of potential



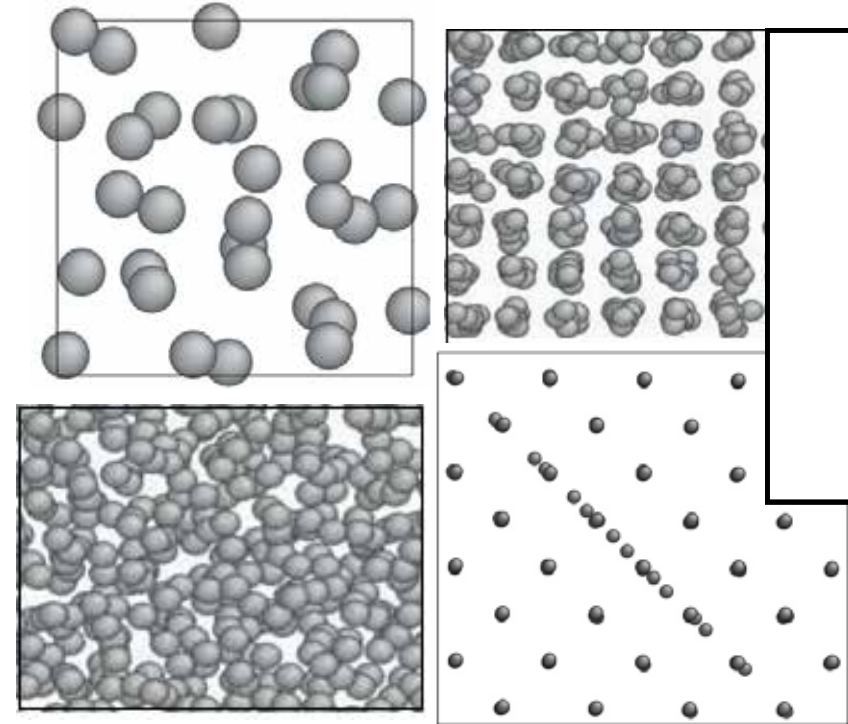
$$E = \frac{\langle j_n | \mathbf{H} | j_n \rangle}{\langle j_n | j_n \rangle}$$

$$\mathbf{F}_i = \frac{\nabla E}{\nabla \mathbf{R}_i}$$

Force matching method for development of potential

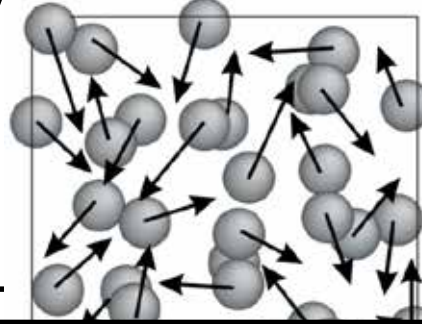


Force matching method for development of potential



$$E = \frac{\langle j_n | \mathbf{H} | j_n \rangle}{\langle j_n | j_n \rangle}$$

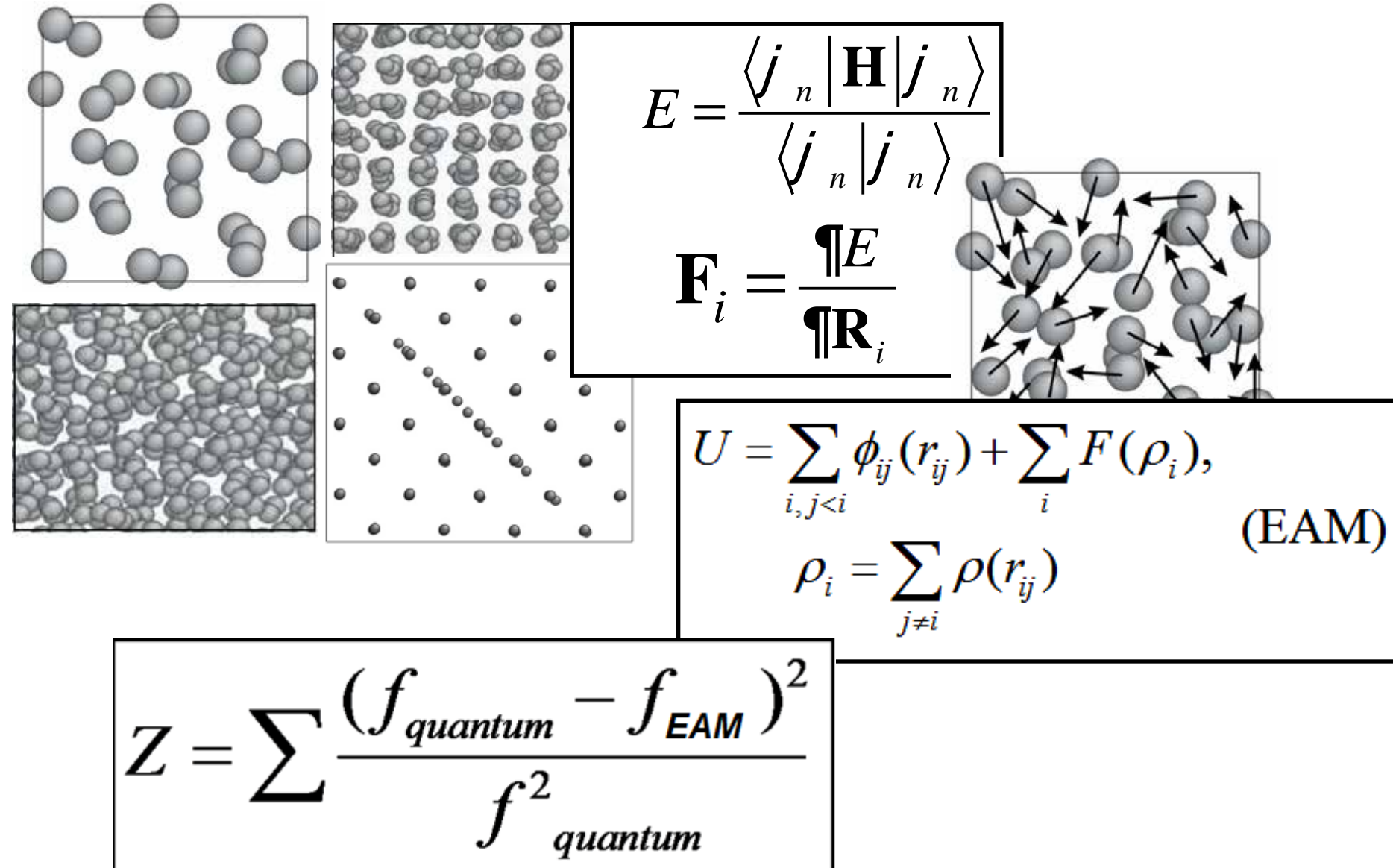
$$\mathbf{F}_i = \frac{\nabla E}{\nabla \mathbf{R}_i}$$



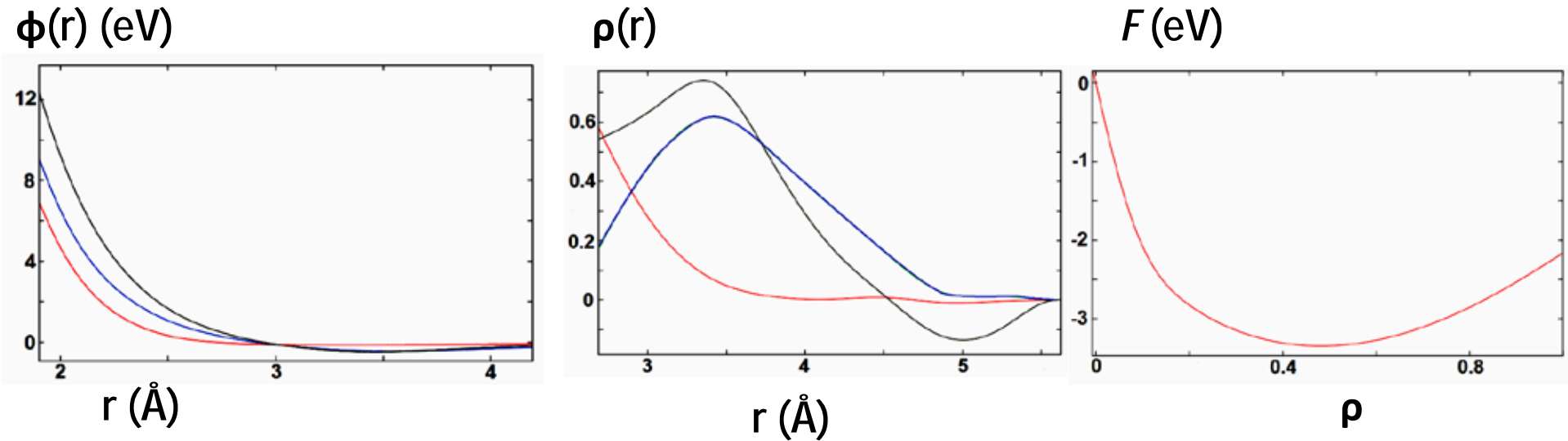
$$U = \sum_{i,j < i} \phi_{ij}(r_{ij}) + \sum_i F(\rho_i), \quad (\text{EAM})$$

$$\rho_i = \sum_{j \neq i} \rho(r_{ij})$$

Force matching method for development of potential



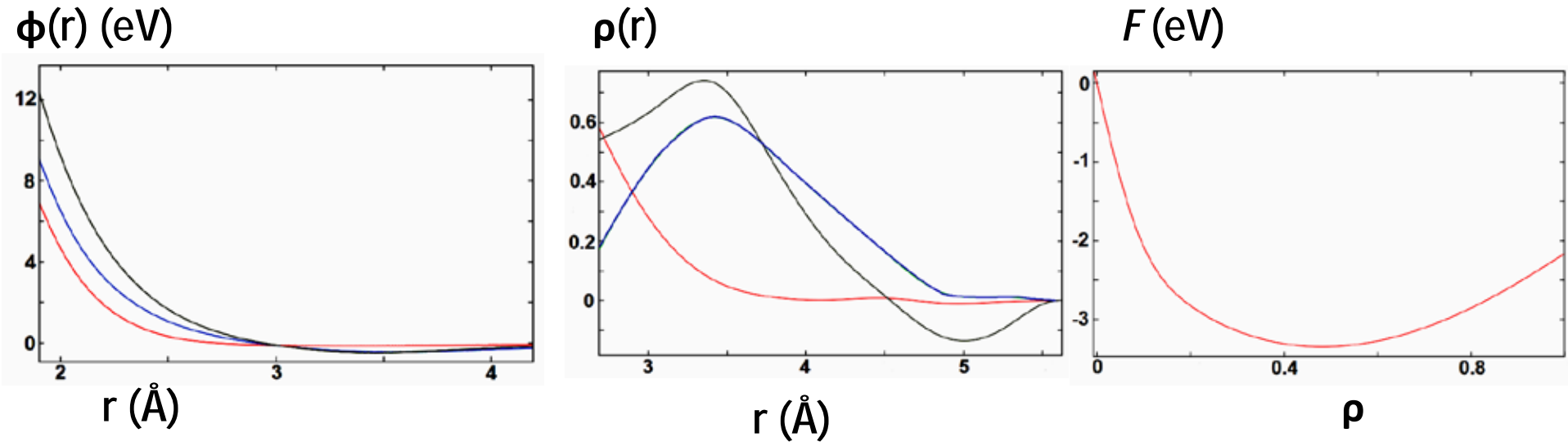
ETD-potential for gold



$$U = \sum_{i,j < i} \phi_{ij}(r_{ij}) + \sum_i F(\rho_i), \quad (\text{EAM})$$
$$\rho_i = \sum_{j \neq i} \rho(r_{ij})$$

— $T_e = 0.1 \text{ eV}$
— $T_e = 3 \text{ eV}$
— $T_e = 6 \text{ eV}$

ETD-potential for gold



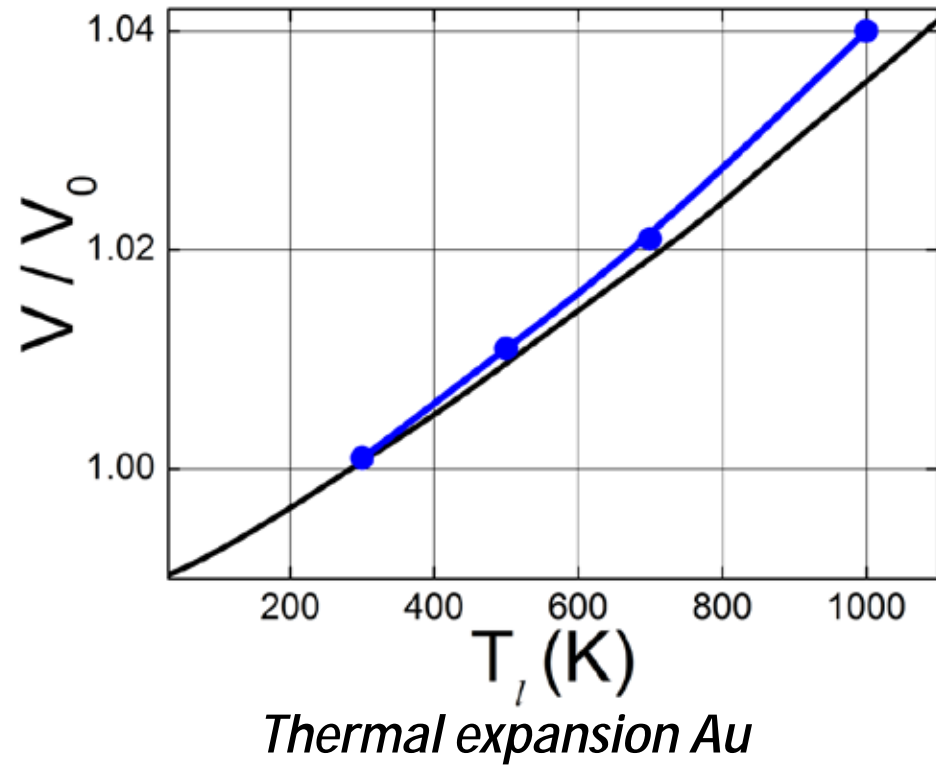
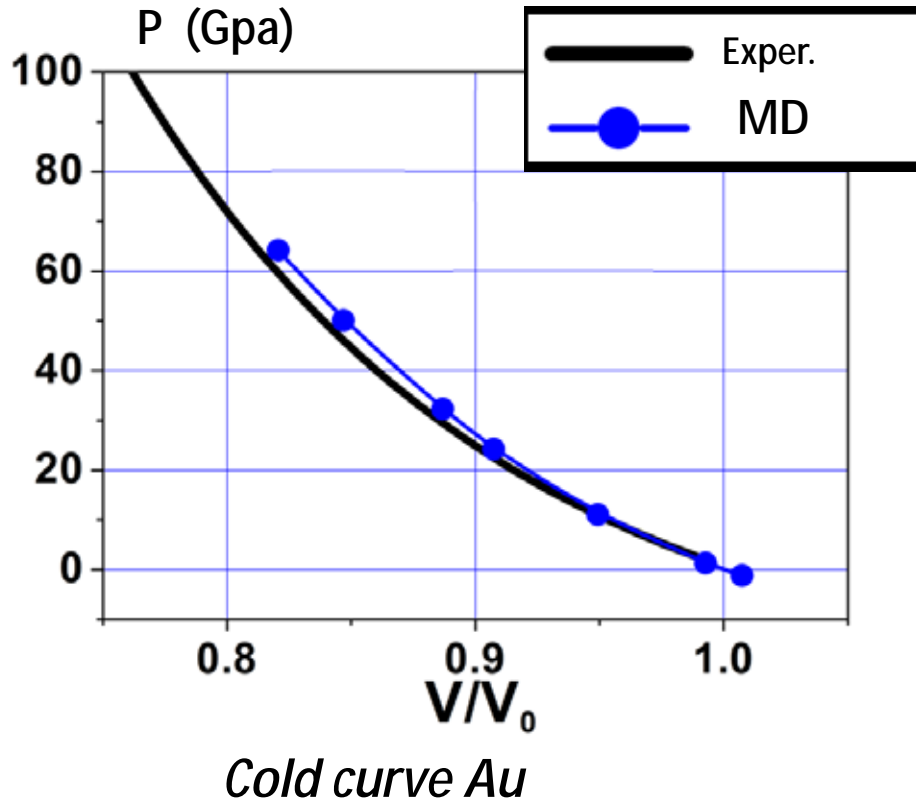
$$E = \sum_j^N \left(\varphi_0(r_j) + \varphi_1(r_j) \cdot T_e + \varphi_2(r_j) \cdot T_e^2 \right) + F \left(\sum_j^N \left\{ \rho_0(r_j) + \rho_1(r_j) \cdot T_e + \rho_2(r_j) \cdot T_e^2 \right\} \right)$$

- $T_e = 0.1$ eV
- $T_e = 3$ eV
- $T_e = 6$ eV

Starikov S.V., Stegailov V.V., Norman G.E. et al. JETP Lett., V. 93, pp. 642-647 (2011)

Норман Г.Э., Старикиов С.В., Стегайлов В.В. ЖЭТФ, том 141, выпуск 5, С. 910-917 (2012)

Verification of ETD-potential for Au at $T_e = 0.05$ eV



	V_0 , Å³	E_c , eV	C_{11} , GPa	C_{12} , GPa	T_{melt} , K
experiment	10.22	3.8	202	170	1338
MD	10.23	4.1	225	180	1210

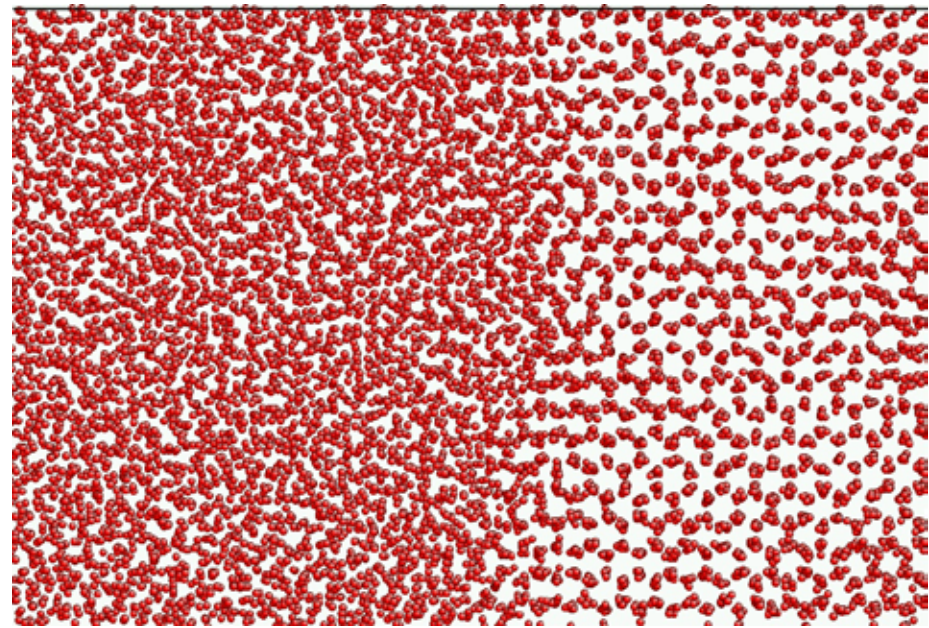
Melting curve calculation, Fe Two-phase 3D modeling

$$E_{conf} = \sum_i \phi_i E_i$$

$$E_i = \frac{1}{2} \sum_{j \neq i}^N \phi_j f(r_{ij}) + F(r_i)$$

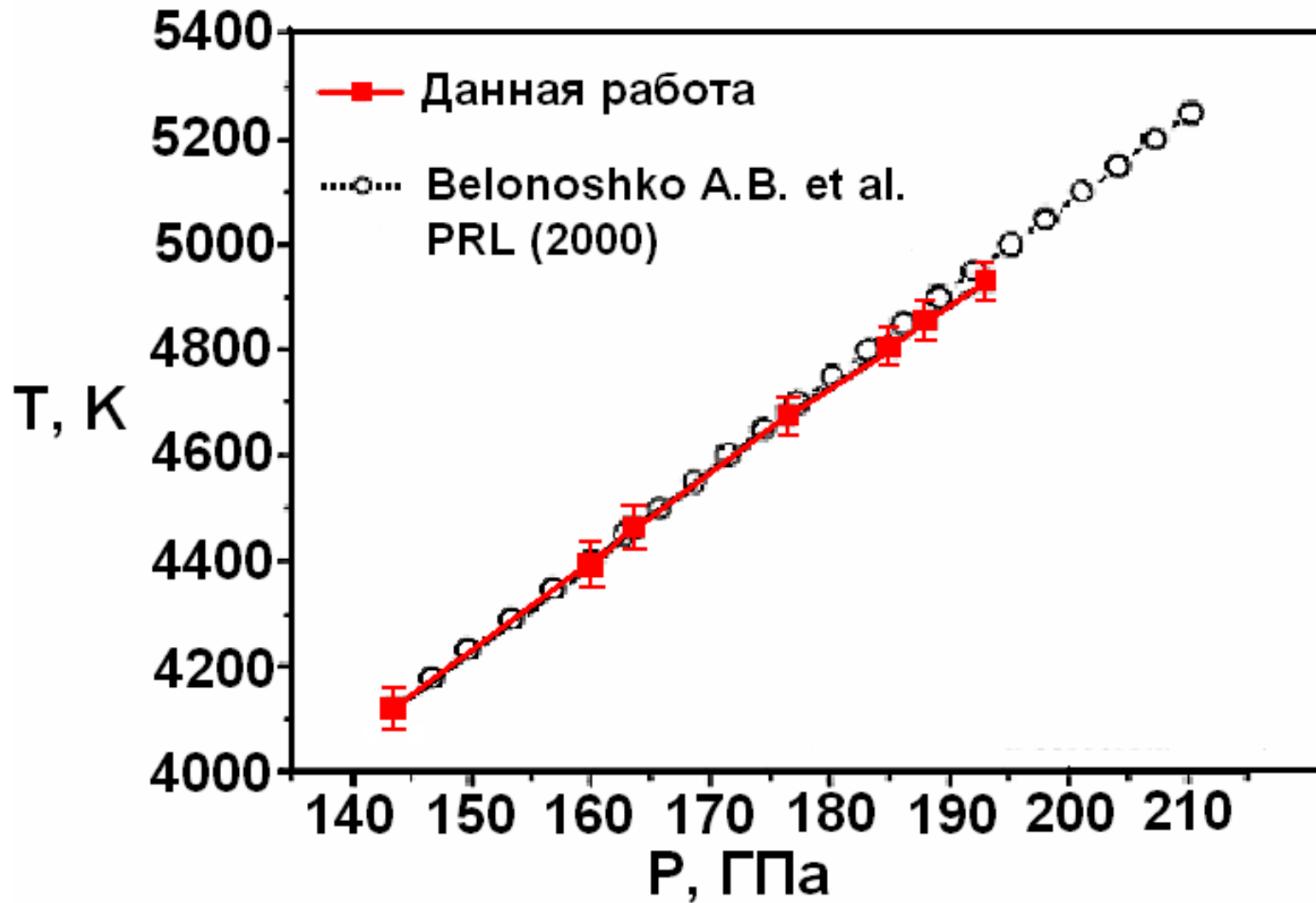
$$r_i = \sum_{j \neq i}^N r_{ij}$$

EAM potential

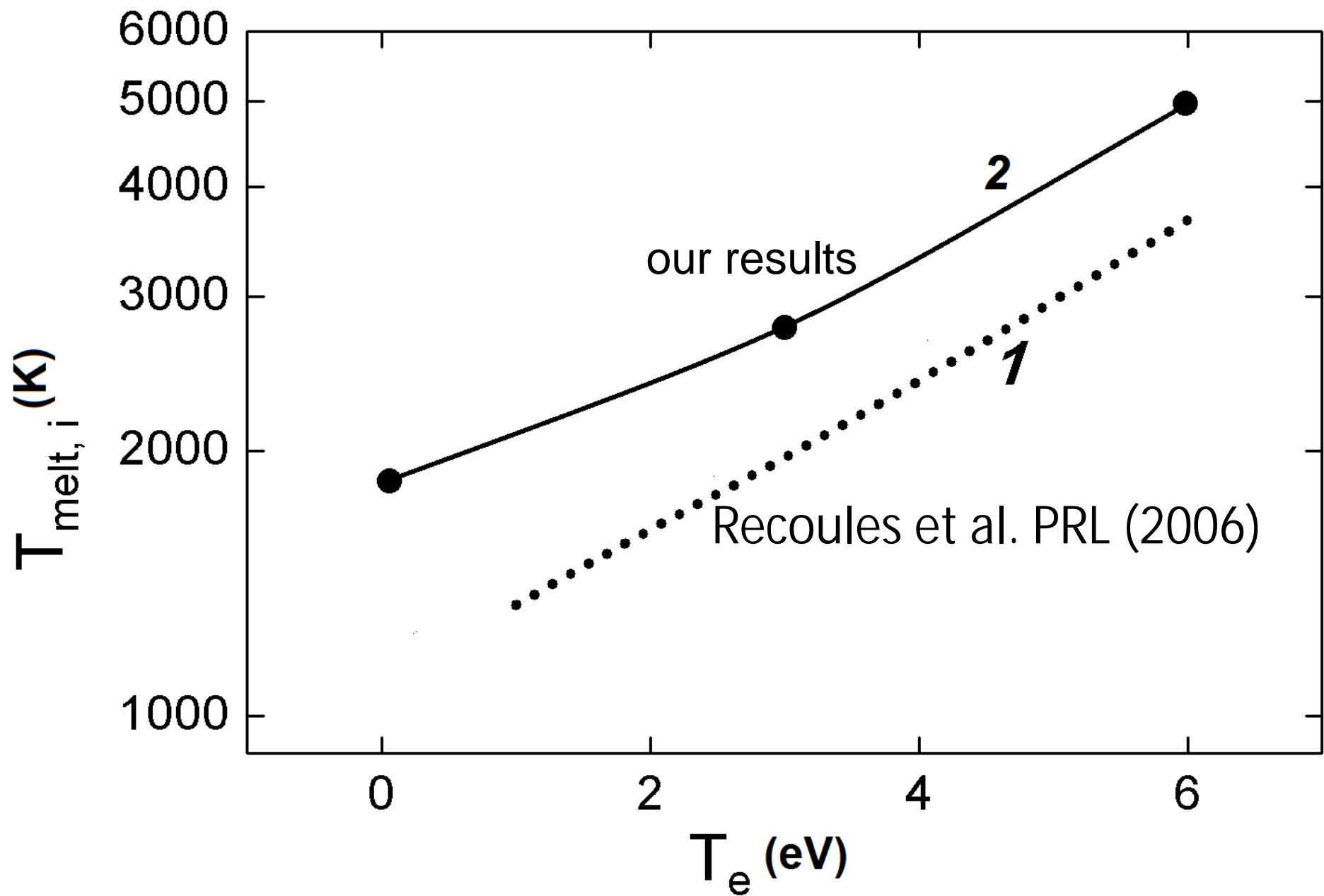


Projection onto xy plane

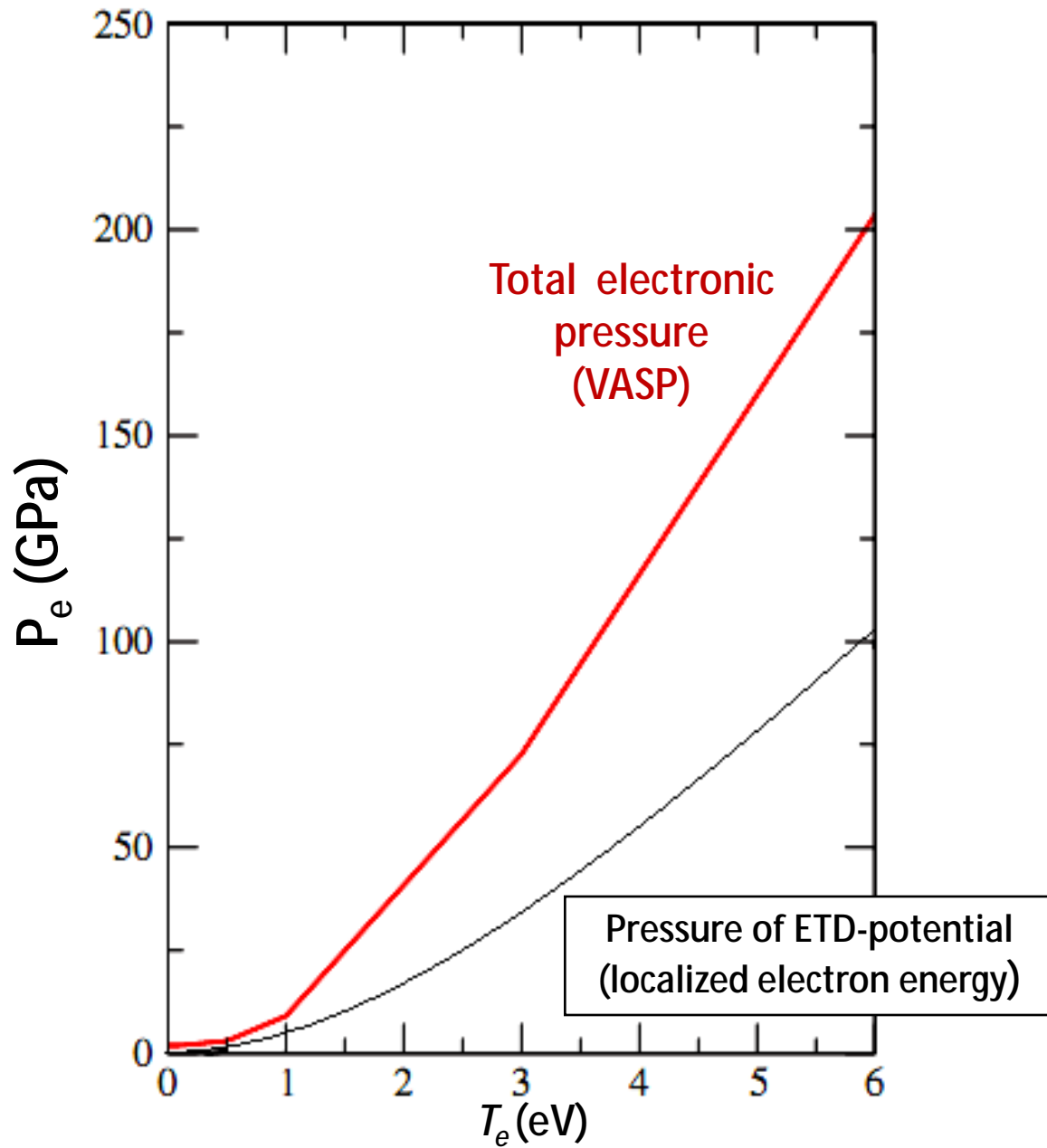
Melting curve $T_m(P)$ for Fe



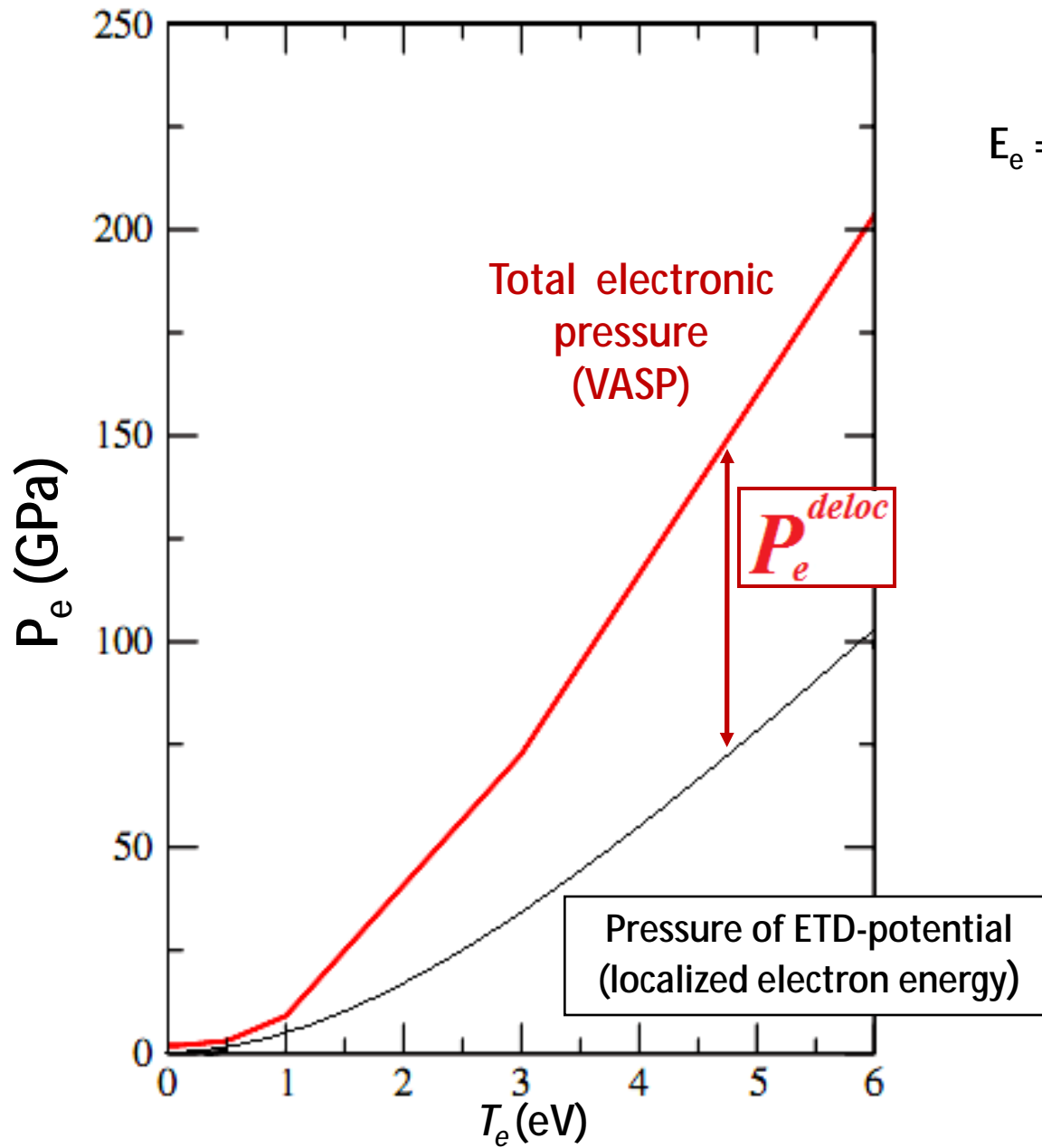
T_e -dependence of Au crystal melting temperature



Electronic pressure in gold



Electronic pressure in gold



$$E_e = E(R_1 \dots R_i \dots R_N, T_e) + E(\text{volume}, T_e)$$

Like gas of free-electrons

$$P_e^{deloc} = A \cdot T_e^2$$

$$B = \frac{\tilde{N} P_e^{deloc}}{r_{ion}}$$

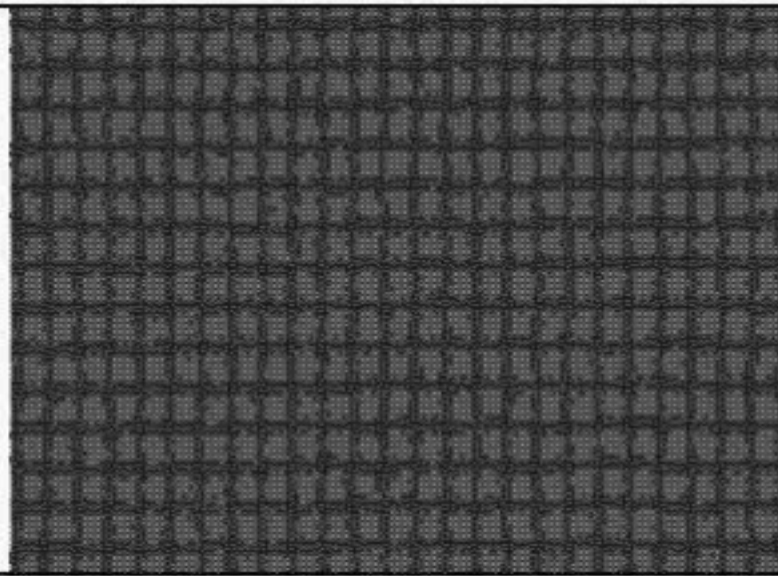
Electron blast force

[Gan, Chen // APL (2009)]

Laser ablation of gold

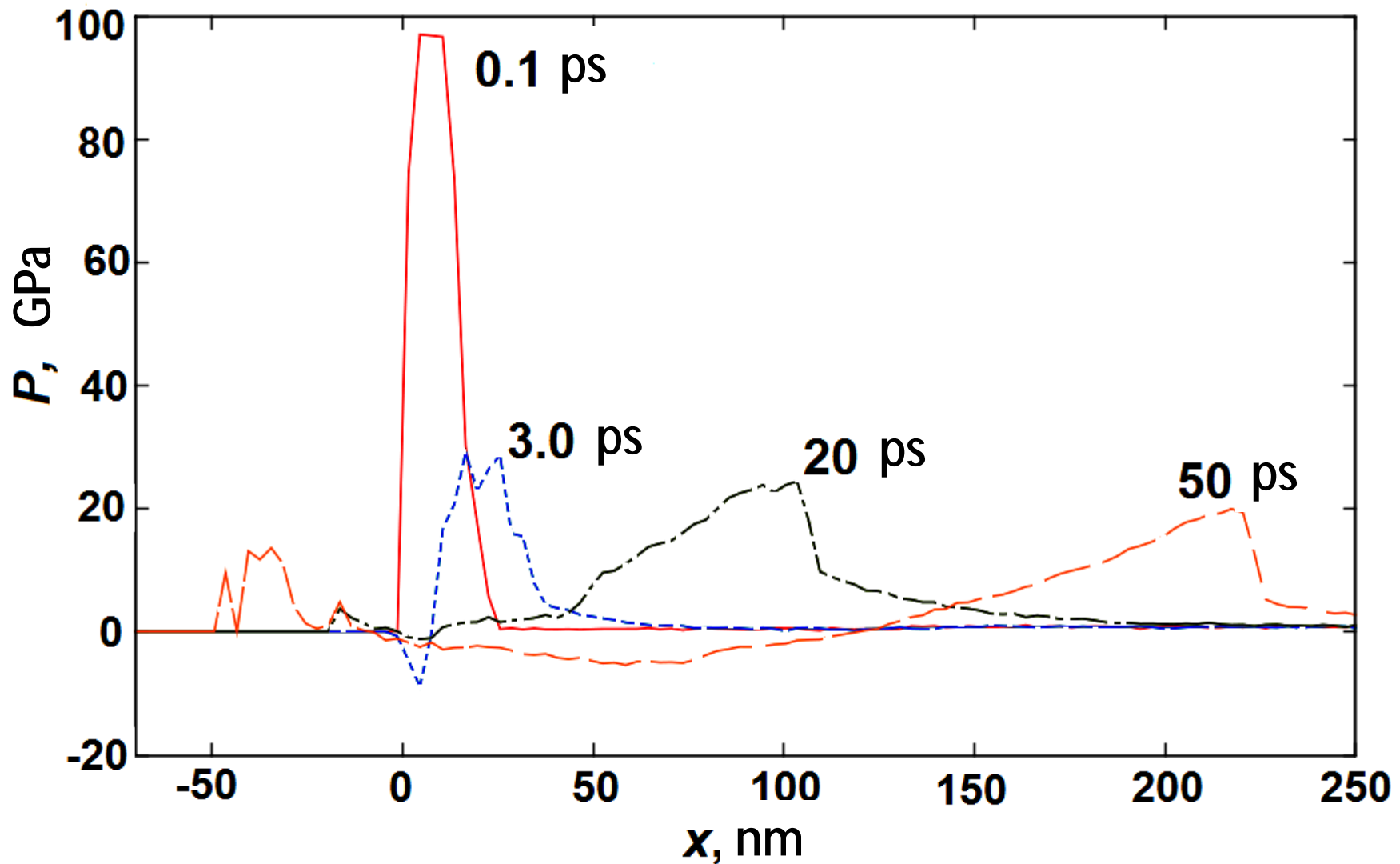
“short” and “long” ablation mechanisms for sub-*ps* pulses

Laser pulse



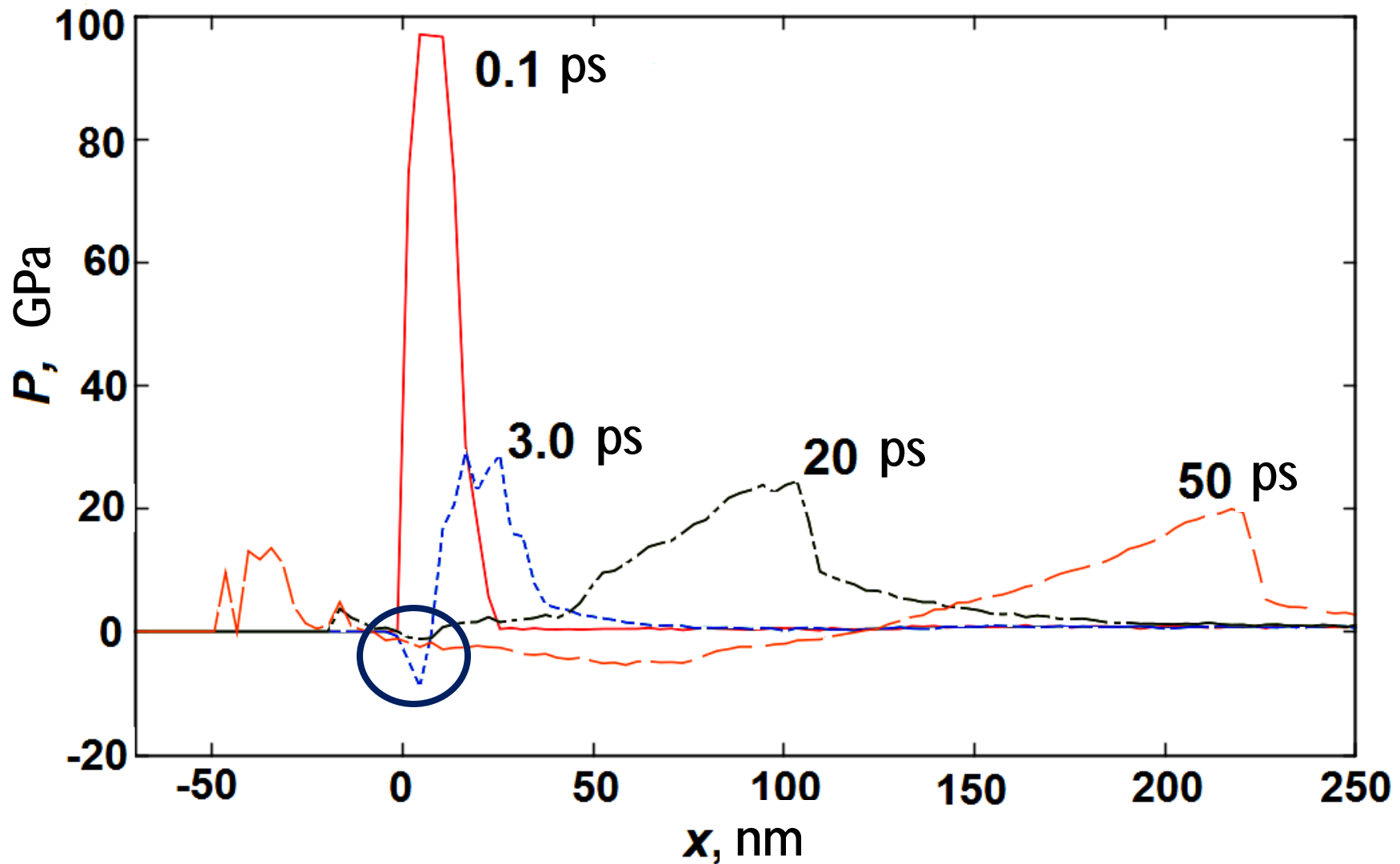
$$F = 1600 \text{ J/m}^2$$

ablation mechanism



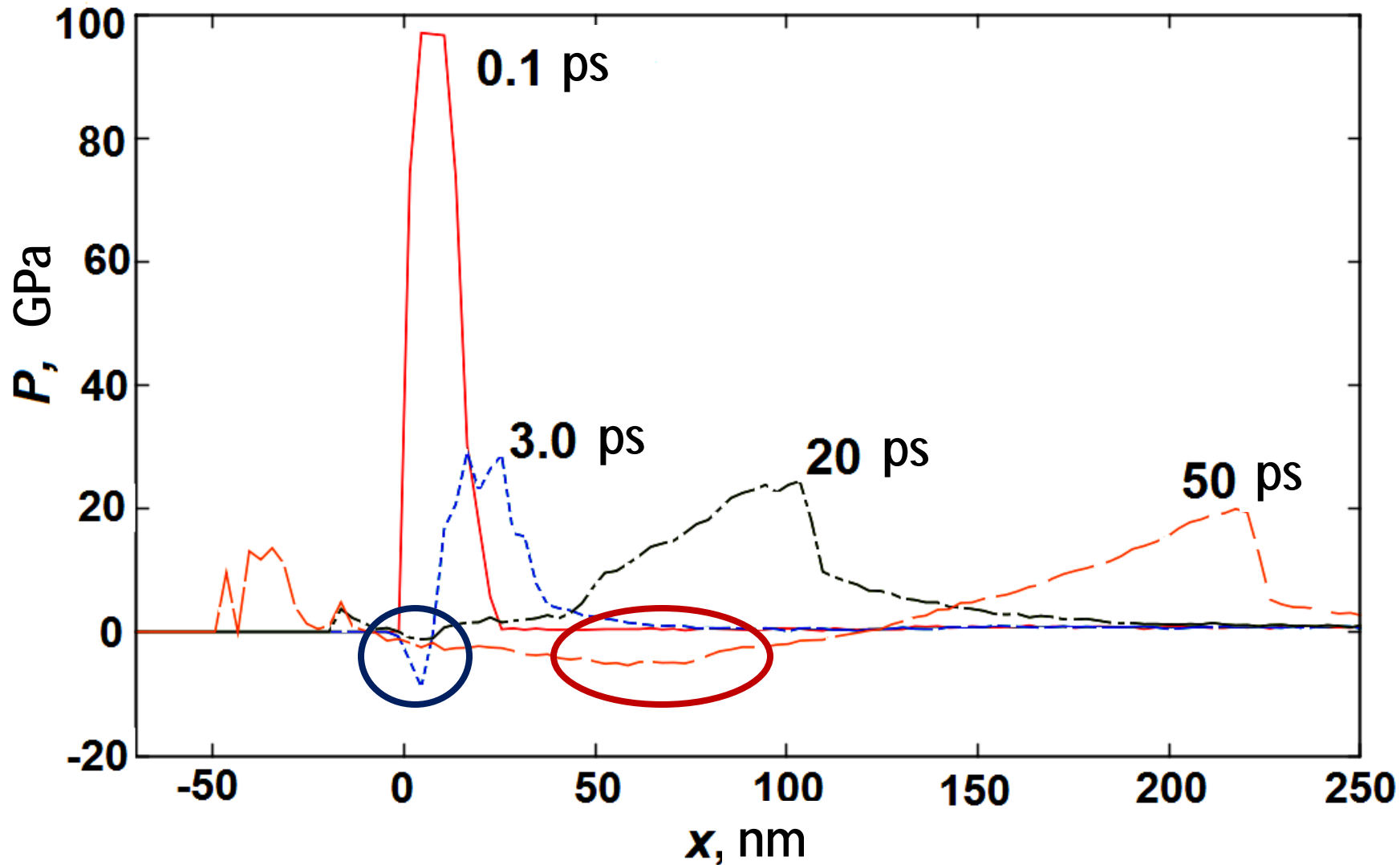
$$F = 1600 \text{ J/m}^2$$

“short” ablation mechanism



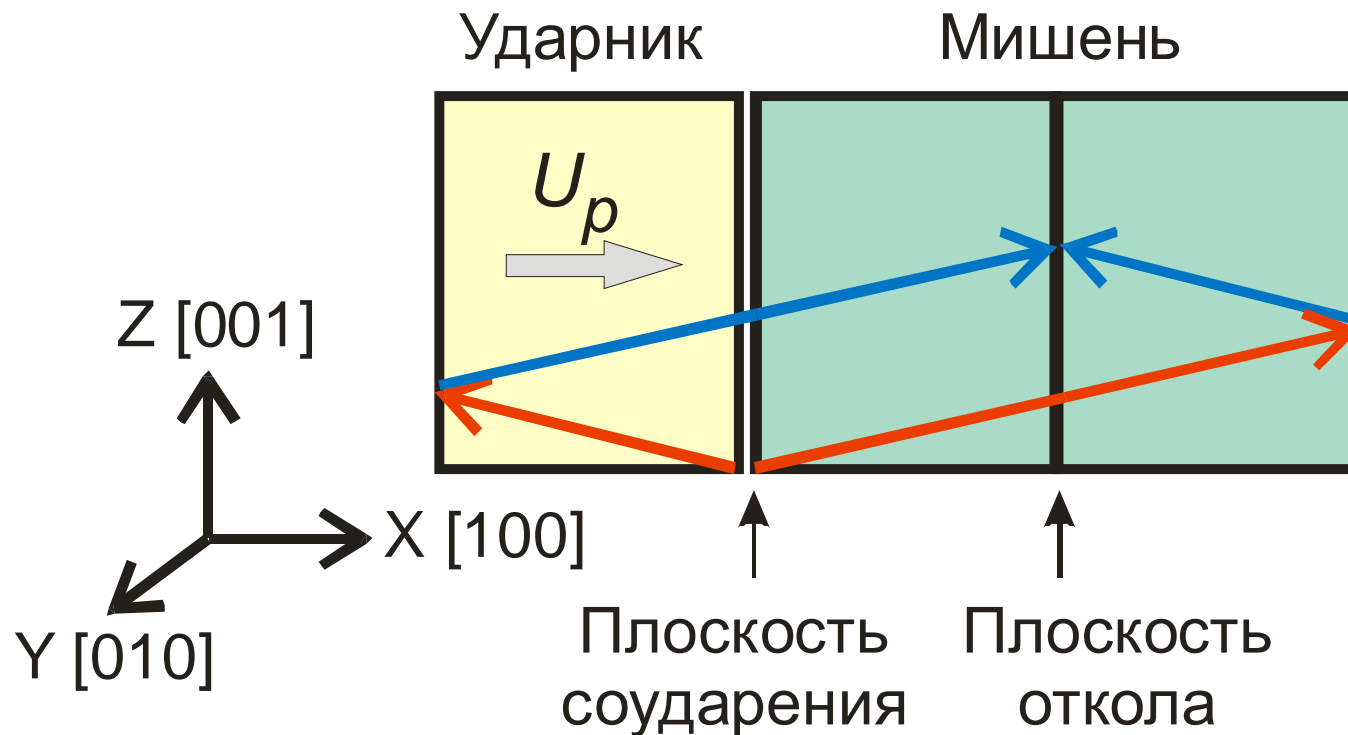
$$F = 1600 \text{ J/m}^2$$

“long” and “short” ablation mechanisms

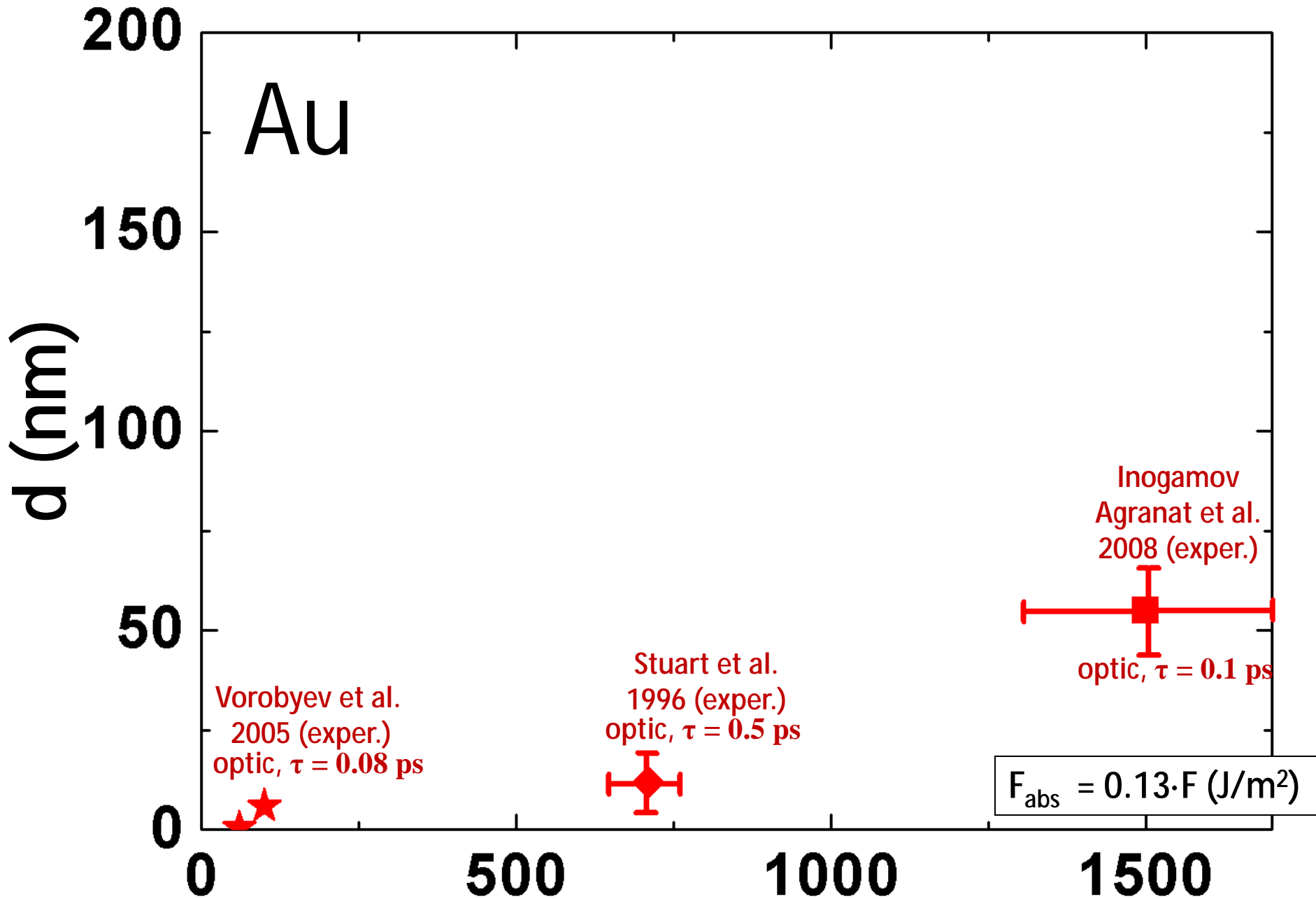


$$F = 1600 \text{ J/m}^2$$

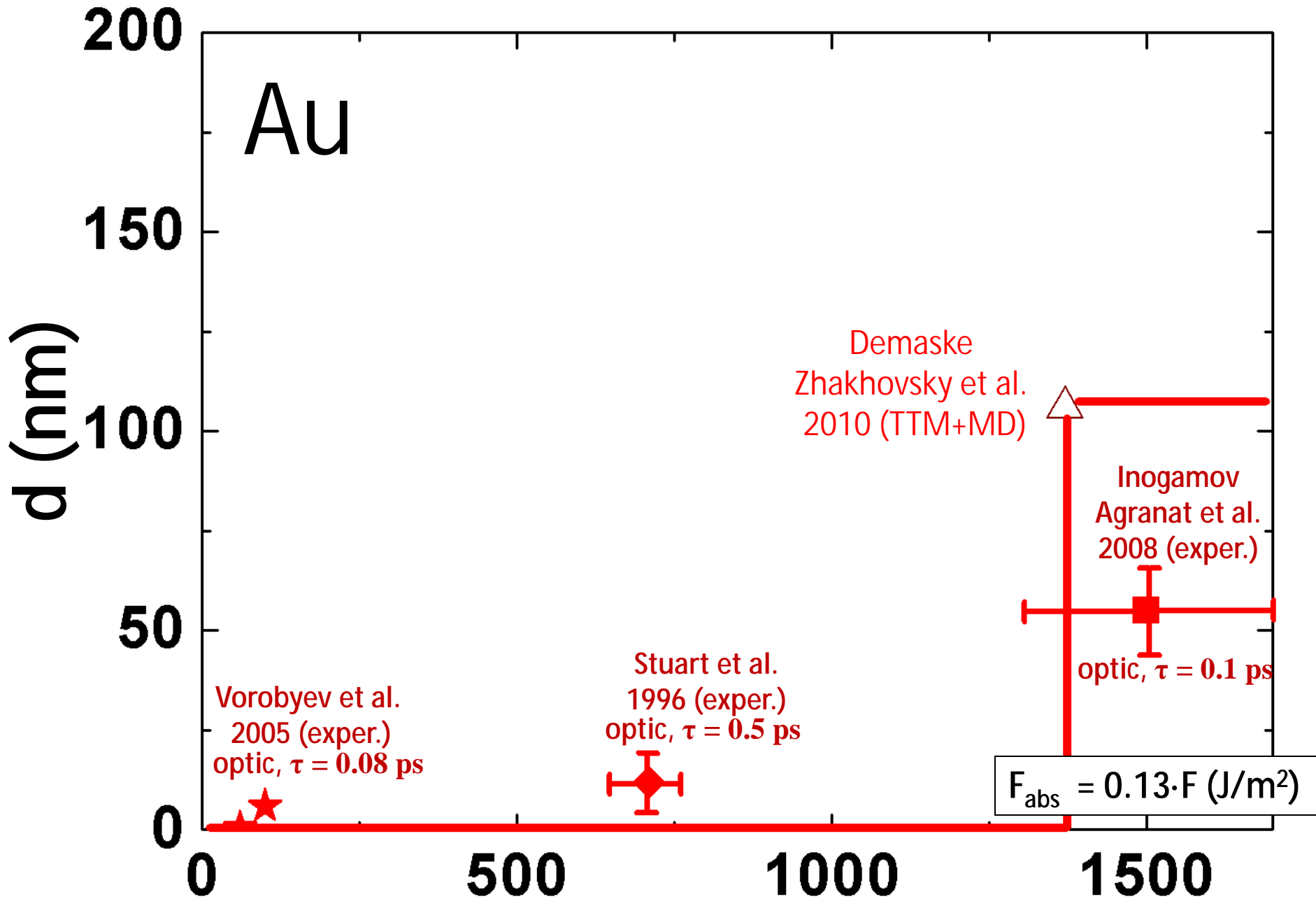
Схема откола при УВ нагружении



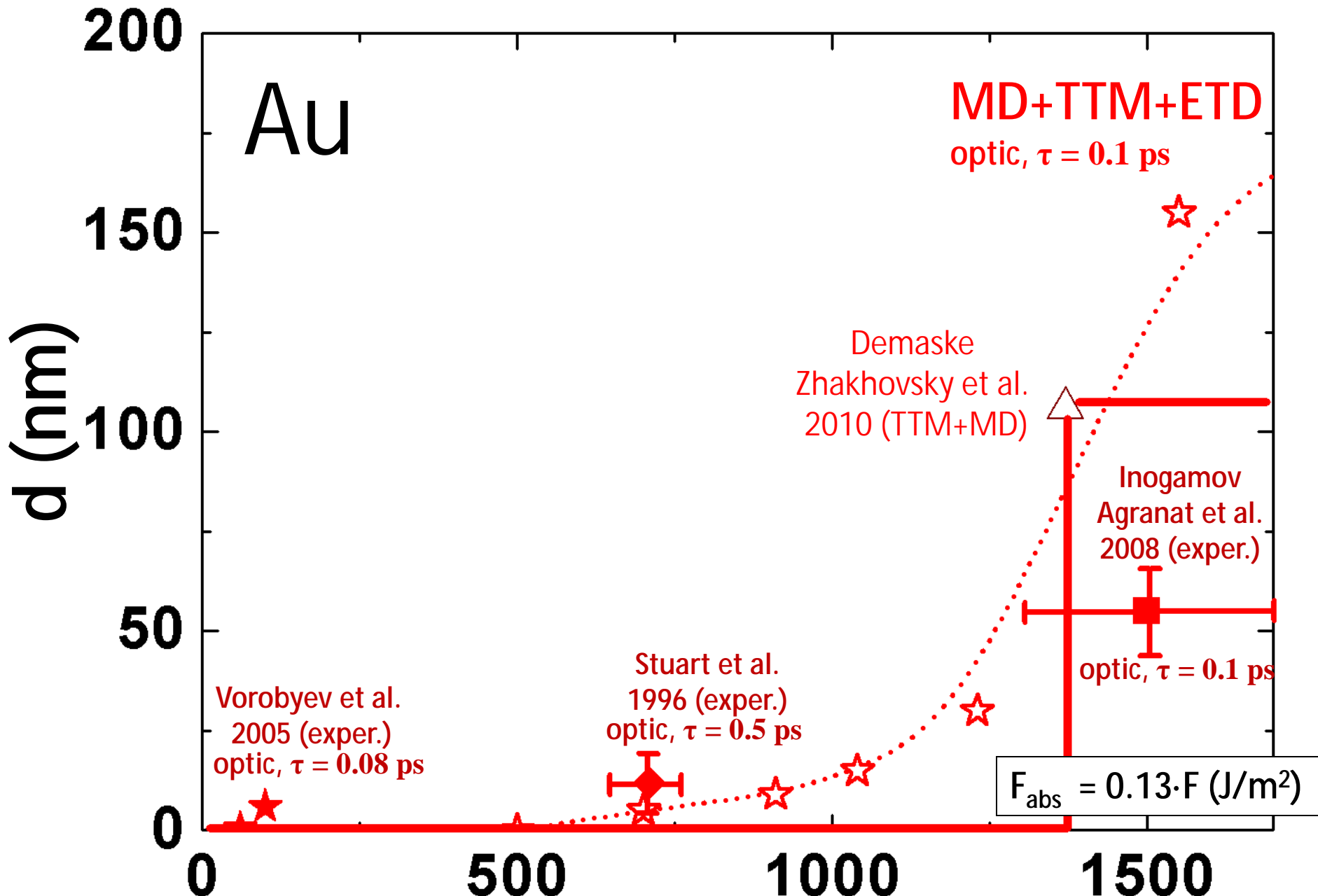
Dependence of crater depth on absorbed fluence (sub-ps pulses)



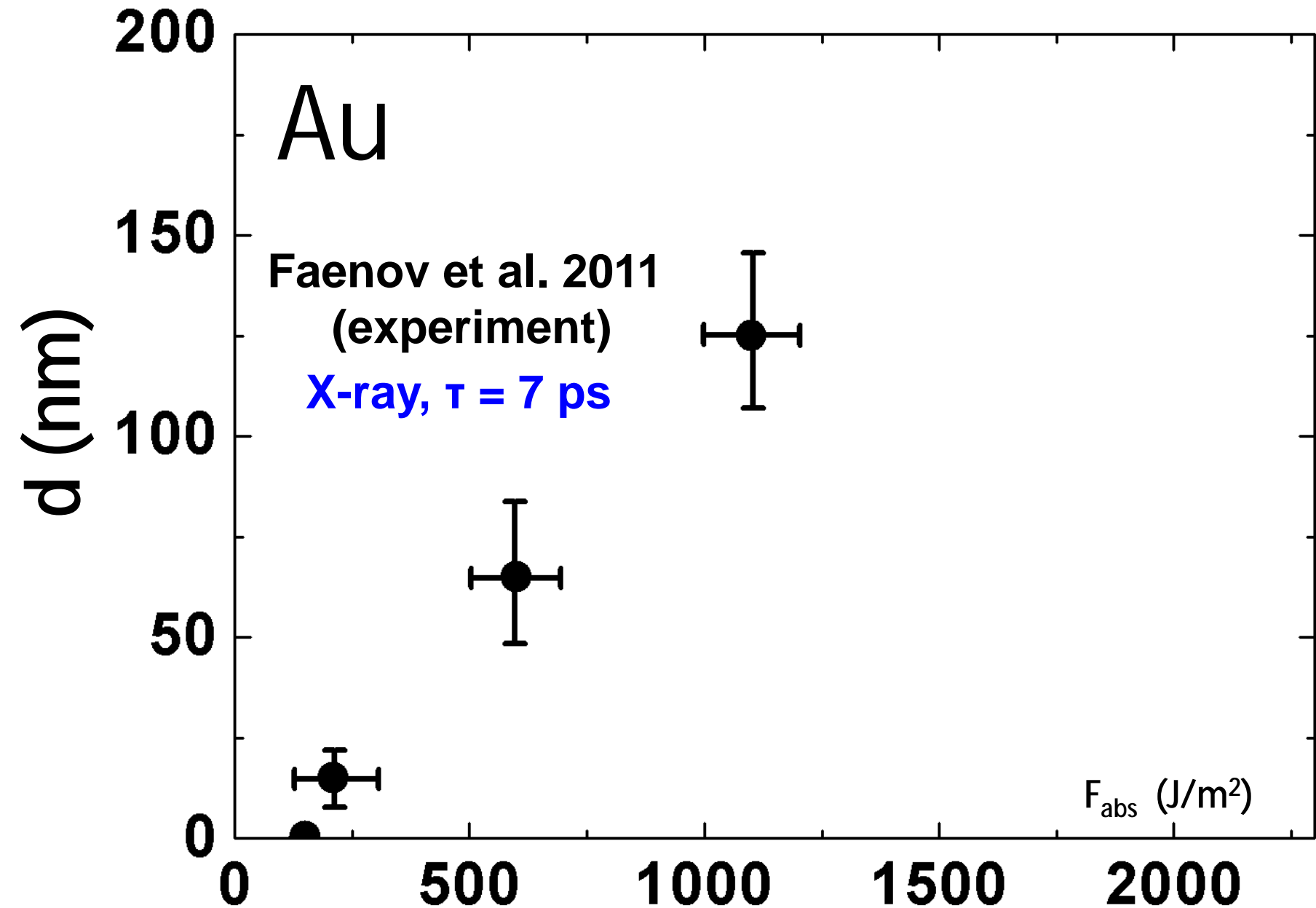
Dependence of crater depth on absorbed fluence (sub-ps pulses)



Dependence of crater depth on absorbed fluence (sub-ps pulses)

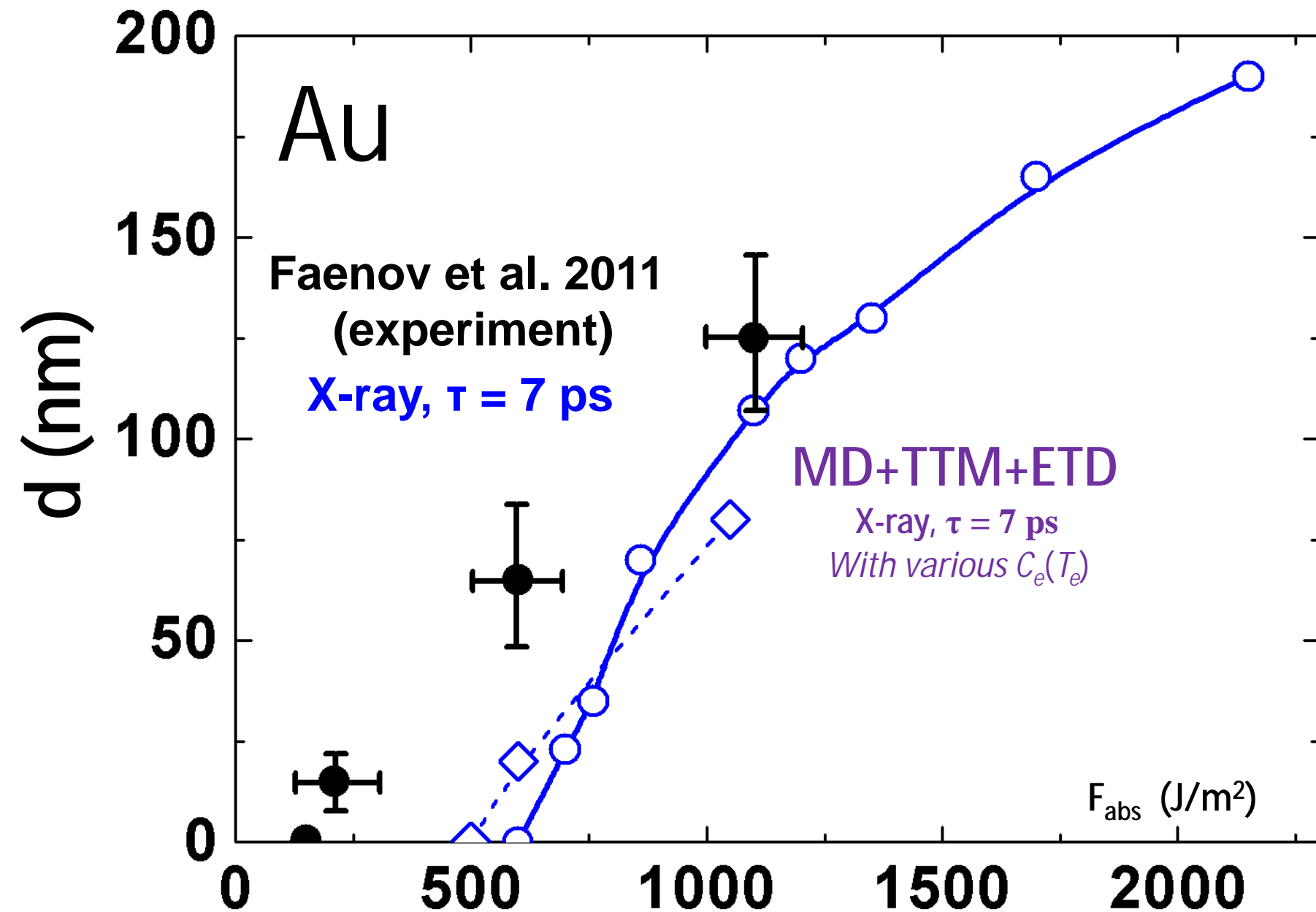


Laser ablation of gold (ps pulses)
Dependence of crater depth on absorbed fluence



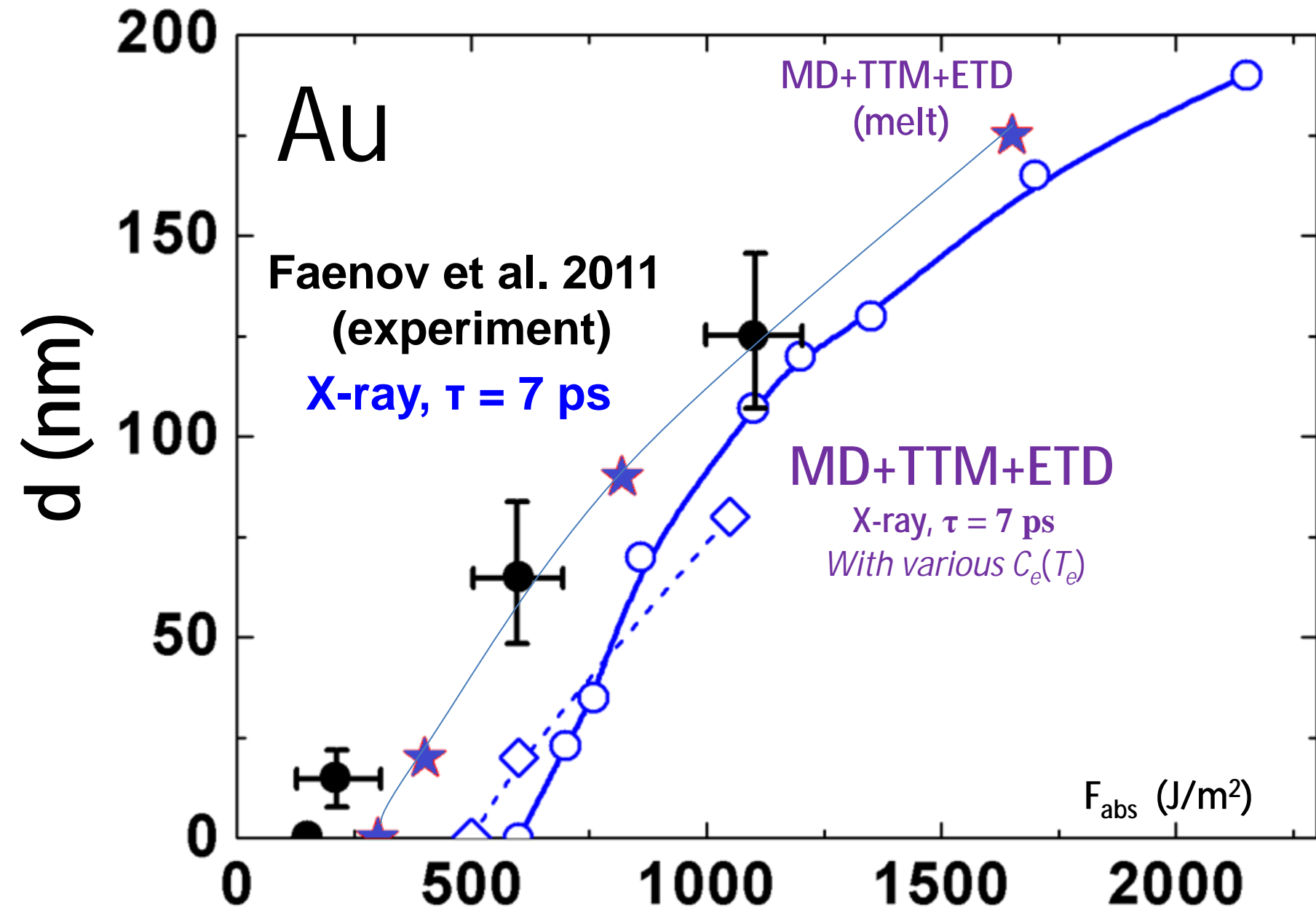
Laser ablation of gold

Dependence of crater depth on absorbed fluence (ps pulse)



Laser ablation of gold

Dependence of crater depth on absorbed fluence (ps pulse)



Norman G.E., Skobelev I.Yu., Stegailov V.V.

Excited States of Warm Dense Matter

Contrib. Plasma Phys. 2011. V. 51. Issue 5. P. 411-418.

Стариков С.В., Стегайлов В.В., Норман Г.Э., Фортов В.Е., Ишино М., Танака М.,
Хасегава Н., Нишикино М., Охба Т., Каихори Т., Очи Е., Имазоно Т., Кавачи Т.,
Тамотсу С., Пикуз Т.А., Скобелев И.Ю., Фаенов А.Я.

Лазерная абляция золота: эксперимент и атомистическое моделирование

Письма в ЖЭТФ 2011. Т.93, №11. С.719-725

Г.Э. Норман, С.В. Старикин, В.В. Стегайлов,

"Атомистическое моделирование лазерной абляции золота:

эффект релаксации давления"

ЖЭТФ. Т 141. выпуск 5. С. 910-918 (2012)

G.Norman, S.Starikov, V.Stegailov, V.Fortov, I.Skobelev, T.Pikuz, A.Faenov,
S.Tamotsu, Y. Kato, M.Ishino, M.Tanaka, N.Hasegawa, M.Nishikino, T.Ohba,
T. Kaihori, Y.Ochi, T.Imazono, Y. Fukuda, M.Kando, T.Kawachi

"Nanomodification of gold surface by picosecond soft X-ray laser pulse"

Journal of Applied Physics. 112, Issue 1, 3 July 2012 [9 pages]

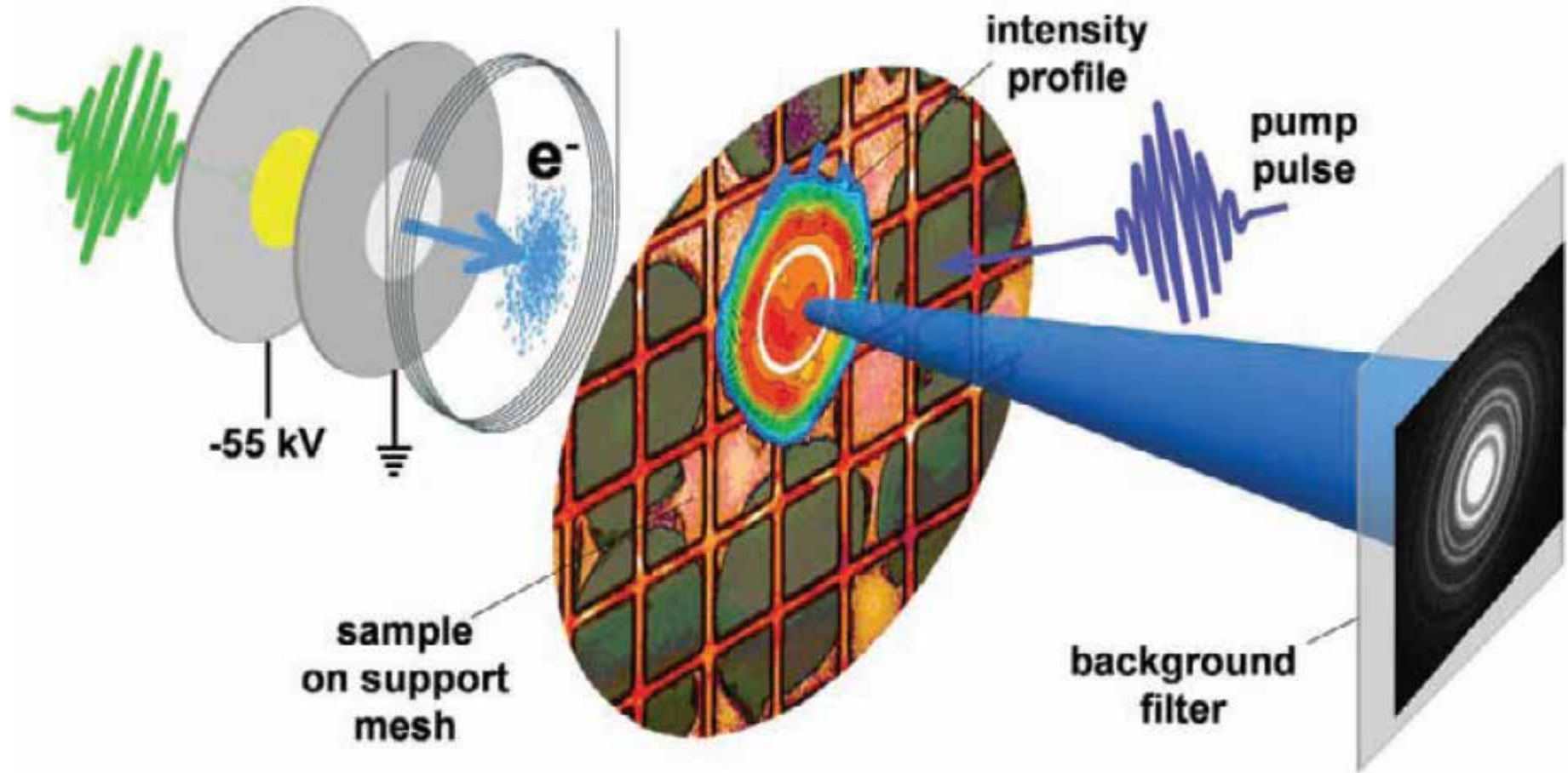
G. E. Norman, I. M. Saitov, S. V. Starikov, V.V. Stegailov and P. A. Zhilyaev.
Atomistic Modeling of Warm Dense Matter in the Two-Temperature State
submitted to Contrib. Plasma Phys.

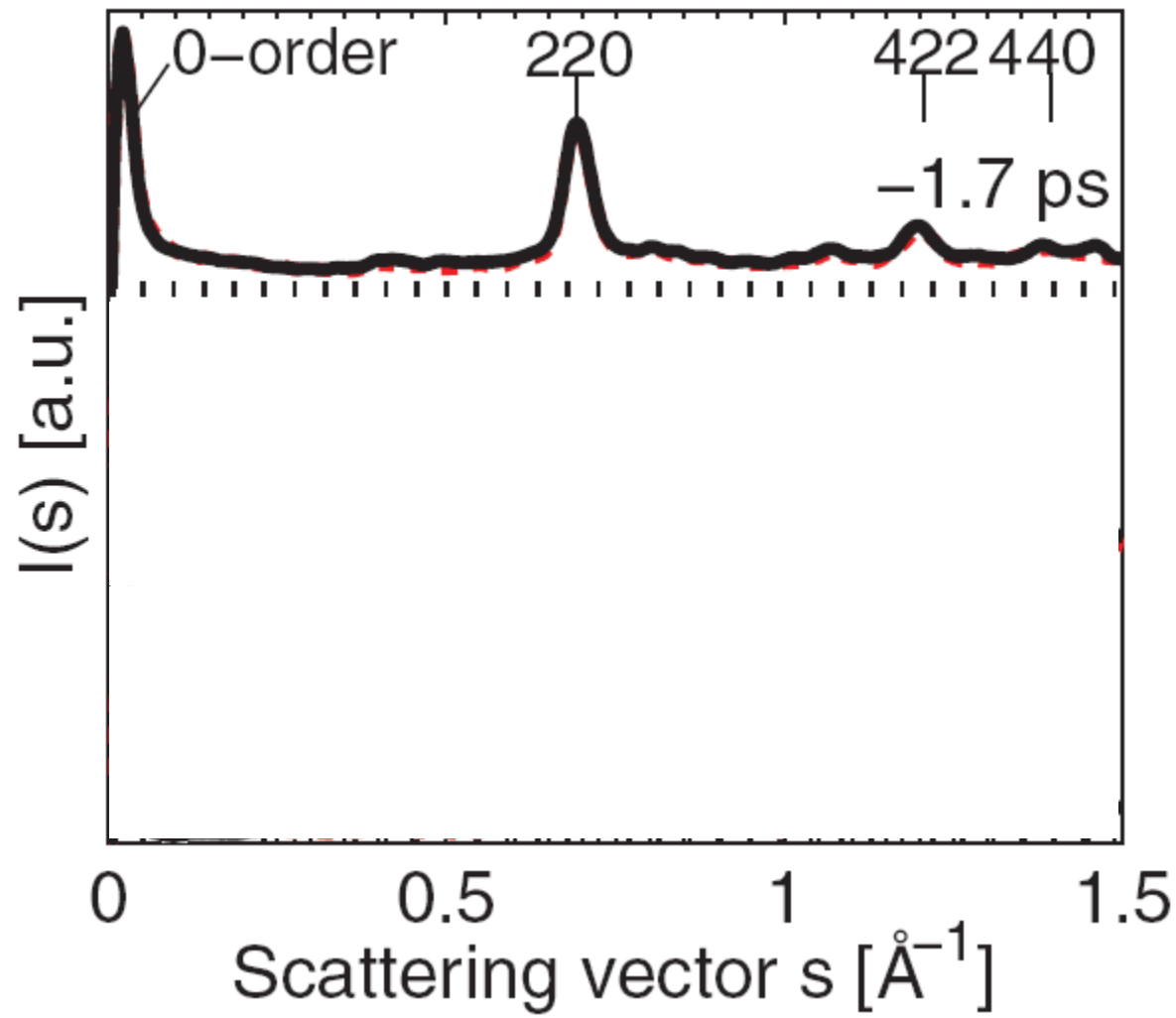
Г.Э. Норман, В.В. Стегайлов.
Стохастическая теория метода классической молекулярной динамики
Математическое моделирование. 2012 год, том 24, номер 6, стр. 3-44

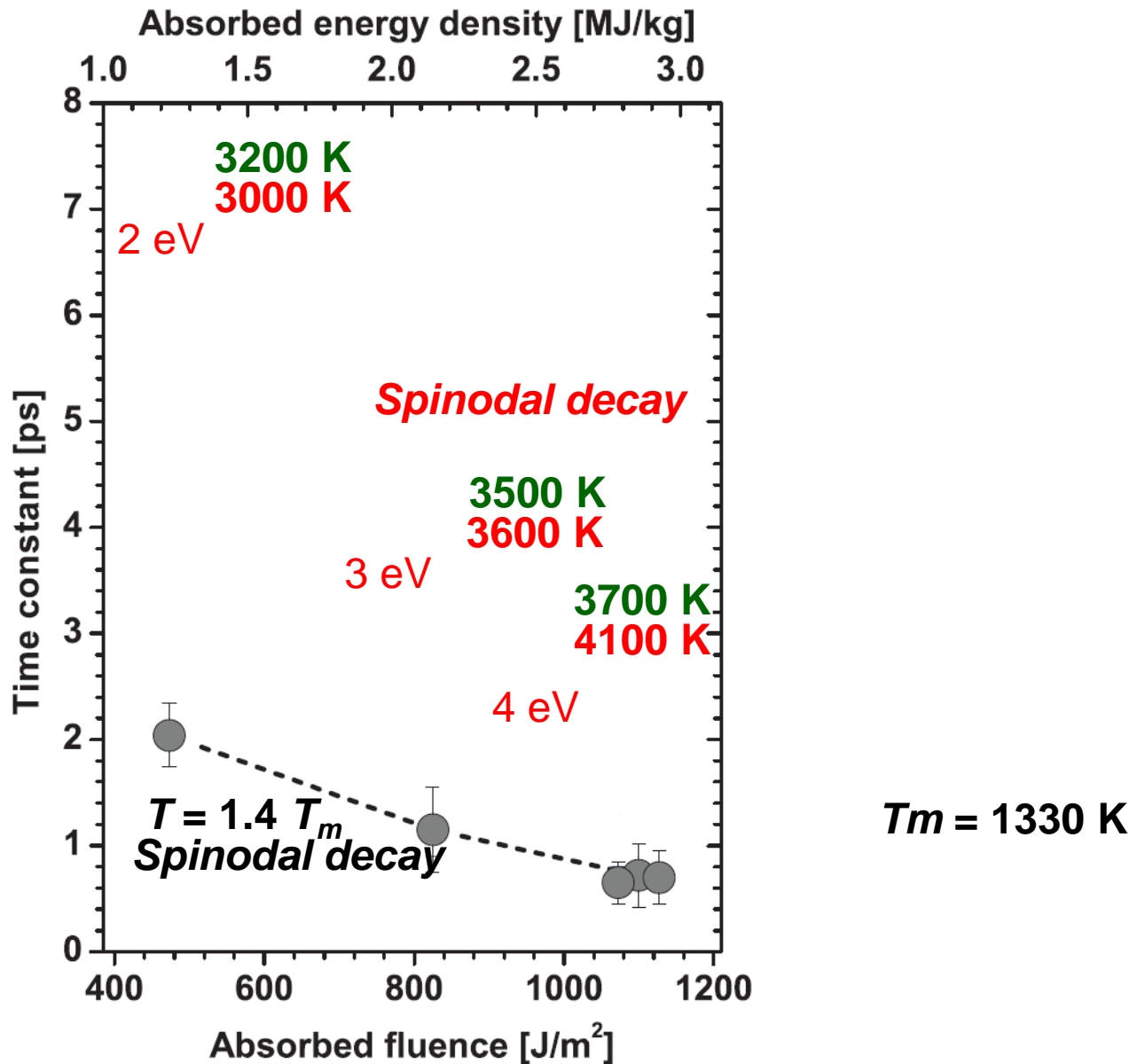
В.М.Замалин, Г.Э.Норман, В.С.Филинов.
Метод Монте Карло в статистической термодинамике.
Москва, Наука, 1977.
http://www.ihed.ras.ru/norman/paper_view.php?p=45

The Formation of Warm Dense Matter: Experimental Evidence for Electronic Bond Hardening in Gold.

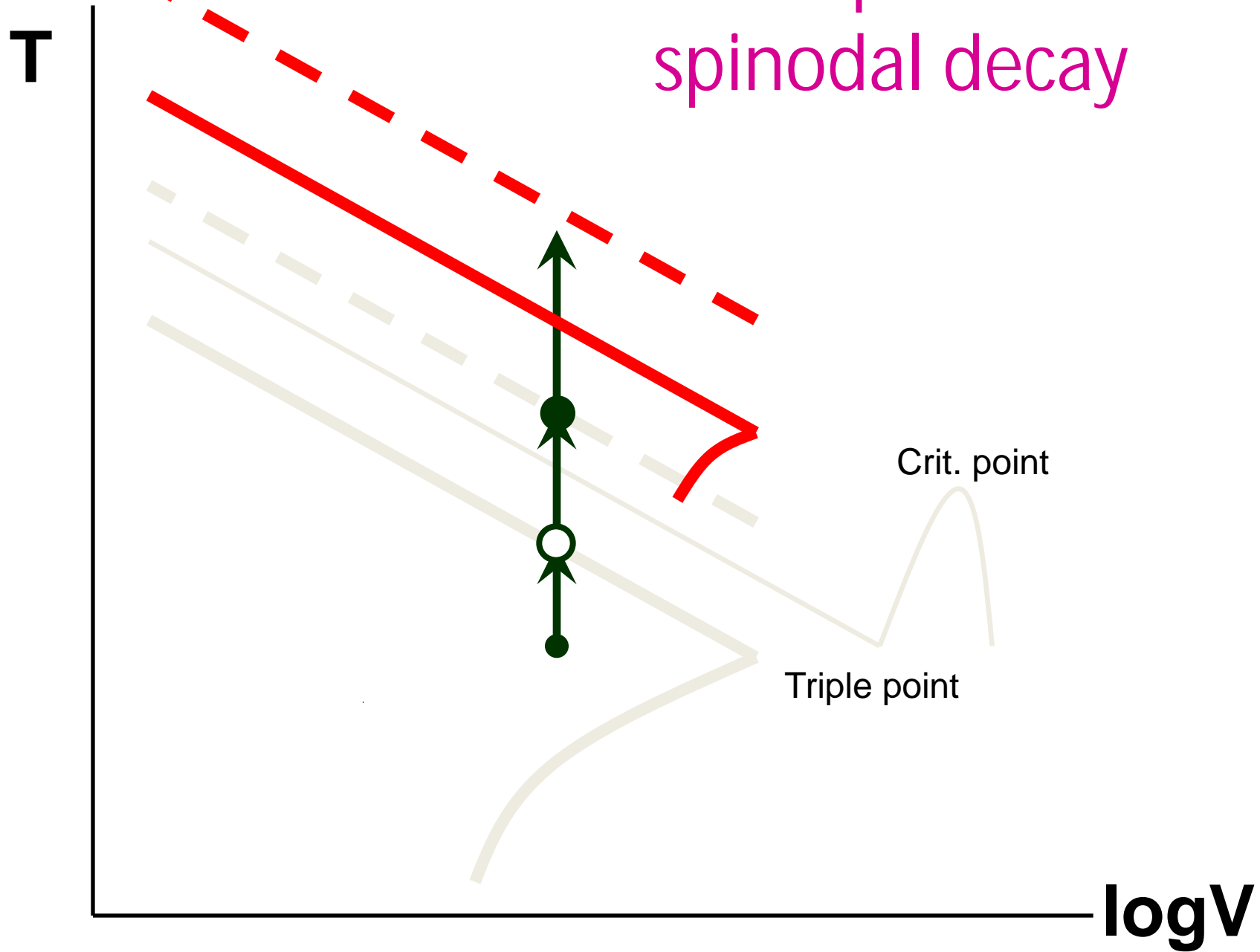
R.Ernstorfer, M.Harb, C.Hebeisen, G.Sciaini, T.Dartigalongue, R.Miller
Science. Vol. 323. no. 5917, pp. 1033 – 1037. **20 February 2009**







Non-equilibrium spinodal decay



The energy deposited in WDM
can be by order of magnitude higher
because of the creation of the
two-temperature state and
corresponding ion lattice hardening

The final explosion can be
a spinodal decay of
a particular two-temperature
metastable state

Formation of two-temperature state: experimental evidence for electronic bond hardening in gold

Ernstorfer R. et al. The formation of warm dense matter: experimental evidence for electronic bond hardening in gold // Science. 2009.

Recoules V. et al. Effect of Intense Laser Irradiation on the Lattice Stability of Semiconductors and Metals// PRL. 2006.

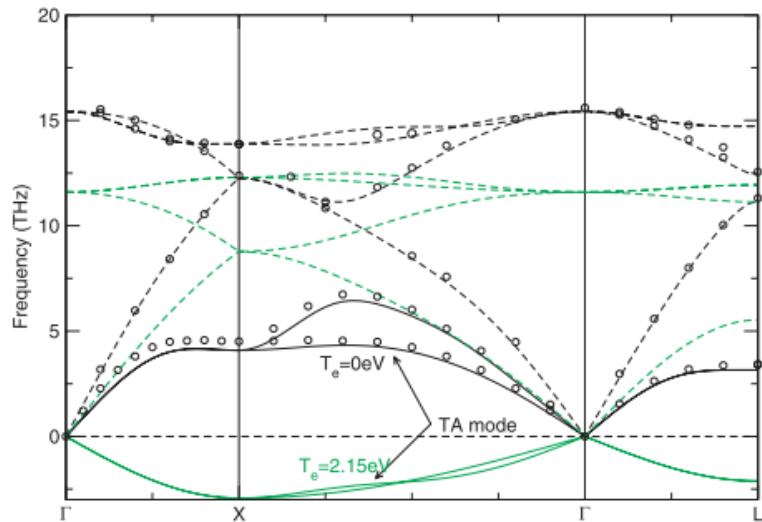


FIG. 1 (color online). Phonon spectrum of Si at different electronic temperature. The black curve is the spectrum for $T_e = 0\text{ eV}$. The green curves are for $T_e = 2.15\text{ eV}$. Open circles are experimental results from [26].

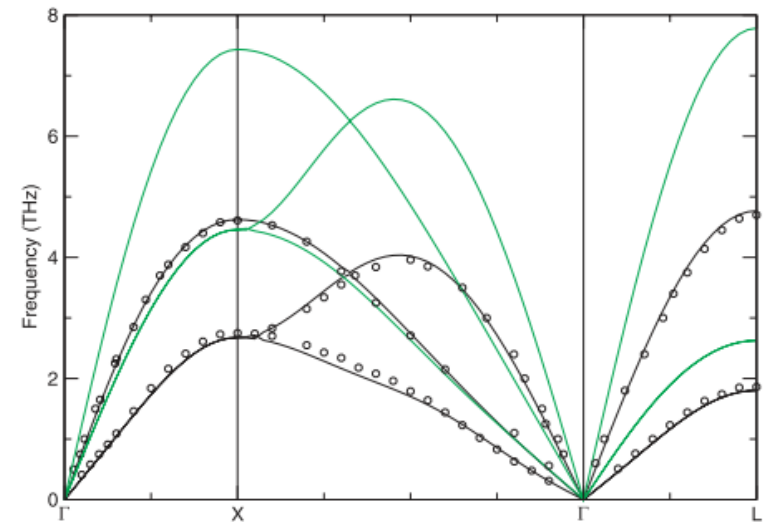
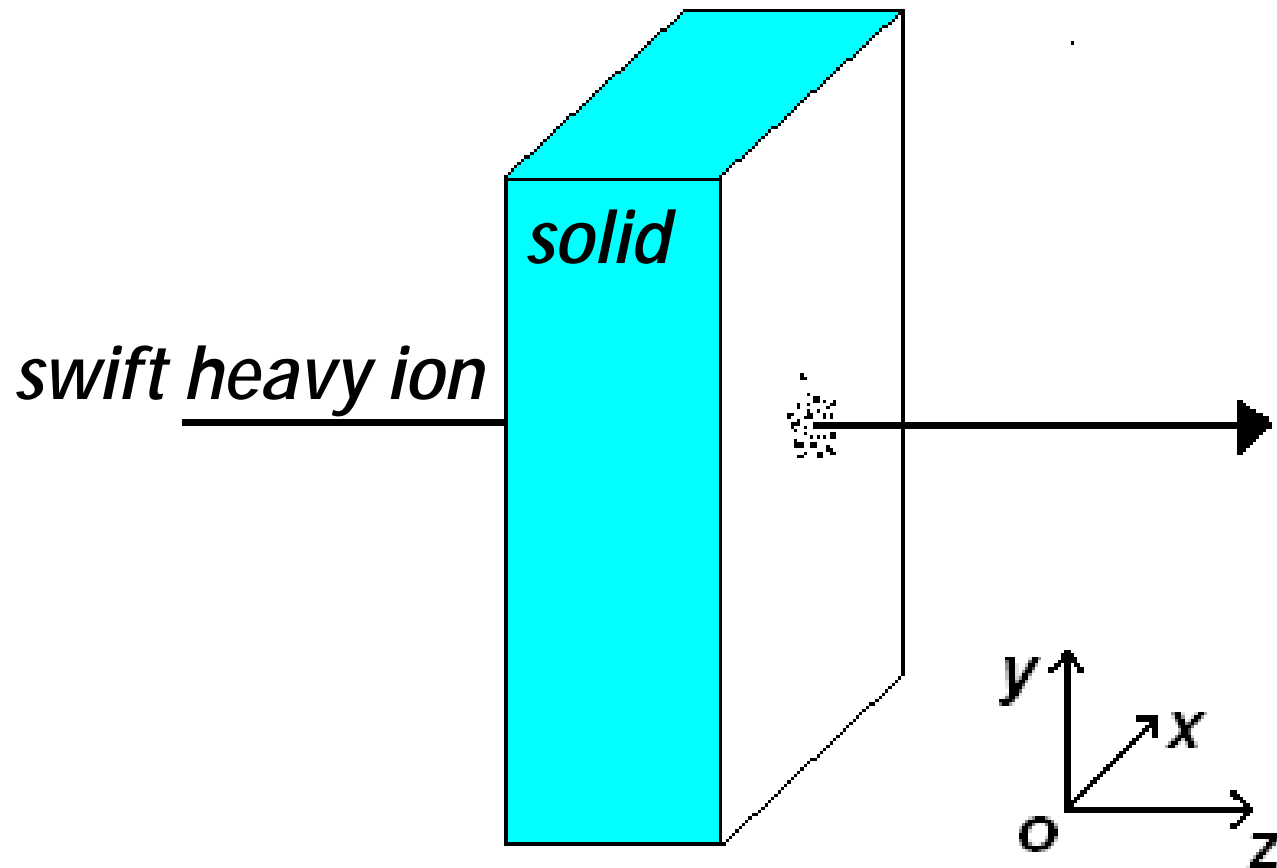


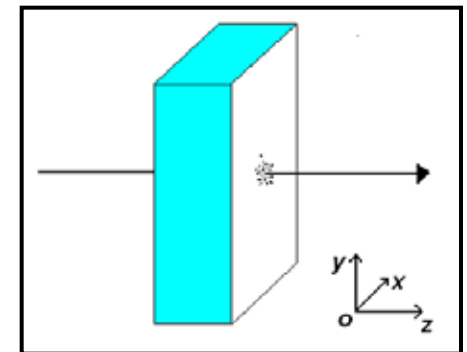
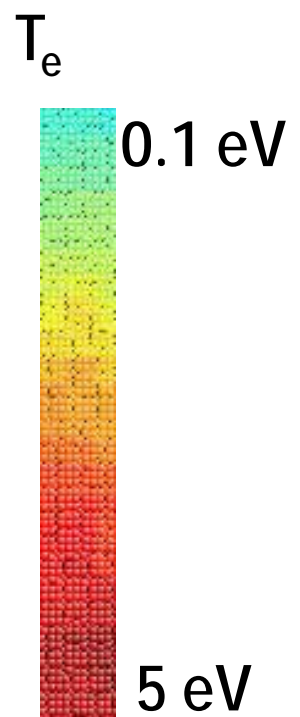
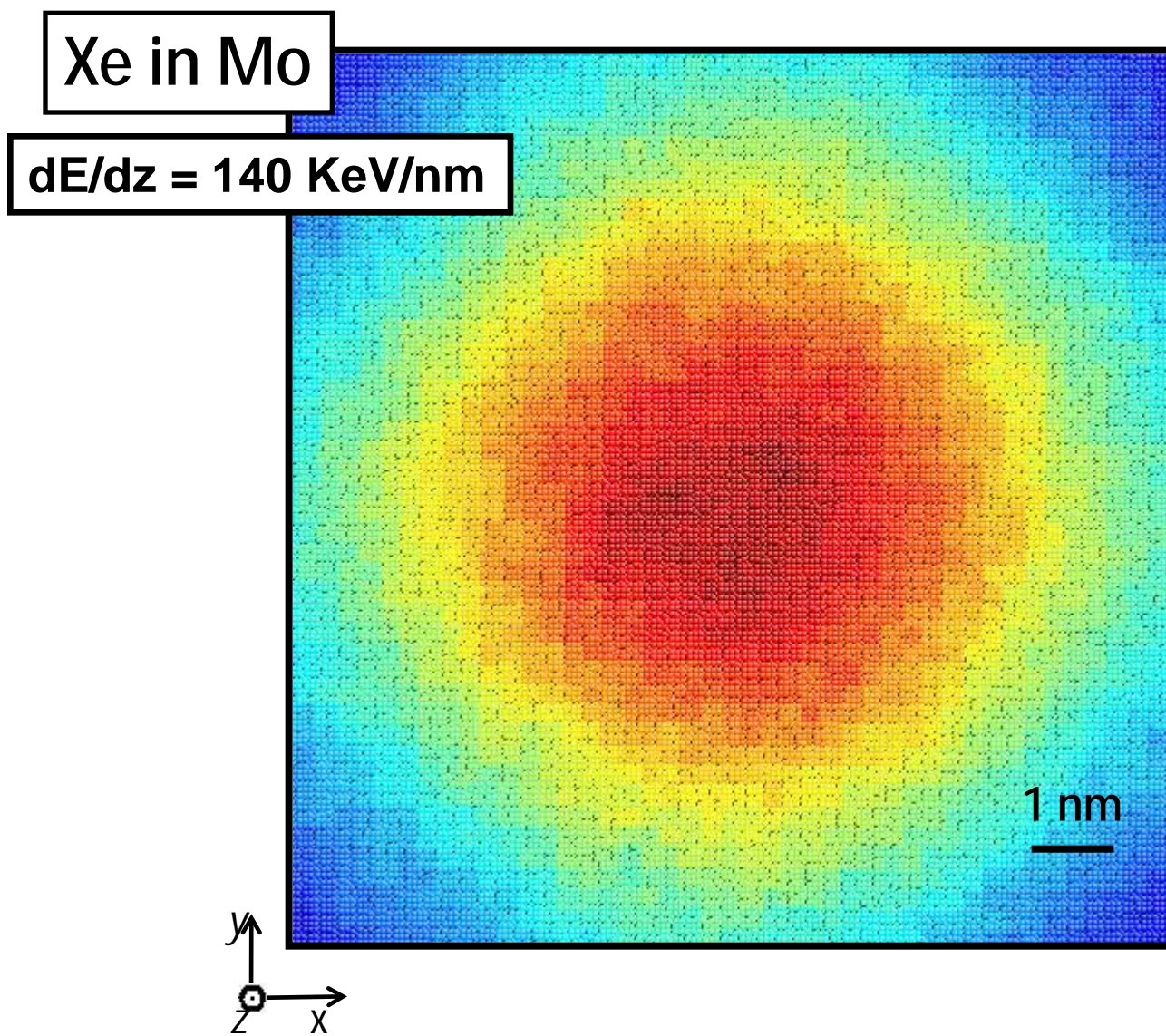
FIG. 2 (color online). Phonon spectrum of Au at different electronic temperatures. The black curves are the spectrum for $T_e = 0\text{ eV}$. The green curves are for $T_e = 6\text{ eV}$. Open circles are experimental results from [27].

Simulation of tracks formation in metals

Moving of high energy ion through matter



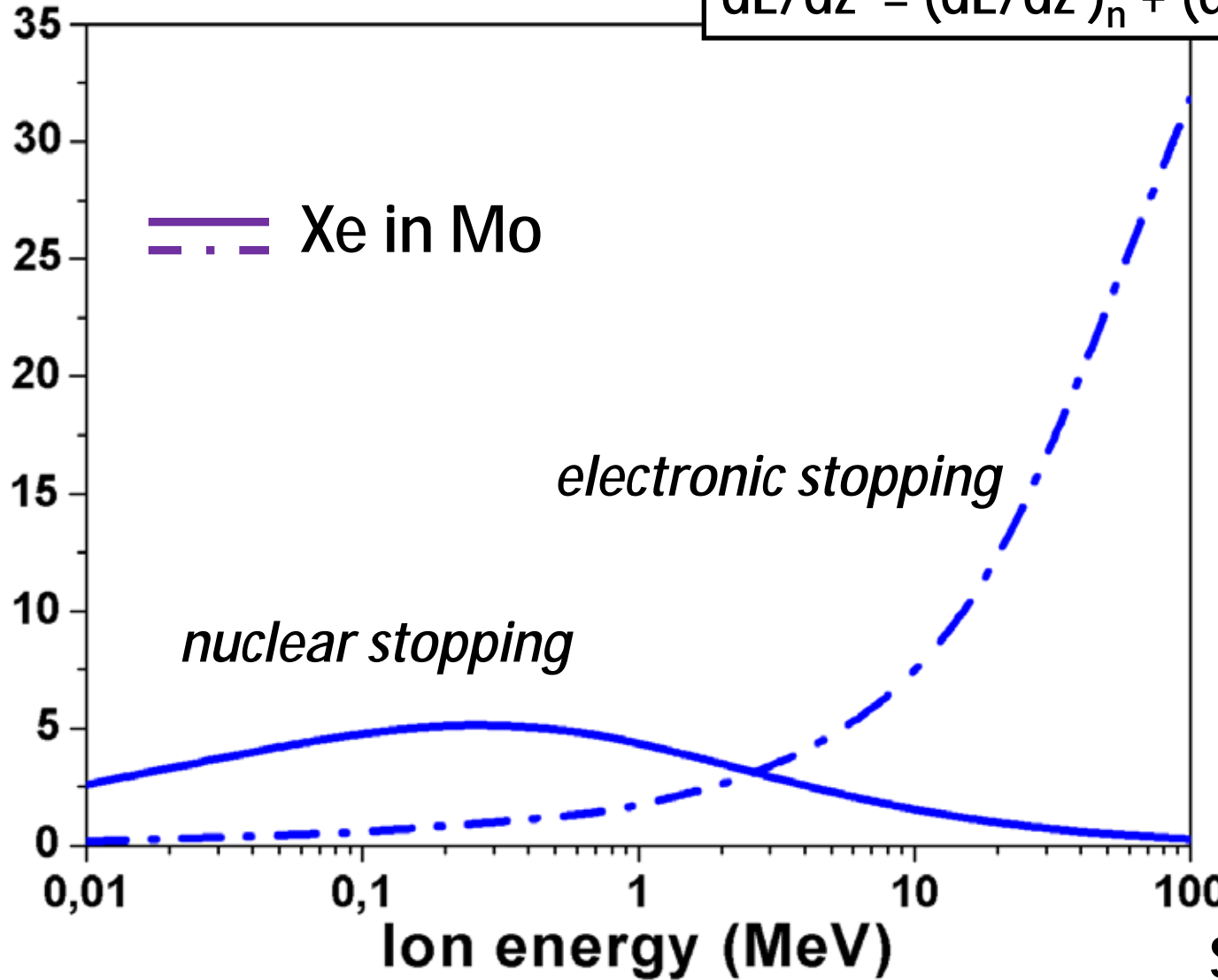
Initial distribution of electronic temperature



Energy loss of Xe ion in metal

dE/dz (KeV/nm)

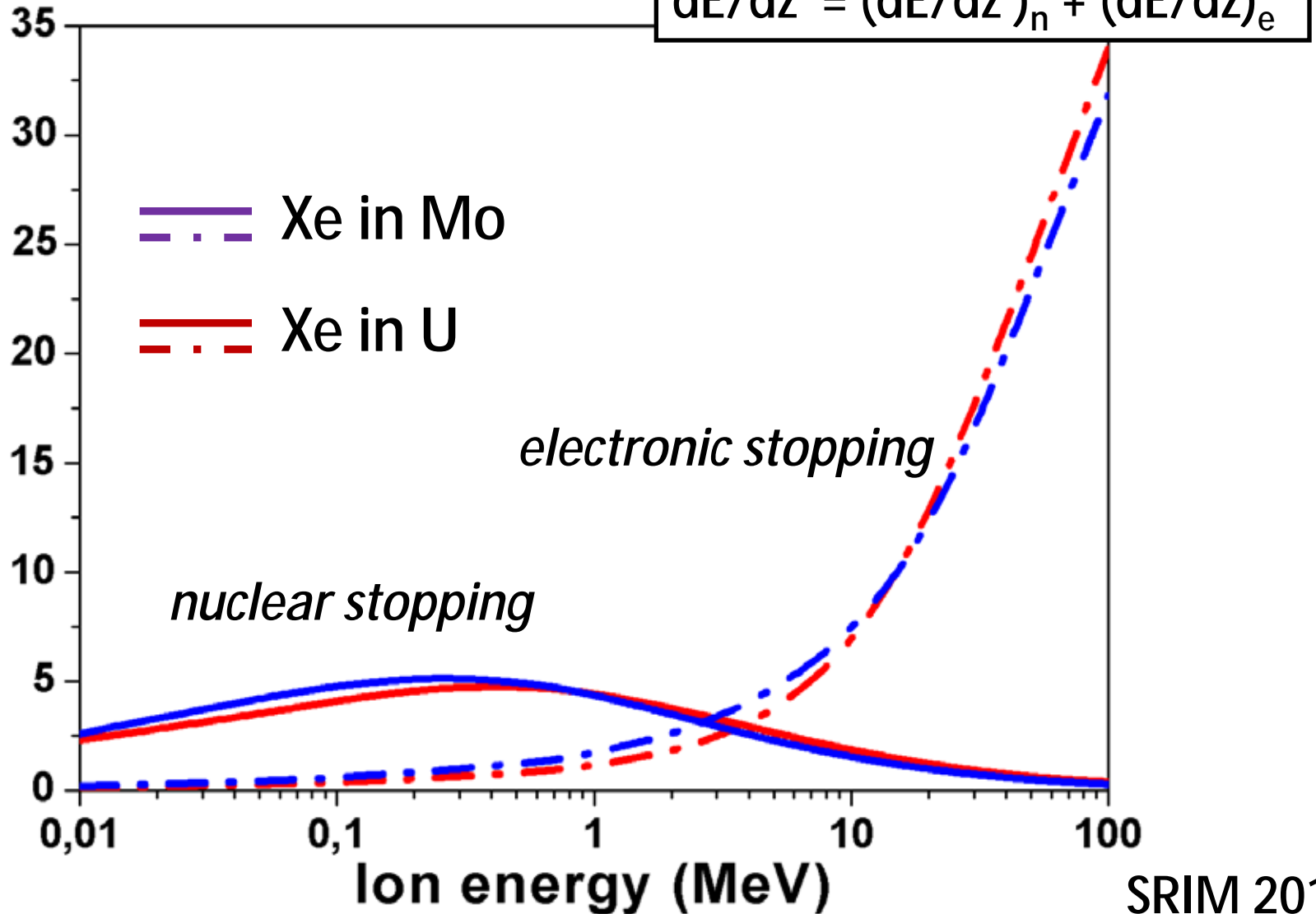
$$dE/dz = (dE/dz)_n + (dE/dz)_e$$



Energy loss of Xe ion in metal

dE/dz (KeV/nm)

$$dE/dz = (dE/dz)_n + (dE/dz)_e$$



Two-temperature model

Ion subsystem

$$m \frac{d\mathbf{v}_i}{dt} = \mathbf{F}_i - b \mathbf{v}_i + \mathbf{F}_i^{Lang}(T_e)$$

Electronic subsystem

$$C_e \frac{\dot{T}_e}{t} = \tilde{N}(K_e \tilde{N} T_e) - G_e(T_e - T_i)$$

Interatomic potential

Mo

Starikov S., Insepov Z., Rest J., Kuksin A., Norman G., Stegailov V., Yanilkin A.
// *Phys. Rev. B* **84** 104109 (2011)

U

Smirnova D., Starikov S., Stegailov V.
// *J. Phys.: Condens. Matter* **24** 015702 (2012)

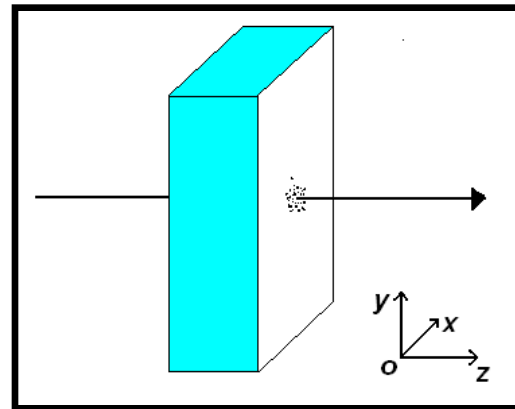
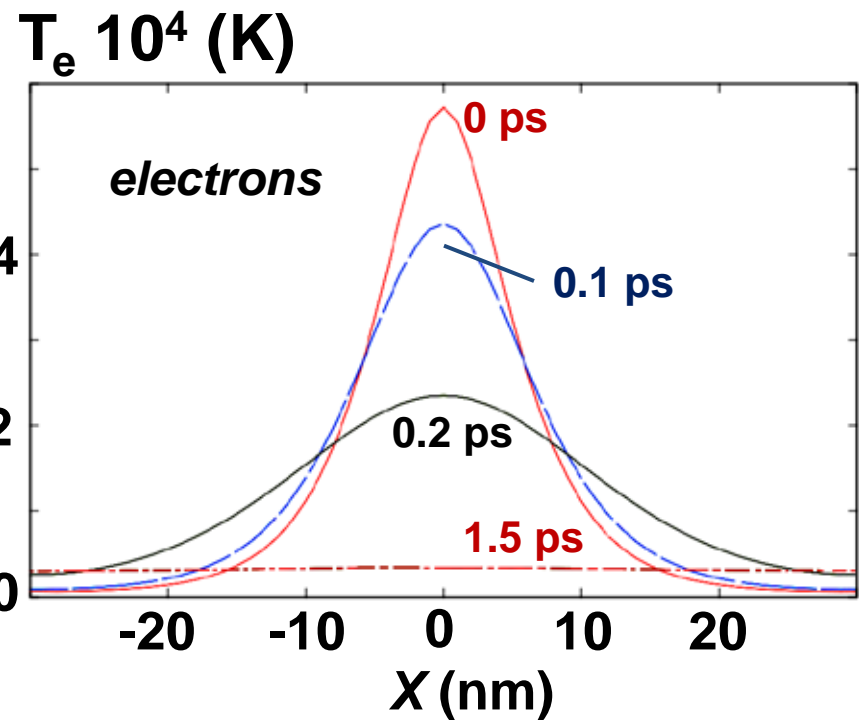
Characteristics of the electronic subsystem

$$C_e = \gamma T_e ; K_e ; G$$

Simulation of track formation in Mo

Profiles of electronic and ionic temperatures

$dE/dz = 140 \text{ KeV/nm}$

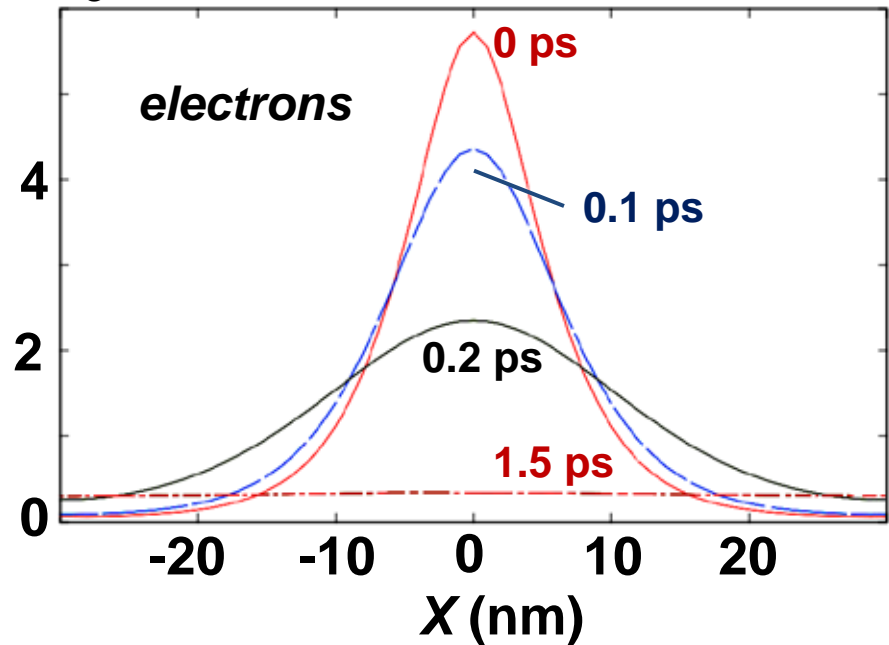


Mo

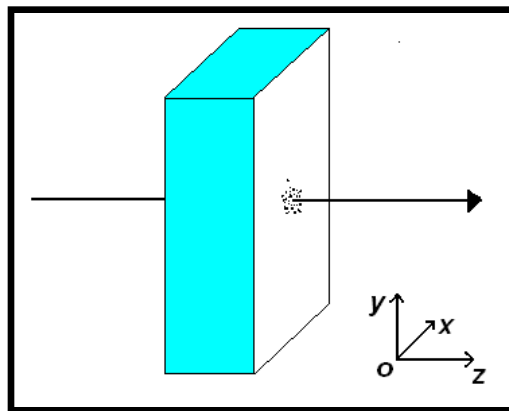
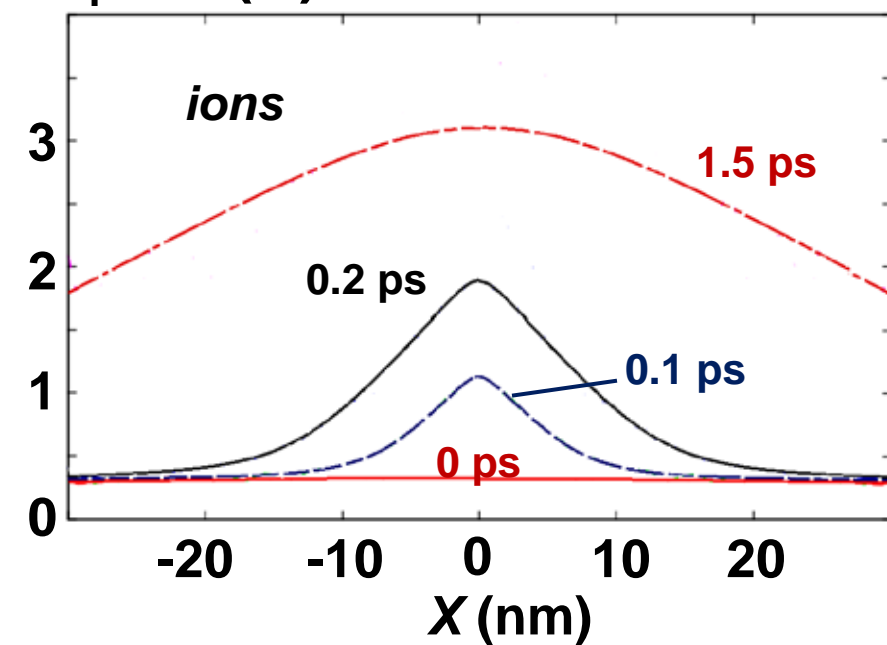
Profiles of electronic and ionic temperatures

$dE/dz = 140 \text{ KeV/nm}$

$T_e 10^4 \text{ (K)}$



$T_i 10^3 \text{ (K)}$



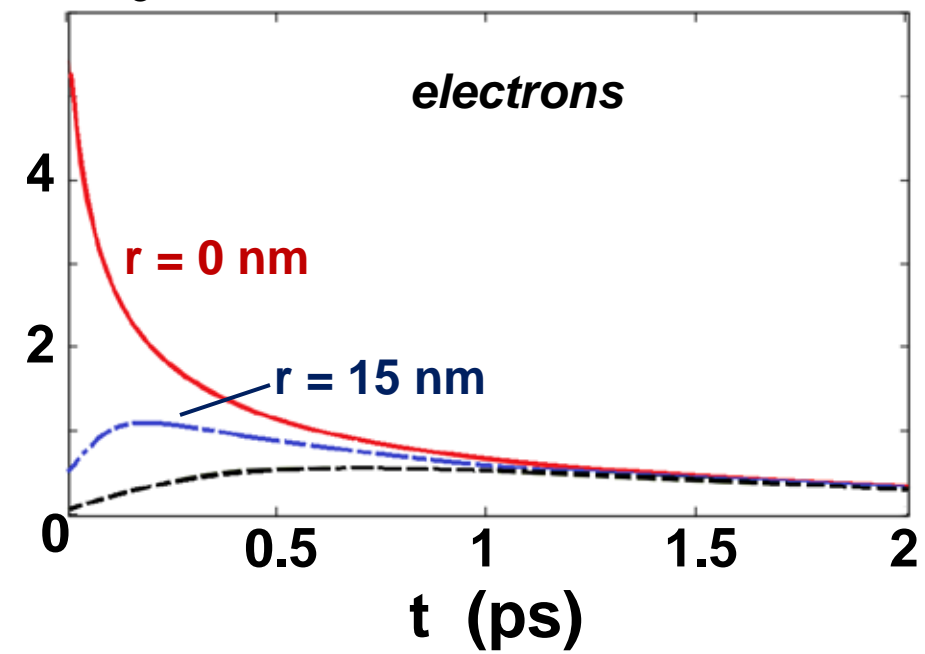
Mo

Dependence of temperature on time

$dE/dz = 140 \text{ KeV/nm}$

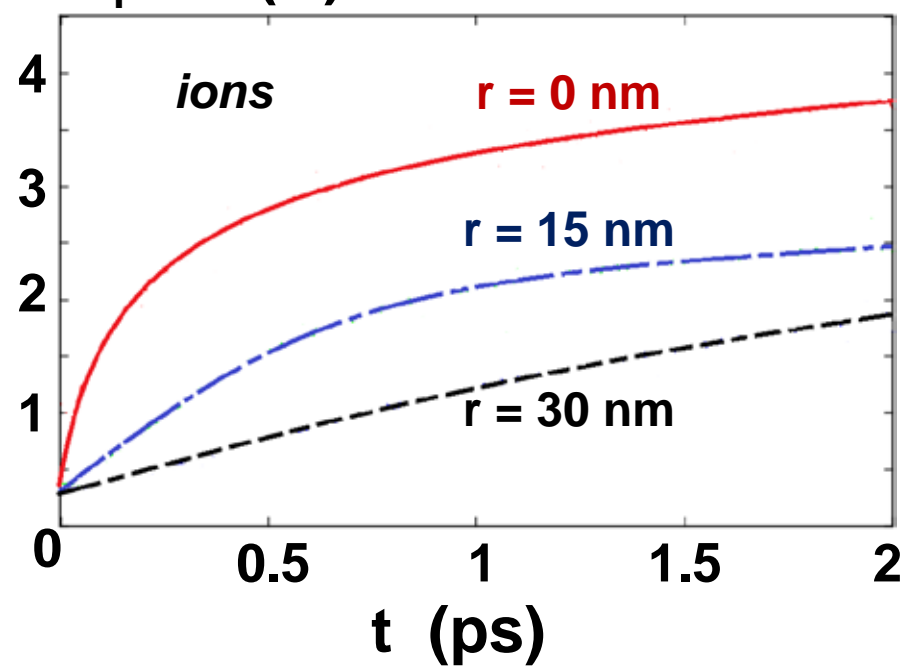
$T_e 10^4 \text{ (K)}$

electrons



$T_i 10^3 \text{ (K)}$

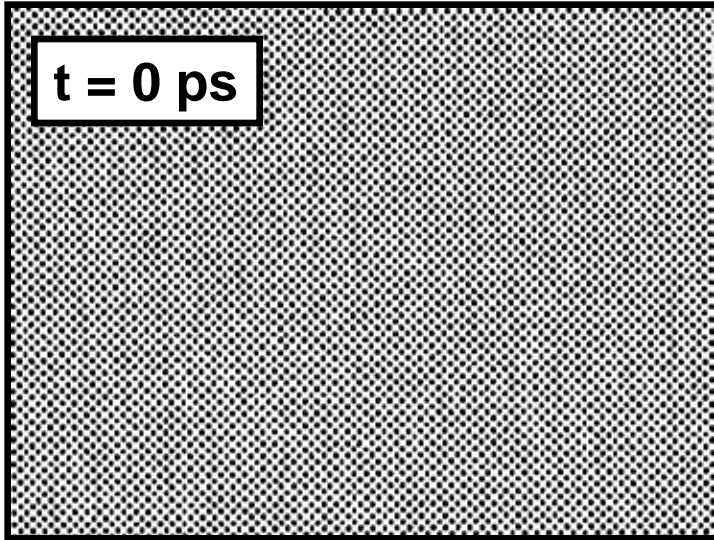
ions



Mo

Defect formation at heating/melting of ionic subsystem

$dE/dz = 160 \text{ KeV/nm}$

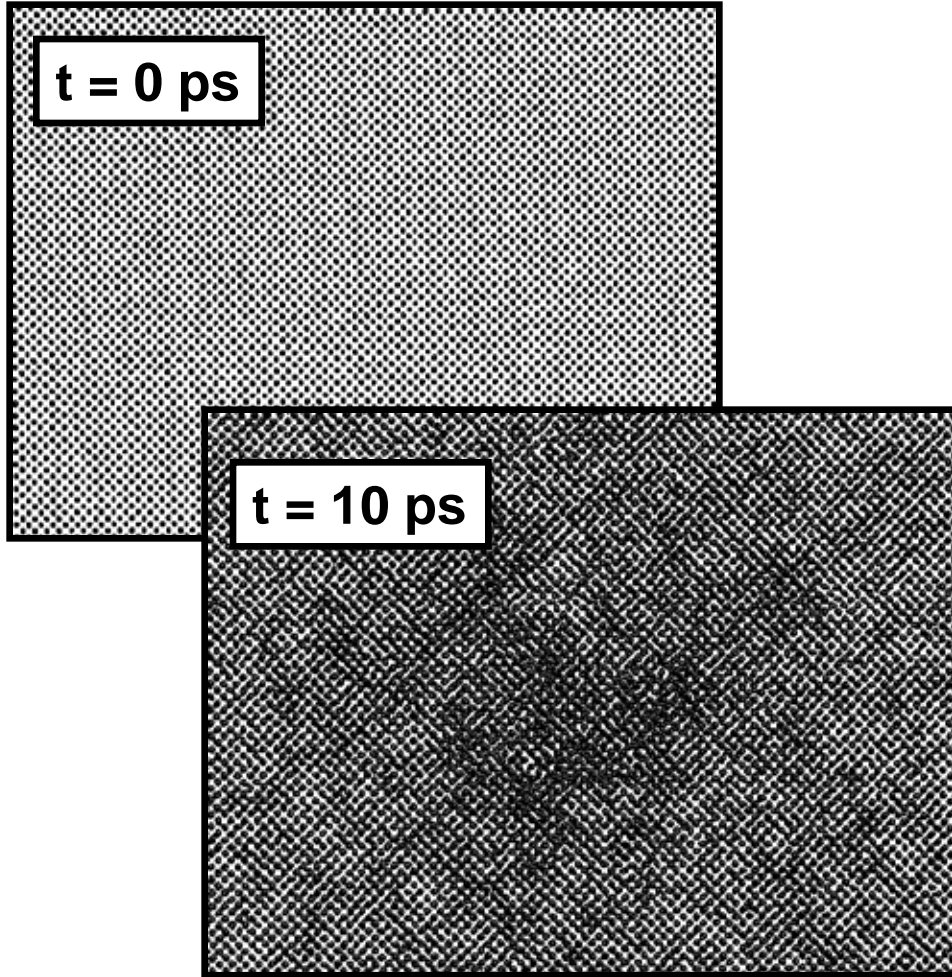


$t = 0 \text{ ps}$

Mo

Defect formation at heating/melting of ionic subsystem

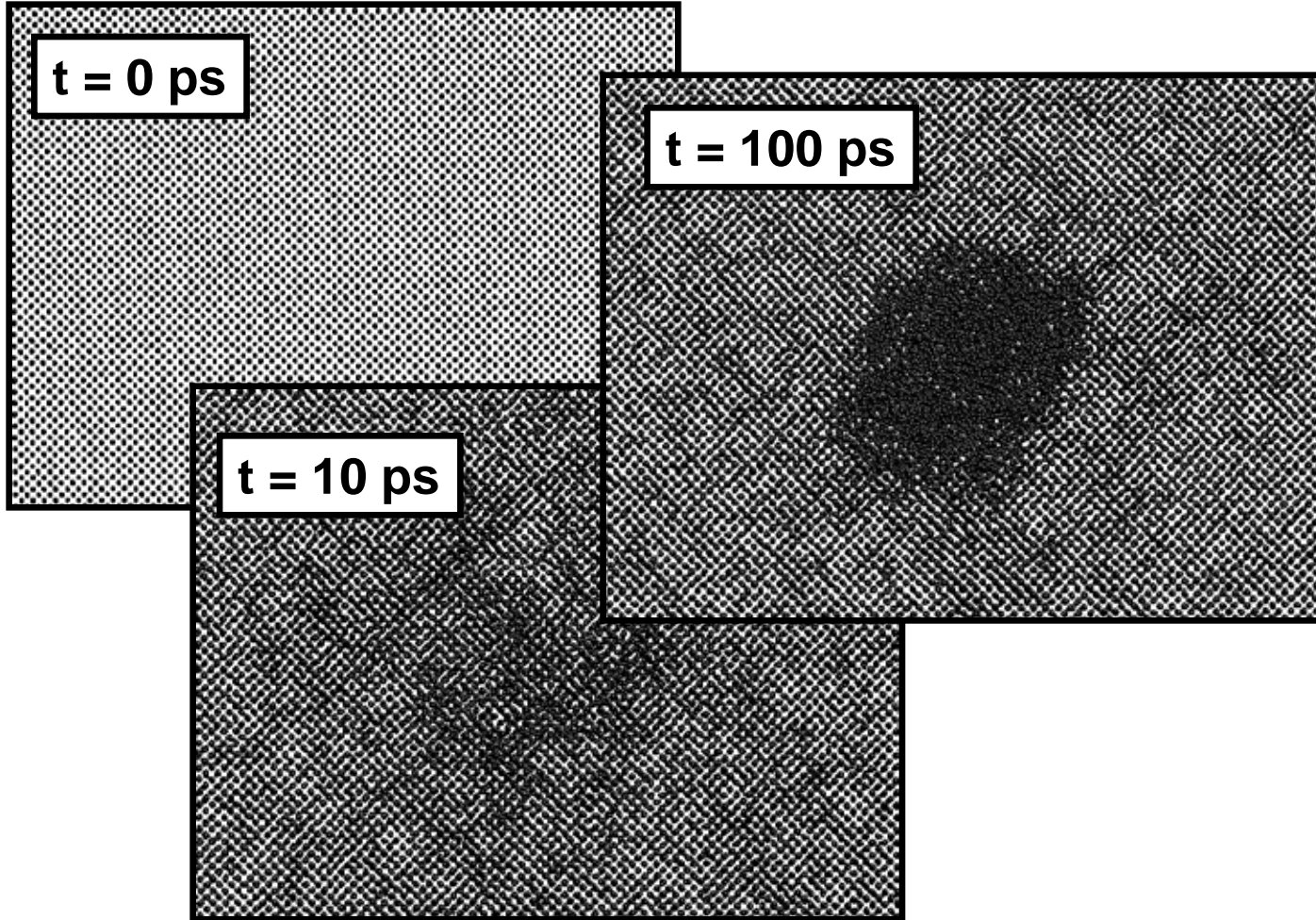
$dE/dz = 160 \text{ KeV/nm}$



Mo

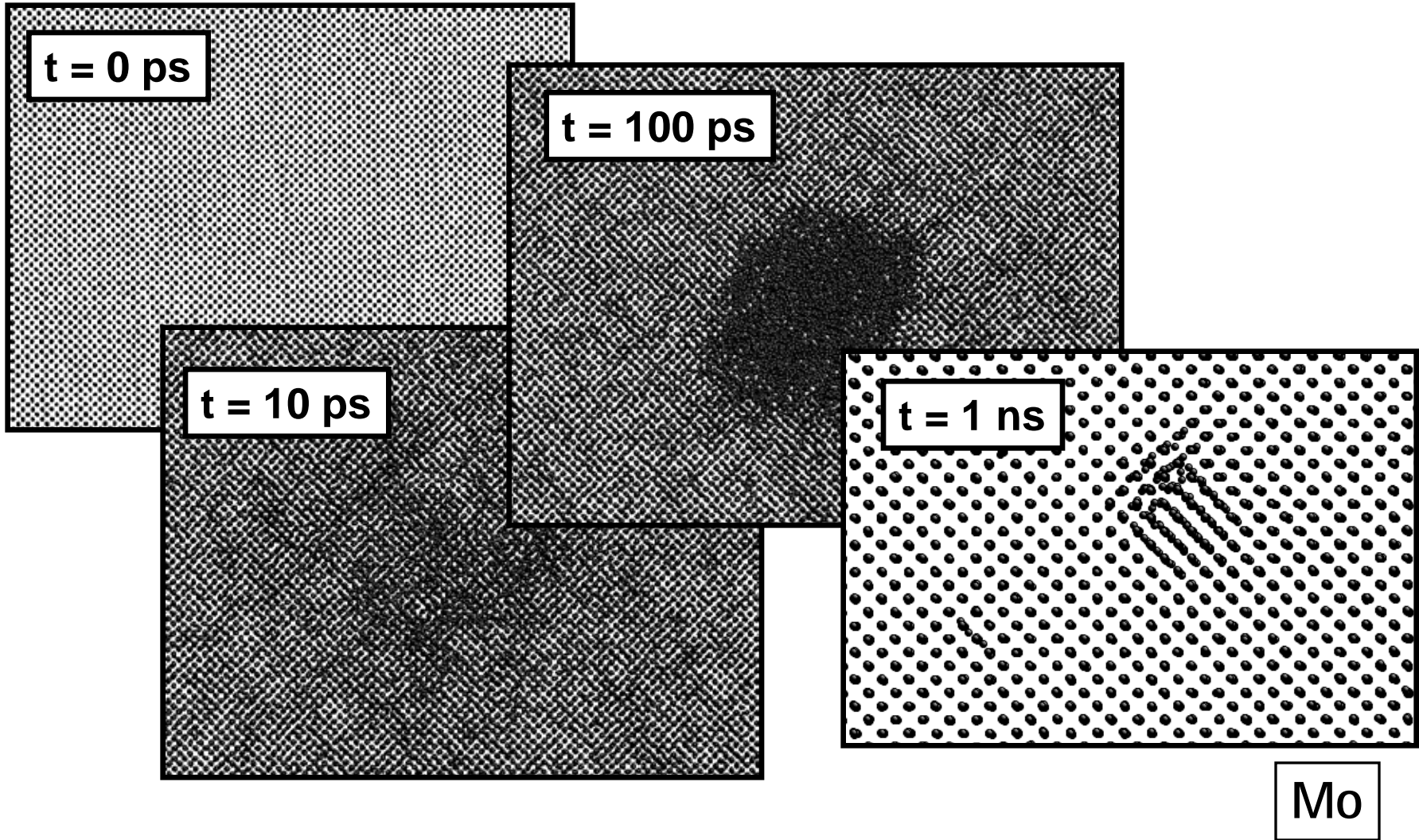
Defect formation at heating/melting of ionic subsystem

$dE/dz = 160 \text{ KeV/nm}$



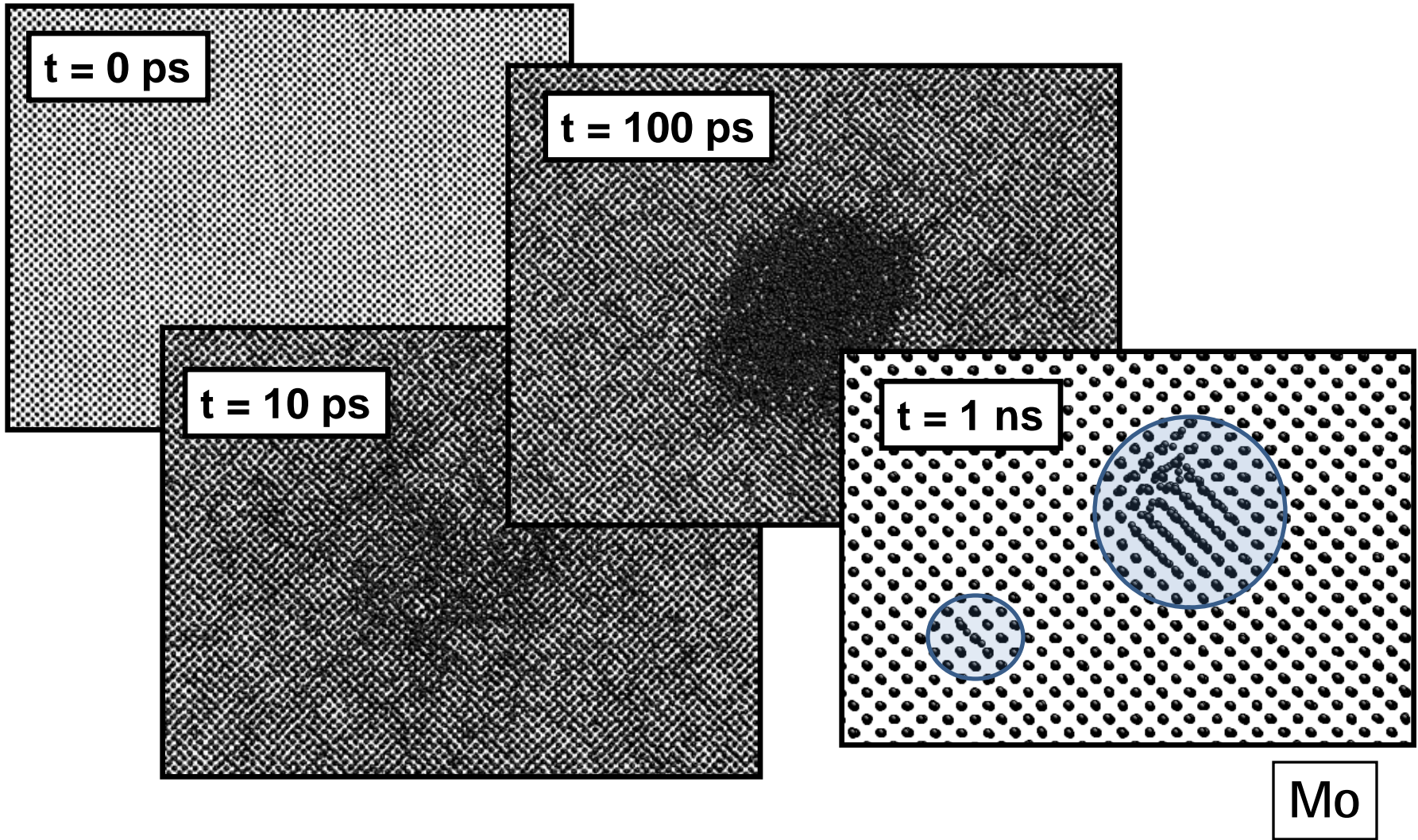
Defect formation at heating/melting of ionic subsystem

$dE/dz = 160 \text{ KeV/nm}$



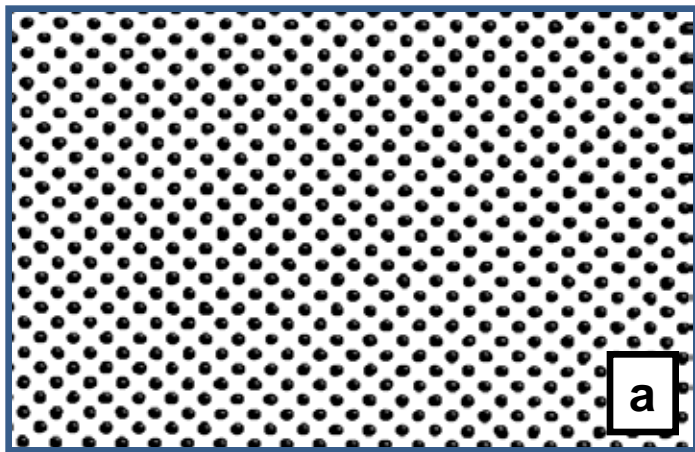
Defect formation at heating/melting of ionic subsystem

$dE/dz = 160 \text{ KeV/nm}$

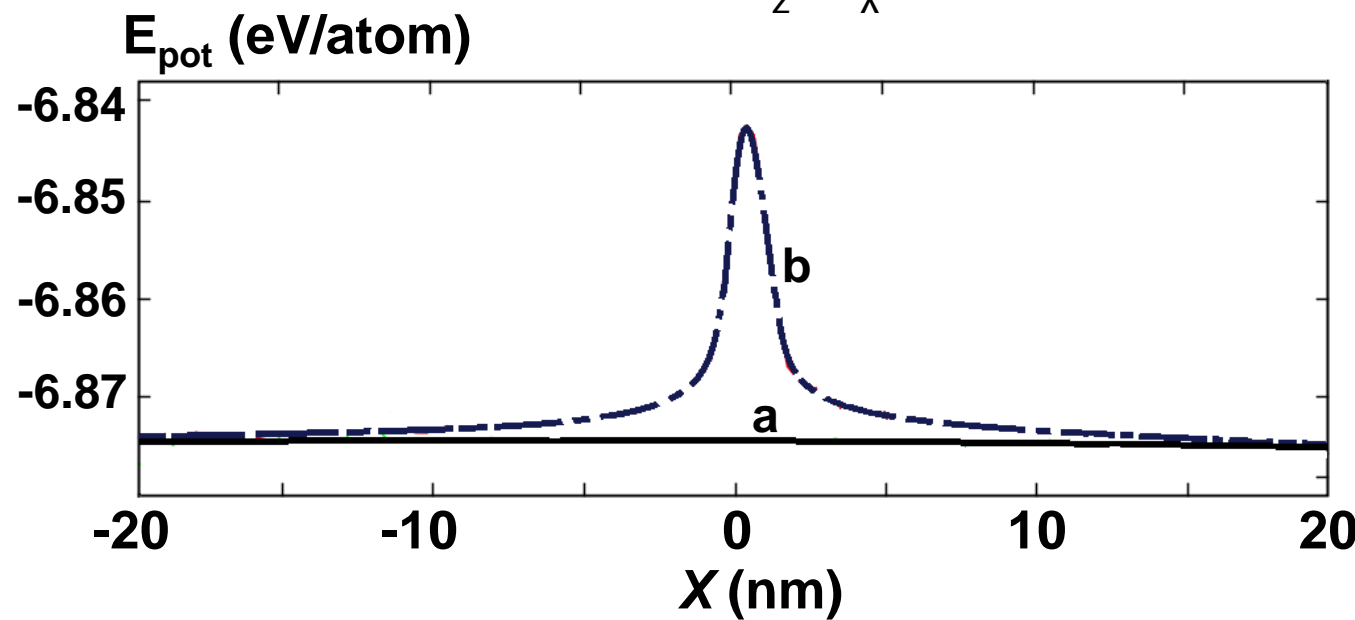
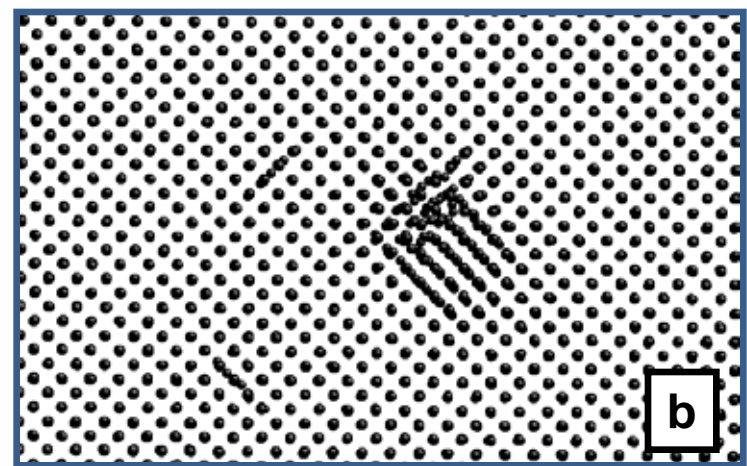


Defect formation at heating/melting of ionic subsystem

$dE/dz = 140 \text{ KeV/nm}$



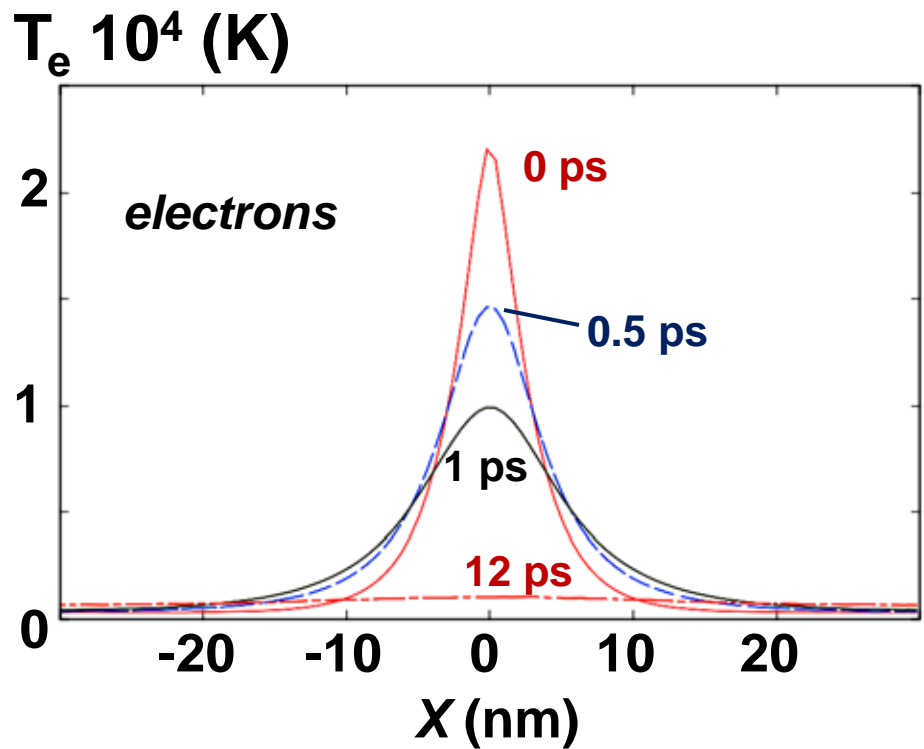
$dE/dz = 160 \text{ KeV/nm}$



Simulation of track formation in **U**

Profiles of electronic and ionic temperatures

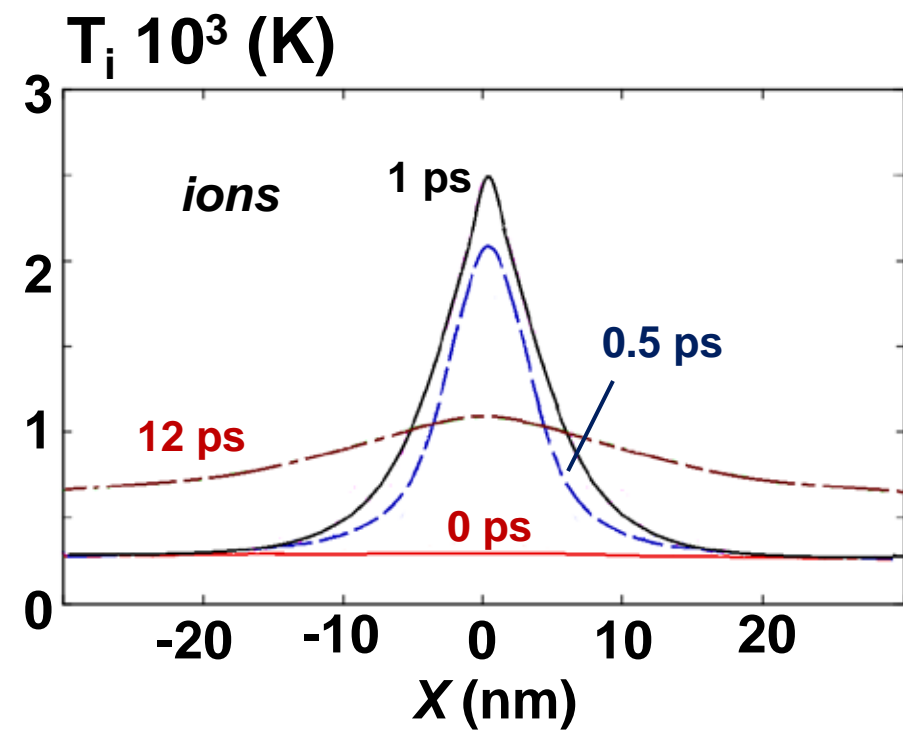
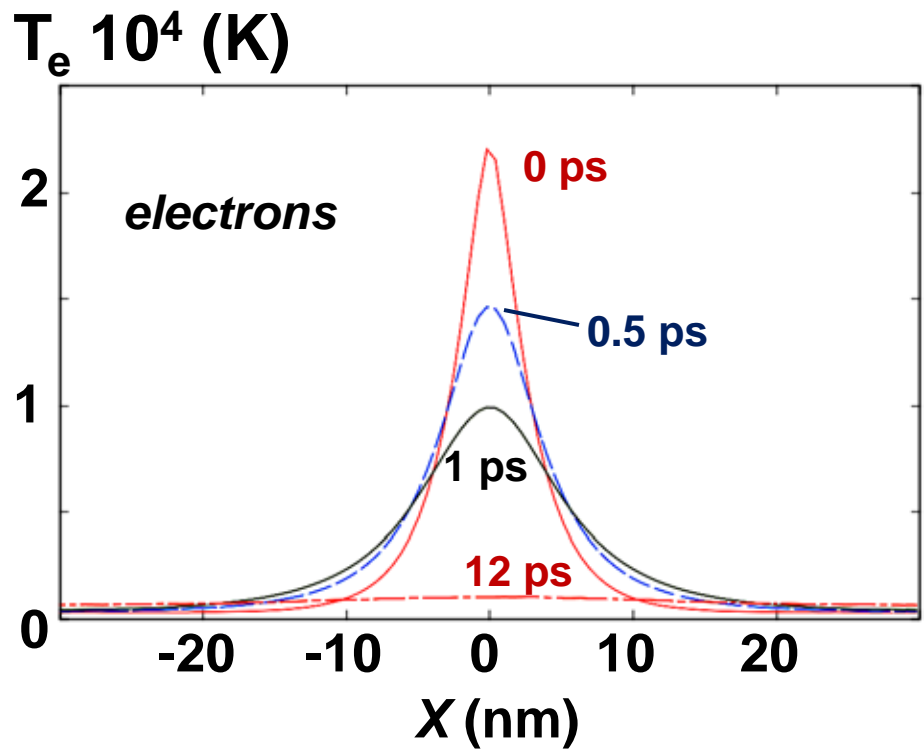
$$dE/dz = 28 \text{ KeV/nm}$$



U

Profiles of electronic and ionic temperatures

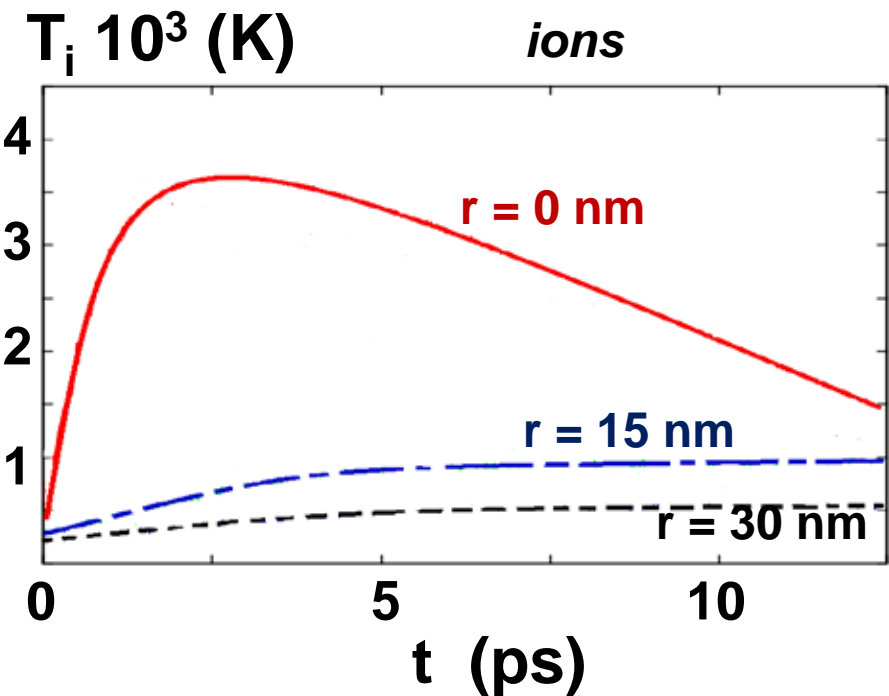
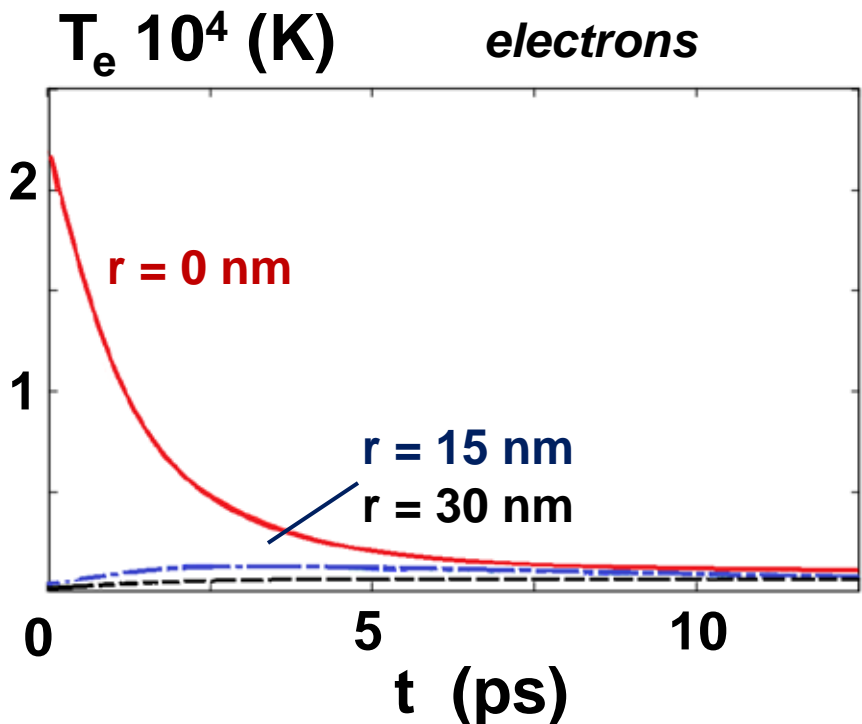
$$dE/dz = 28 \text{ KeV/nm}$$



U

Dependence of temperature on time

$$dE/dz = 28 \text{ KeV/nm}$$

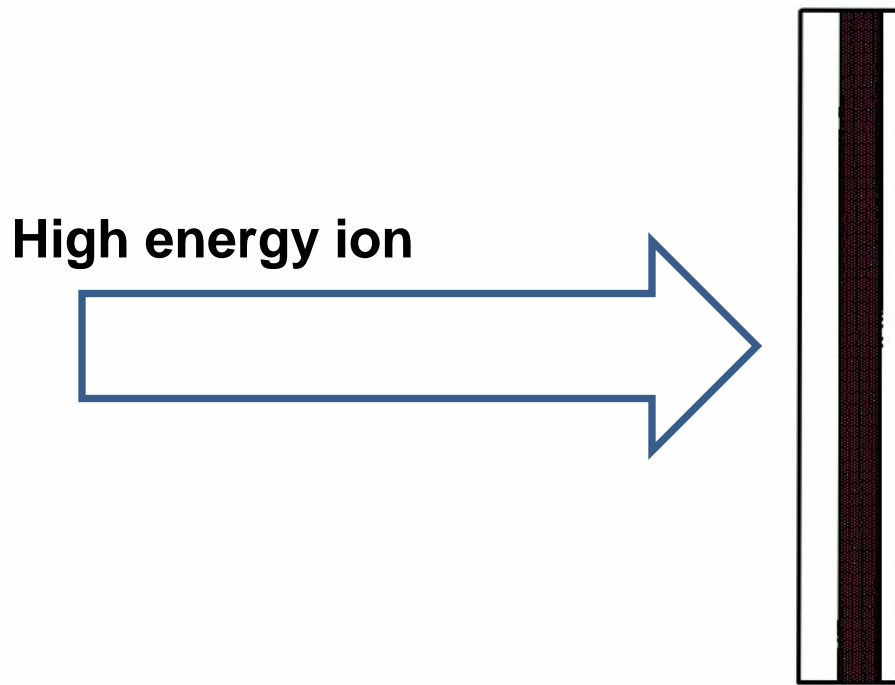


U

Образование дефектов при нагреве/плавлении ионной подсистемы

(атомы раскрашены в соответствии с координационным числом)

$$dE/dz = 28 \text{ KeV/nm}$$



U

Образование дефектов при нагреве/плавлении ионной подсистемы

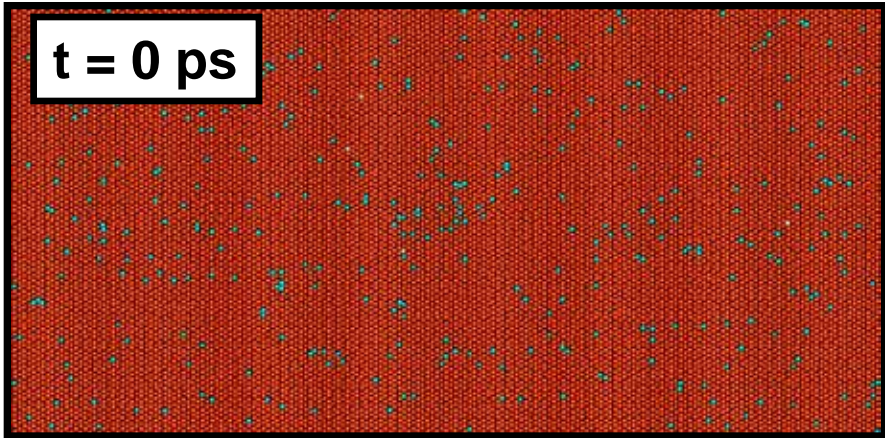
(атомы раскрашены в соответствии с координационным числом)

■ α -U

■ γ -U

$dE/dz = 28 \text{ KeV/nm}$

$t = 0 \text{ ps}$



Образование дефектов при нагреве/плавлении ионной подсистемы

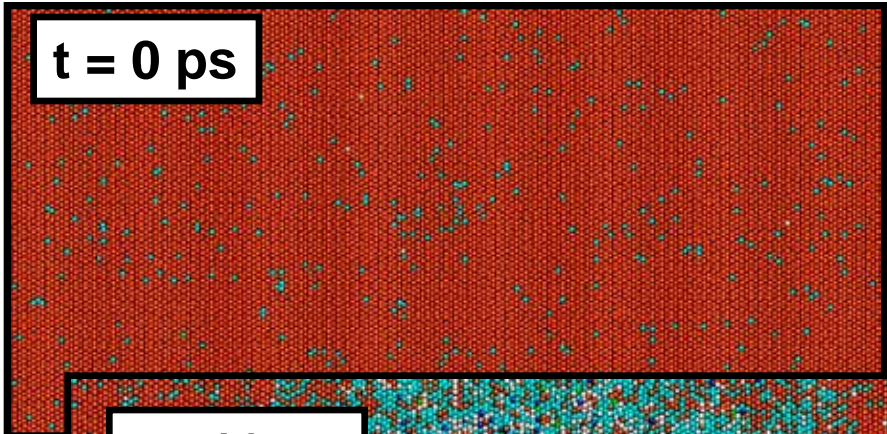
(атомы раскрашены в соответствии с координационным числом)

■ α -U

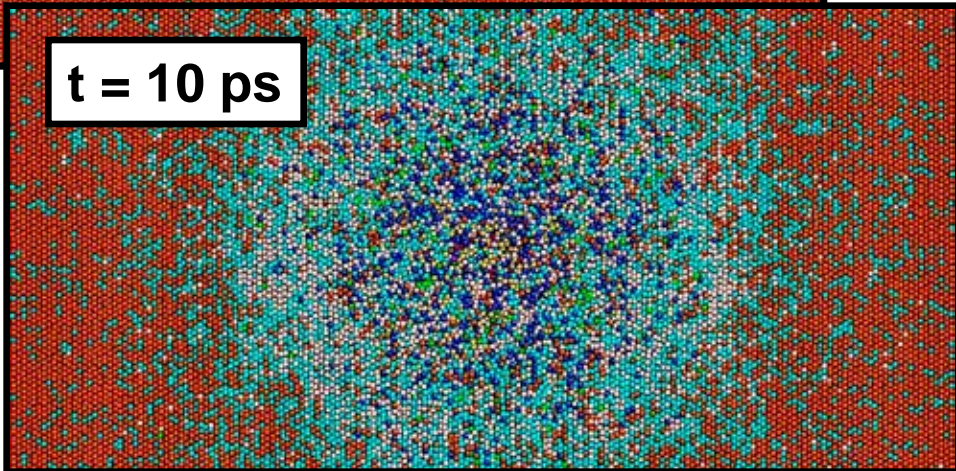
■ γ -U

$dE/dz = 28 \text{ KeV/nm}$

$t = 0 \text{ ps}$



$t = 10 \text{ ps}$



U

Образование дефектов при нагреве/плавлении ионной подсистемы

(атомы раскрашены в соответствии с координационным числом)

■ $\alpha\text{-U}$

■ $\gamma\text{-U}$

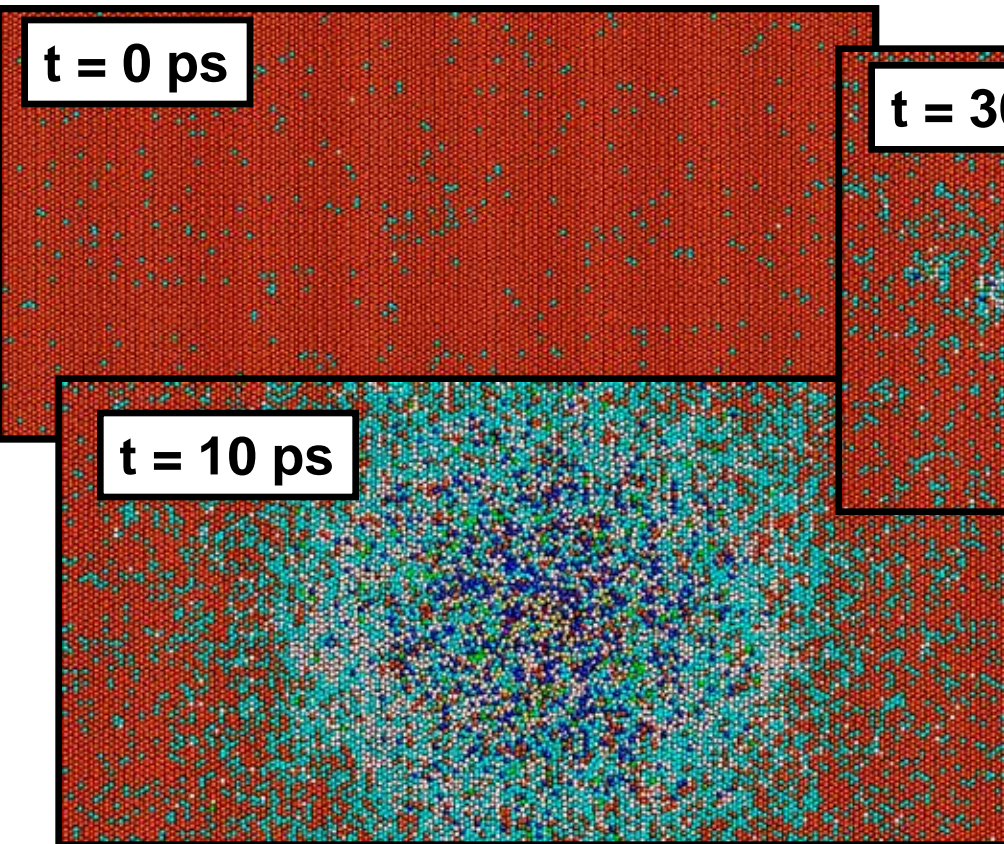
$dE/dz = 28 \text{ KeV/nm}$

$t = 0 \text{ ps}$

$t = 300 \text{ ps}$

$t = 10 \text{ ps}$

U



Образование дефектов при нагреве/плавлении ионной подсистемы

(атомы раскрашены в соответствии с координационным числом)

■ α -U

■ γ -U

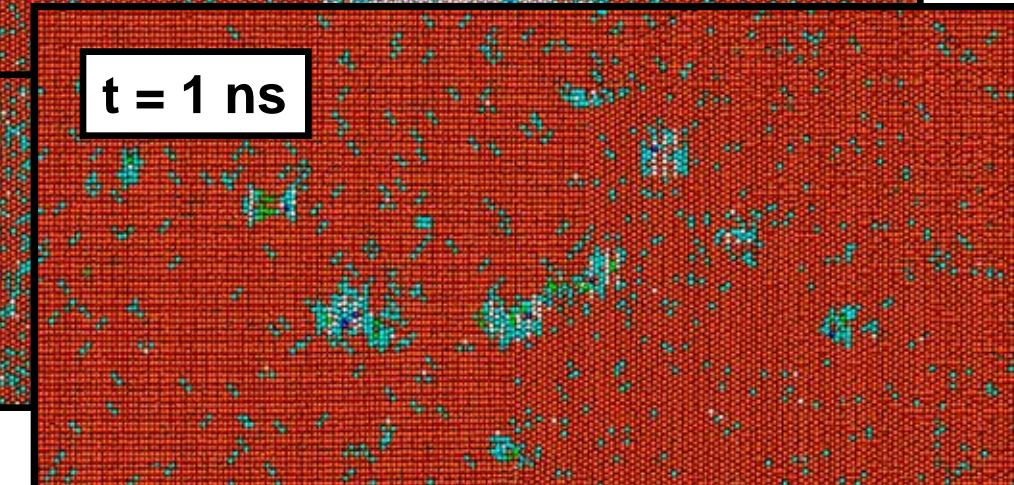
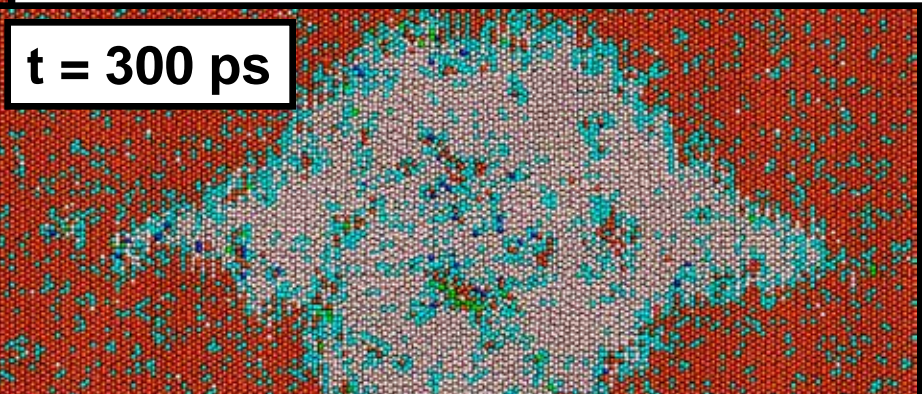
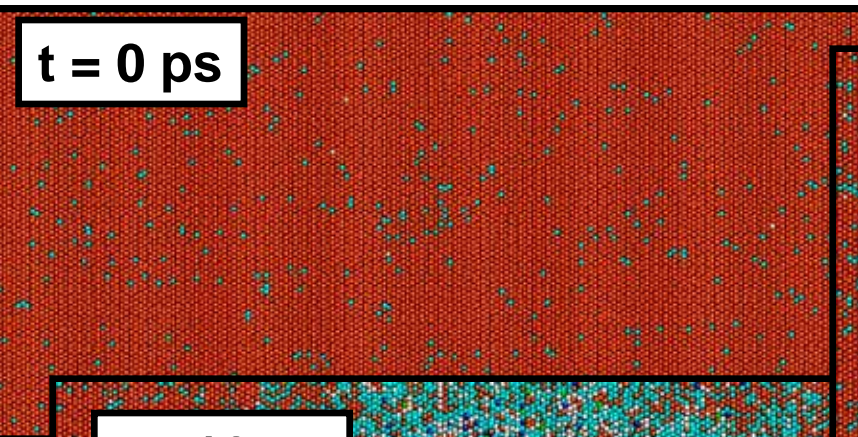
$dE/dz = 28 \text{ KeV/nm}$

$t = 0 \text{ ps}$

$t = 300 \text{ ps}$

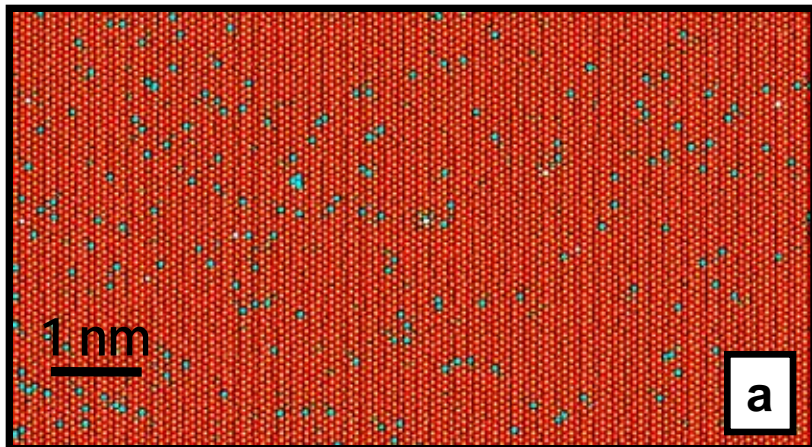
$t = 10 \text{ ps}$

$t = 1 \text{ ns}$

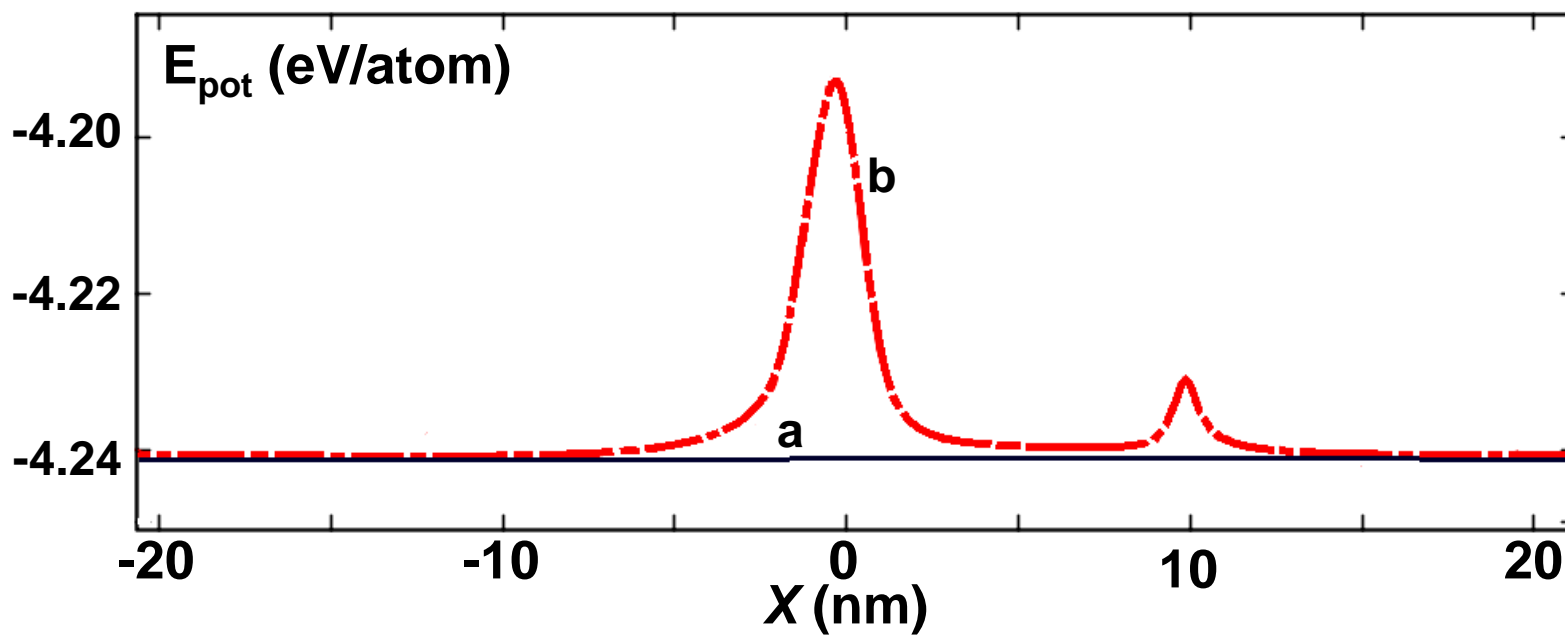
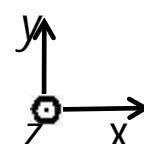
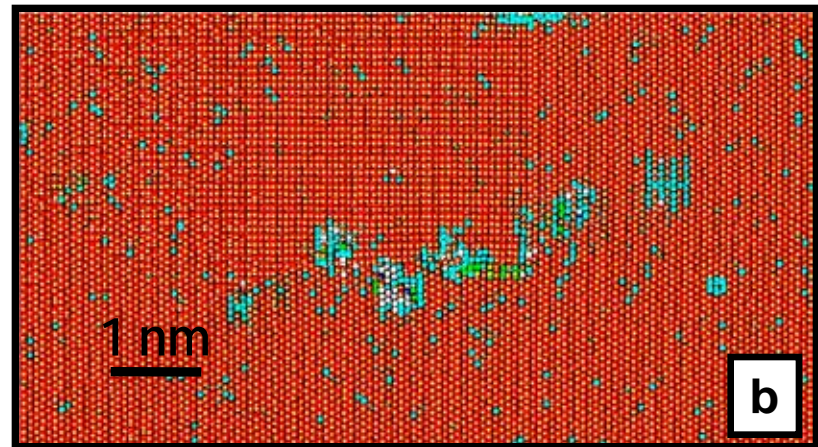


Defect formation at heating/melting of ionic subsystem

$dE/dz = 15 \text{ KeV/nm}$



$dE/dz = 28 \text{ KeV/nm}$

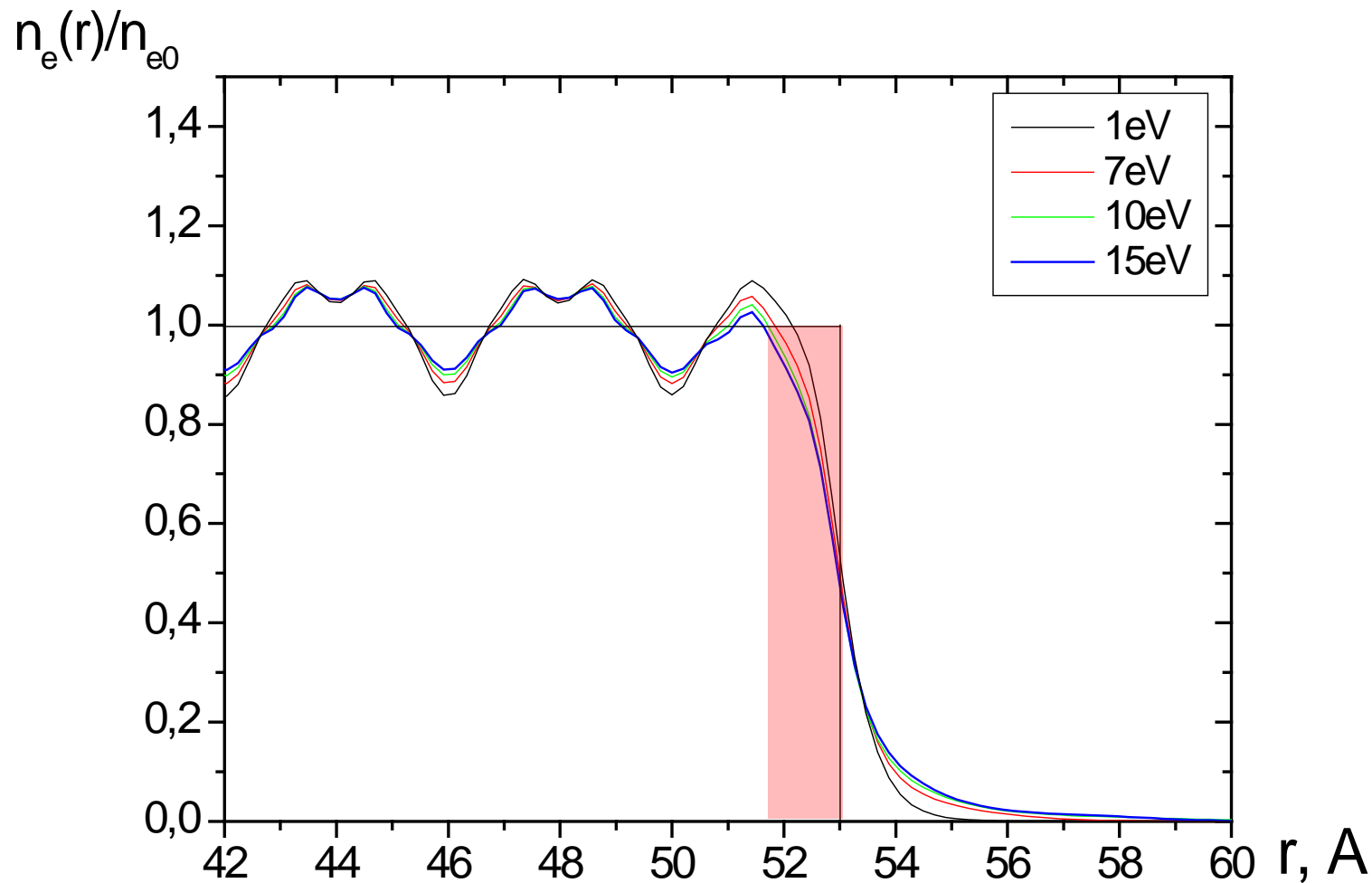


Conclusions

A new approach is developed
to model and simulate
two-temperature warm dense matter
relaxation

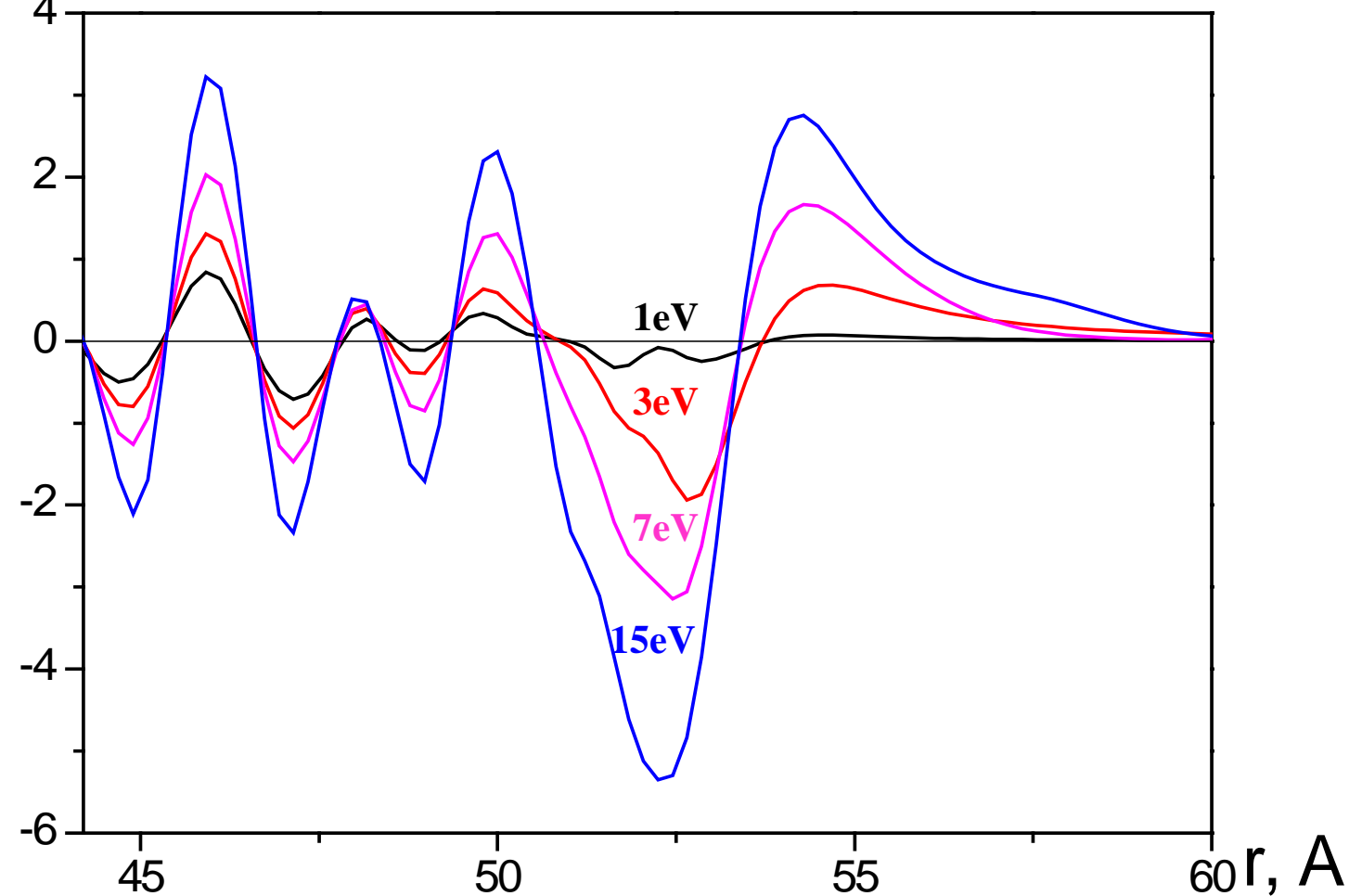
The approach is used to study
some examples of
laser ablation and tracks formation

Distribution of electron density in Aluminium.



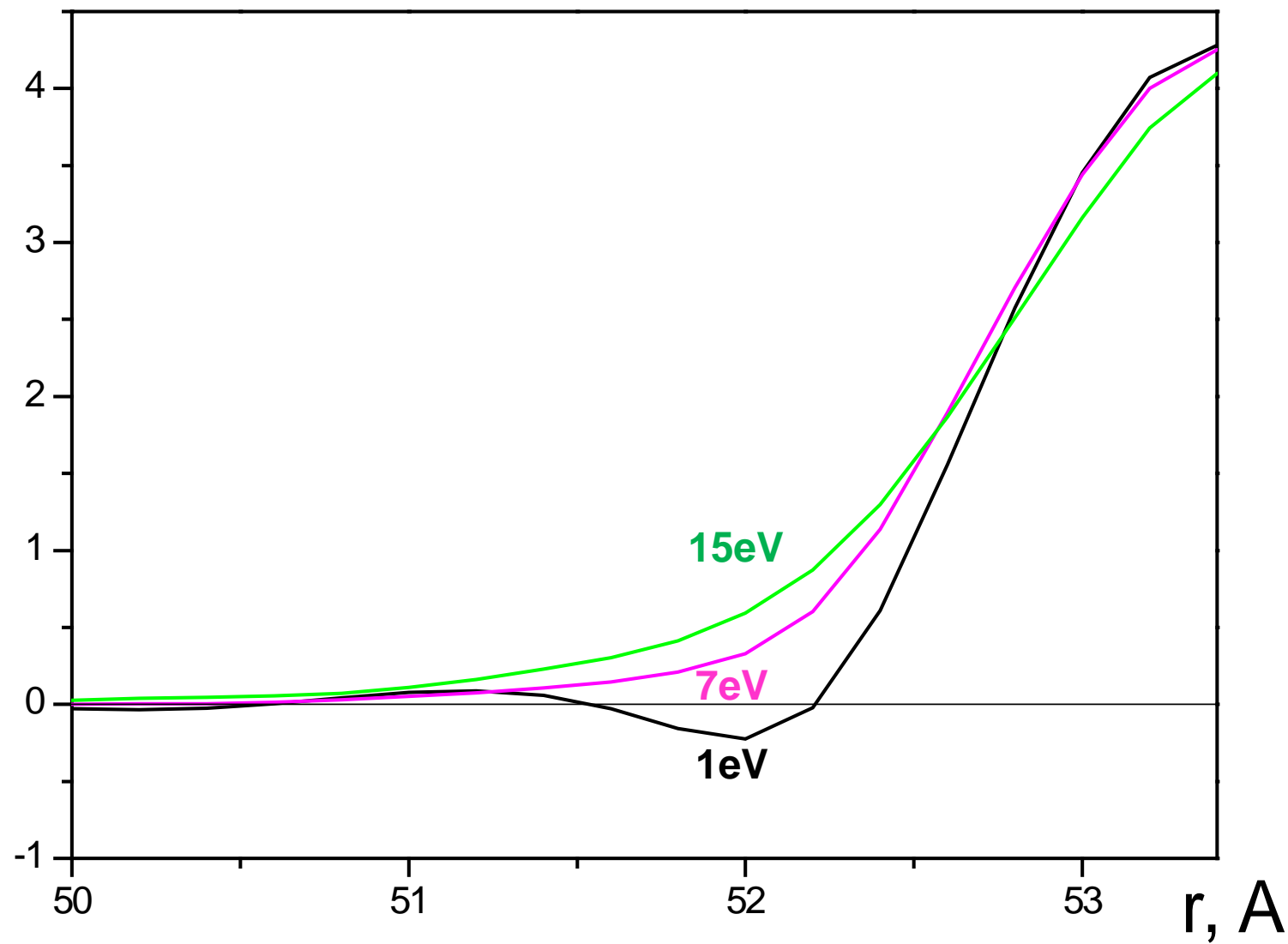
Distribution of electron density in Aluminium.

$$n_e(T) - n_e(0), 10^{21} \text{ cm}^{-3}$$



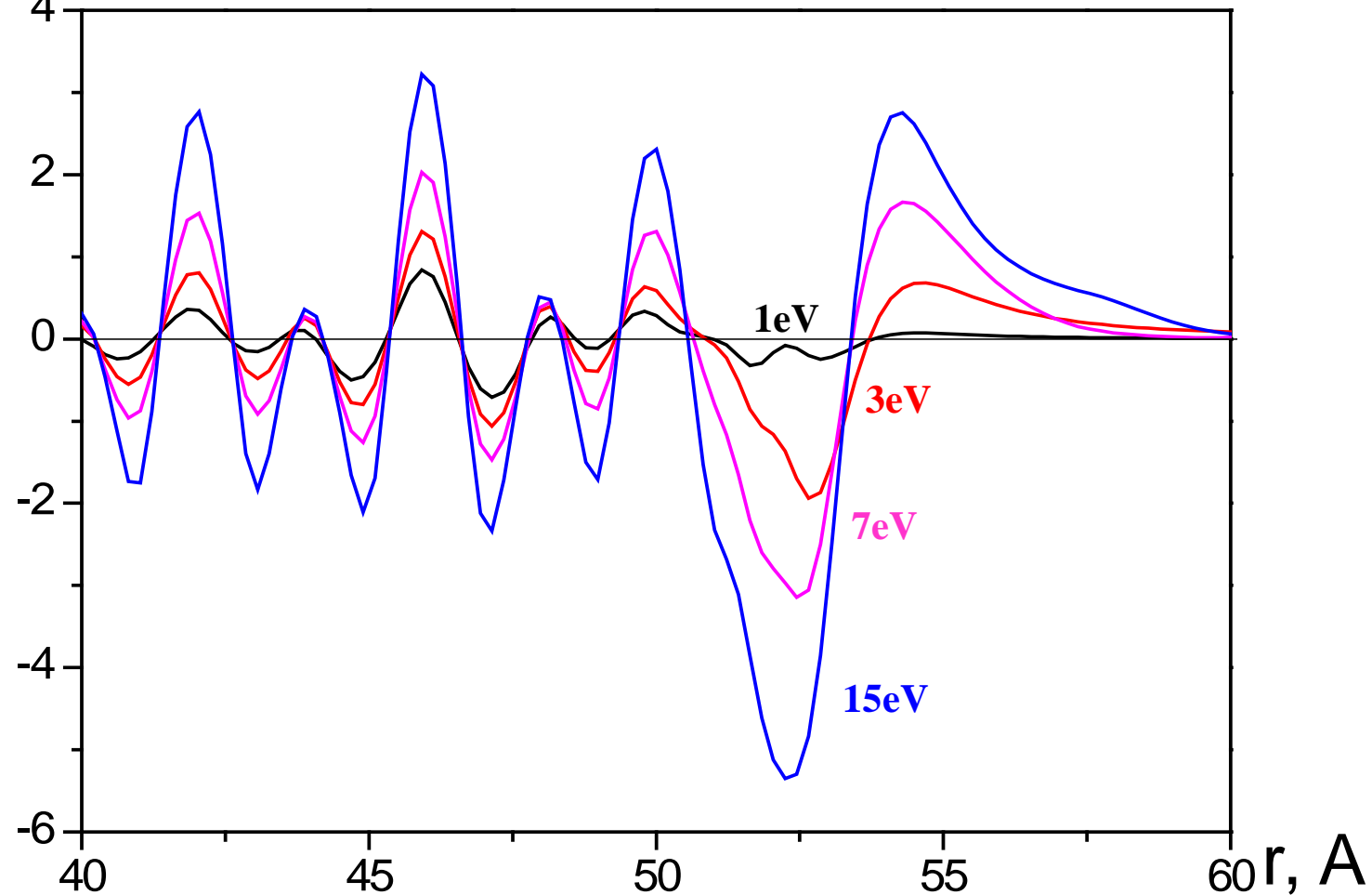
Distribution of electron density in Aluminium.

$$n_e^{\text{bulk}} - n_e^{\text{surface}}, 10^{22} \text{ cm}^{-3}$$

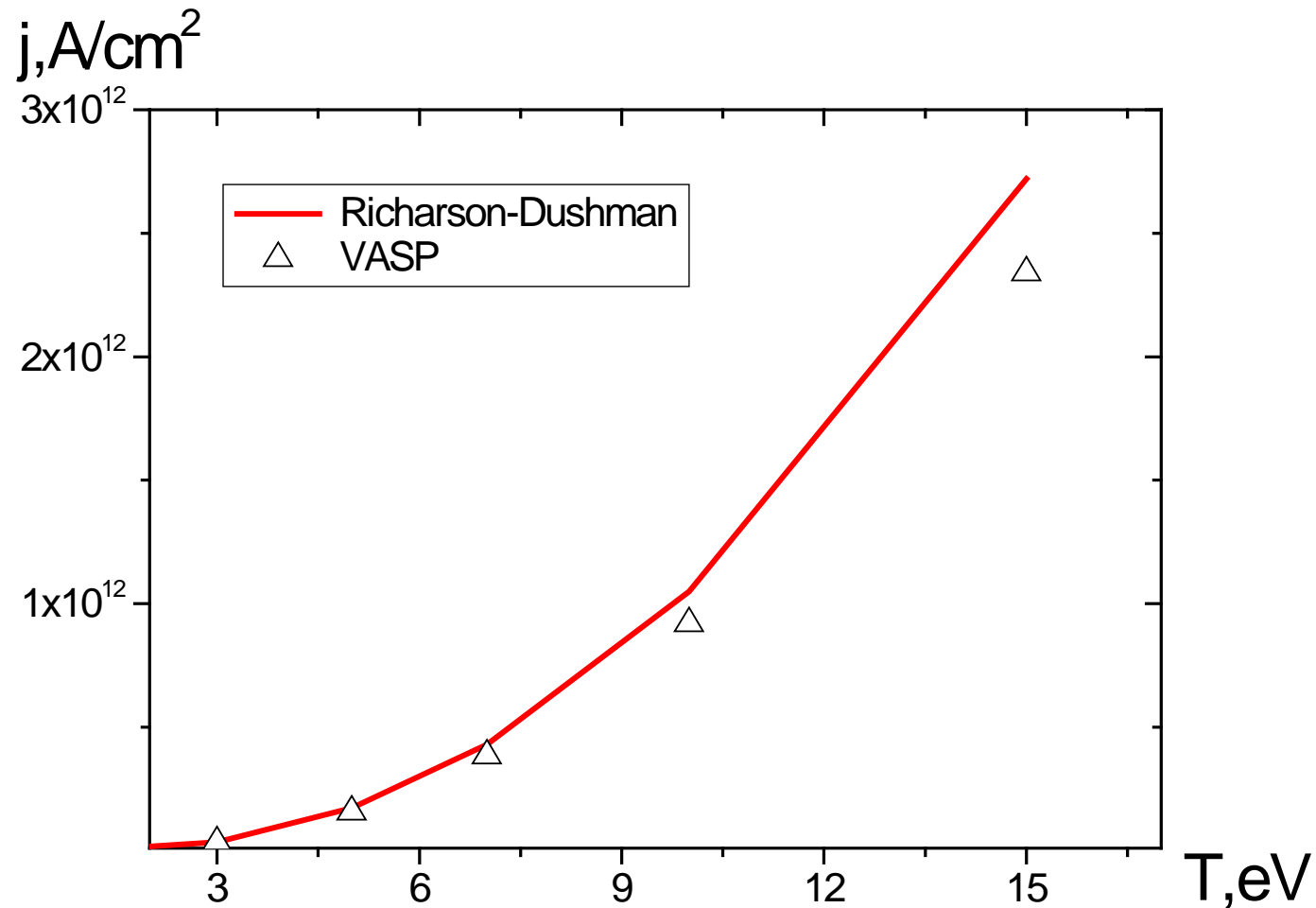


Distribution of electron density in Aluminium.

$$n_e(T) - n_e(0), 10^{21} \text{ cm}^{-3}$$



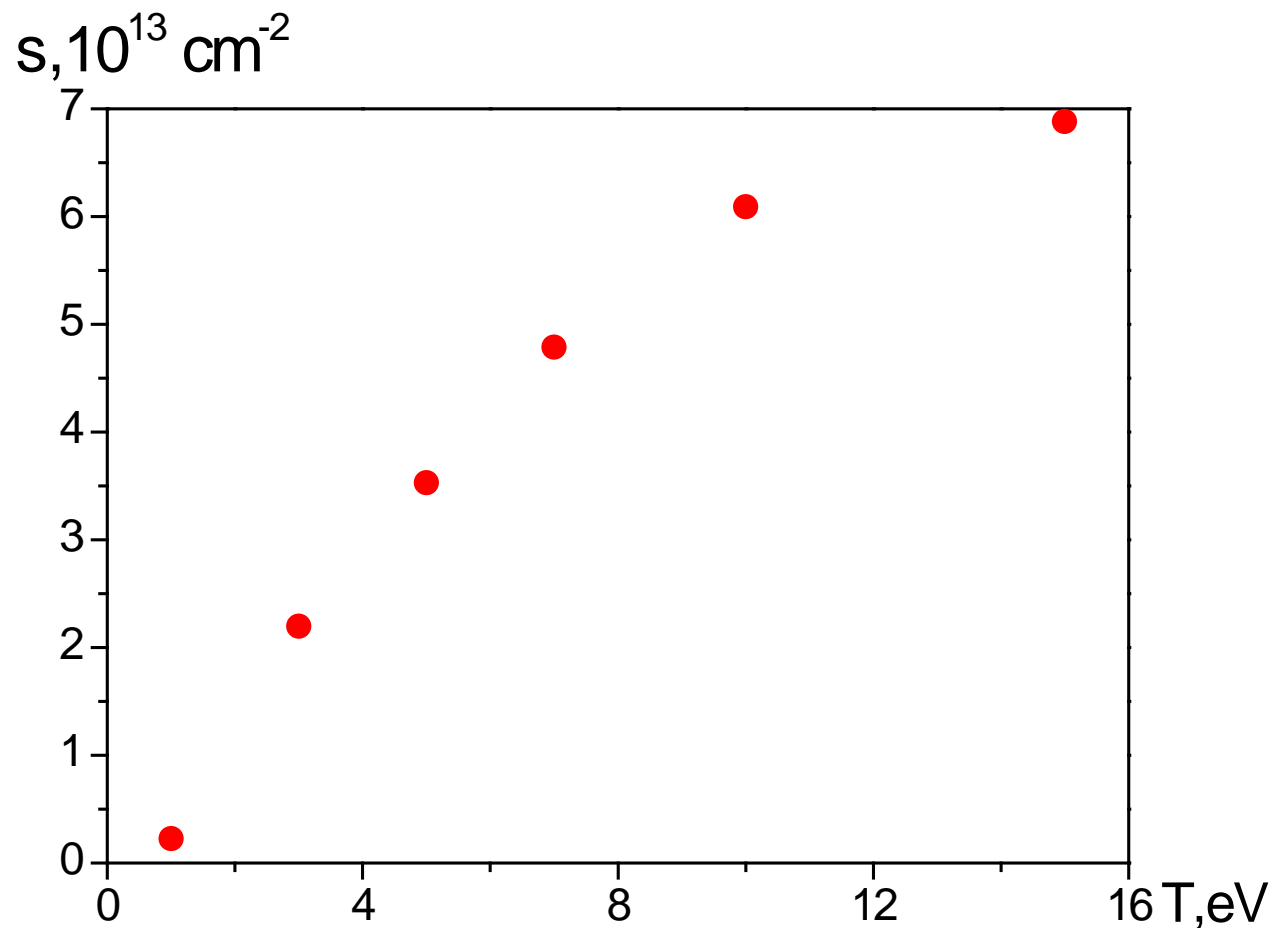
Density of current of thermal emission in Aluminium.



$$j = \frac{4\pi me}{h^3} \int_{\varepsilon_F+A}^{\infty} \frac{[\varepsilon - (\varepsilon_F + A)]}{1 + \exp((\varepsilon - \varepsilon_F)/kT)} d\varepsilon$$

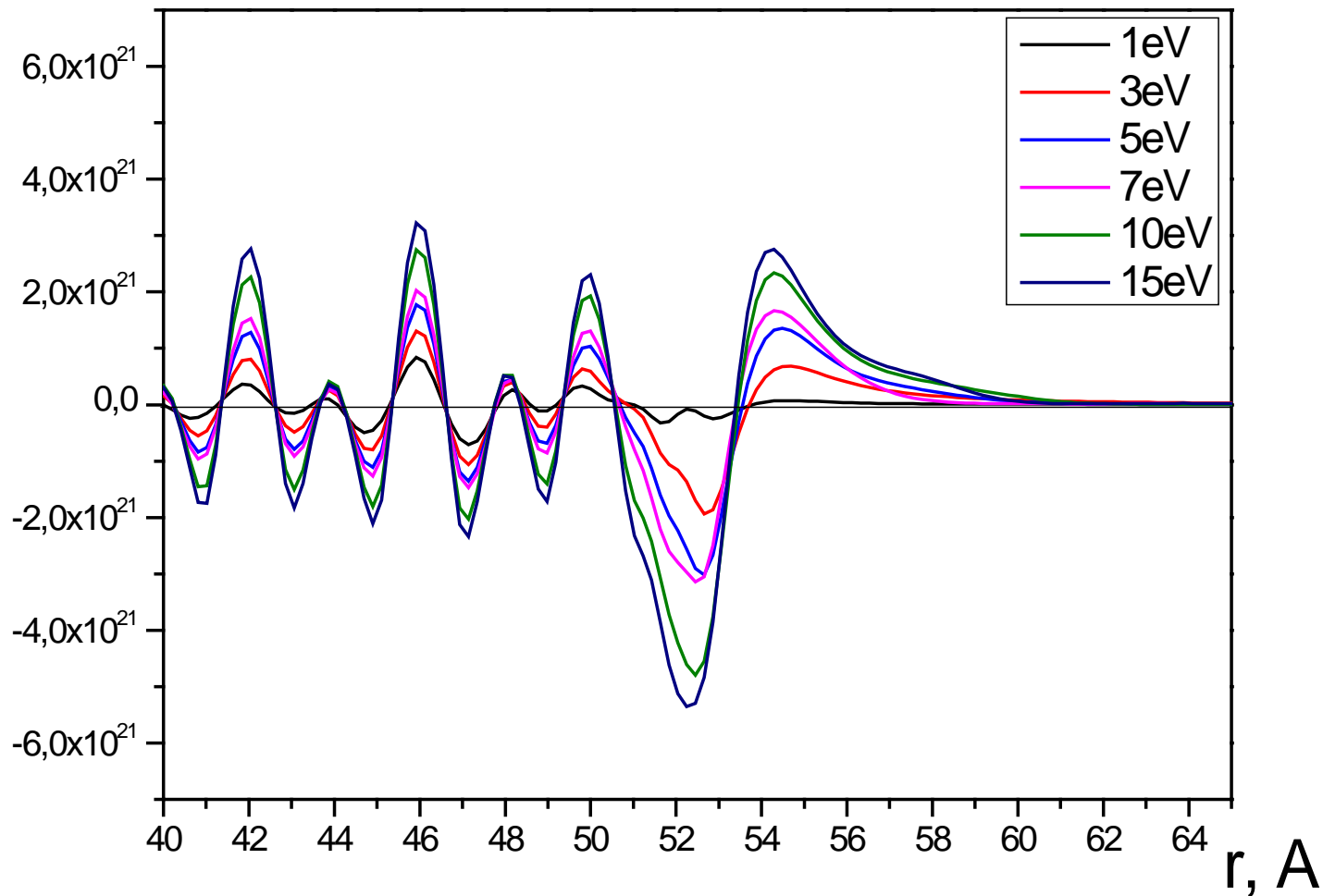
$$j_{R-D} = \frac{4\pi me}{h^3} (kT)^2 \exp\left(-\frac{A}{kT}\right)$$

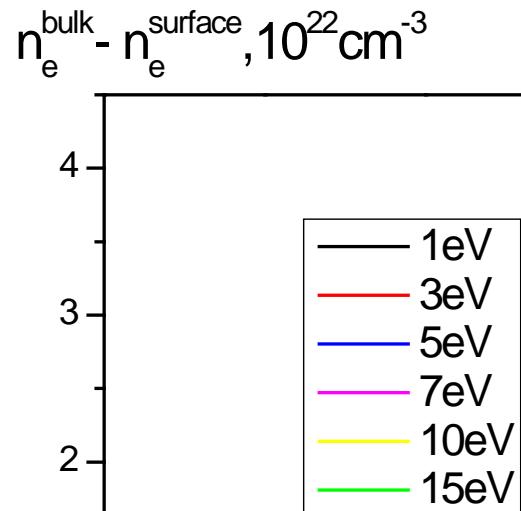
Surface density of uncompensated positive charge.



Distribution of electron density in Aluminium.

$$n_e(T) - n_e(0), \text{ cm}^{-3}$$





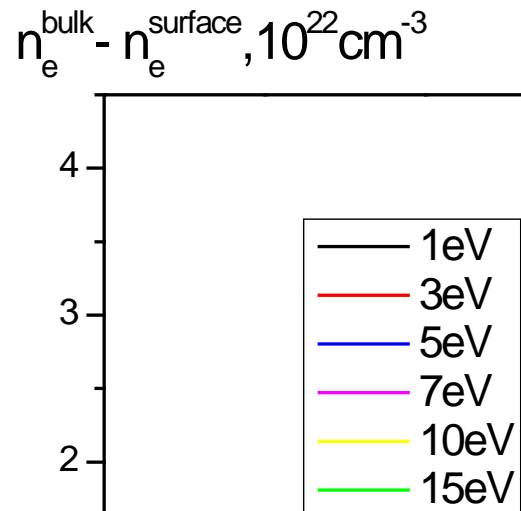
50

51

52

53

 $r, \text{\AA}$



50

51

52

53

 $r, \text{\AA}$

Properties of electronic subsystem

Electronic subsystem:

$$C_e(T_e) \cdot \rho_e \cdot \frac{\partial T_e}{\partial t} = \nabla(K_e(T_e) \cdot \nabla T_e) - g_p(T_e - T_i) + \nabla Q$$

$$T_e \gg T_i$$

Necessary

$$C_e(T_e)$$

$$K_e(T_e)$$

$$g_p(T_e - T_i)$$

?

Electronic subsystem:

$$C_e(T_e) \cdot \rho_e \cdot \frac{\partial T_e}{\partial t} = \nabla(K_e(T_e) \cdot \nabla T_e) - g_p(T_e - T_i) + \nabla Q$$

$$T_e \gg T_i$$

Necessary

$$C_e(T_e)$$

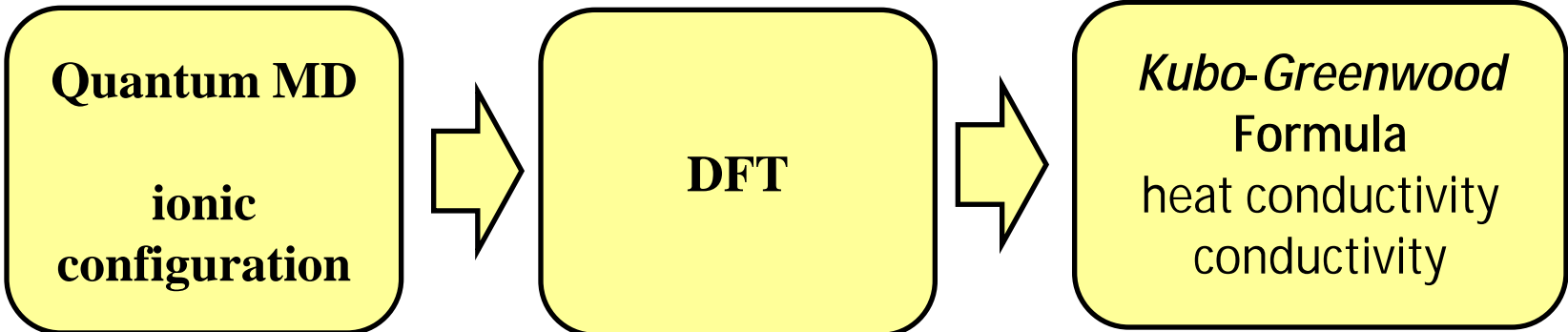
$$K_e(T_e)$$

$$g_p(T_e - T_i)$$

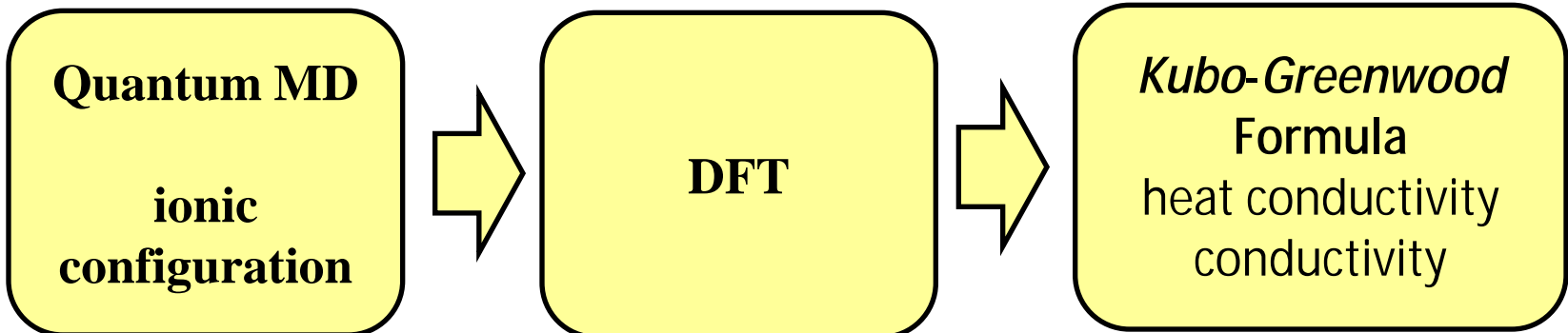


DFT calculation

Calculation of electron heat conductivity



Calculation of electron heat conductivity



Kubo-Greenwood Formula

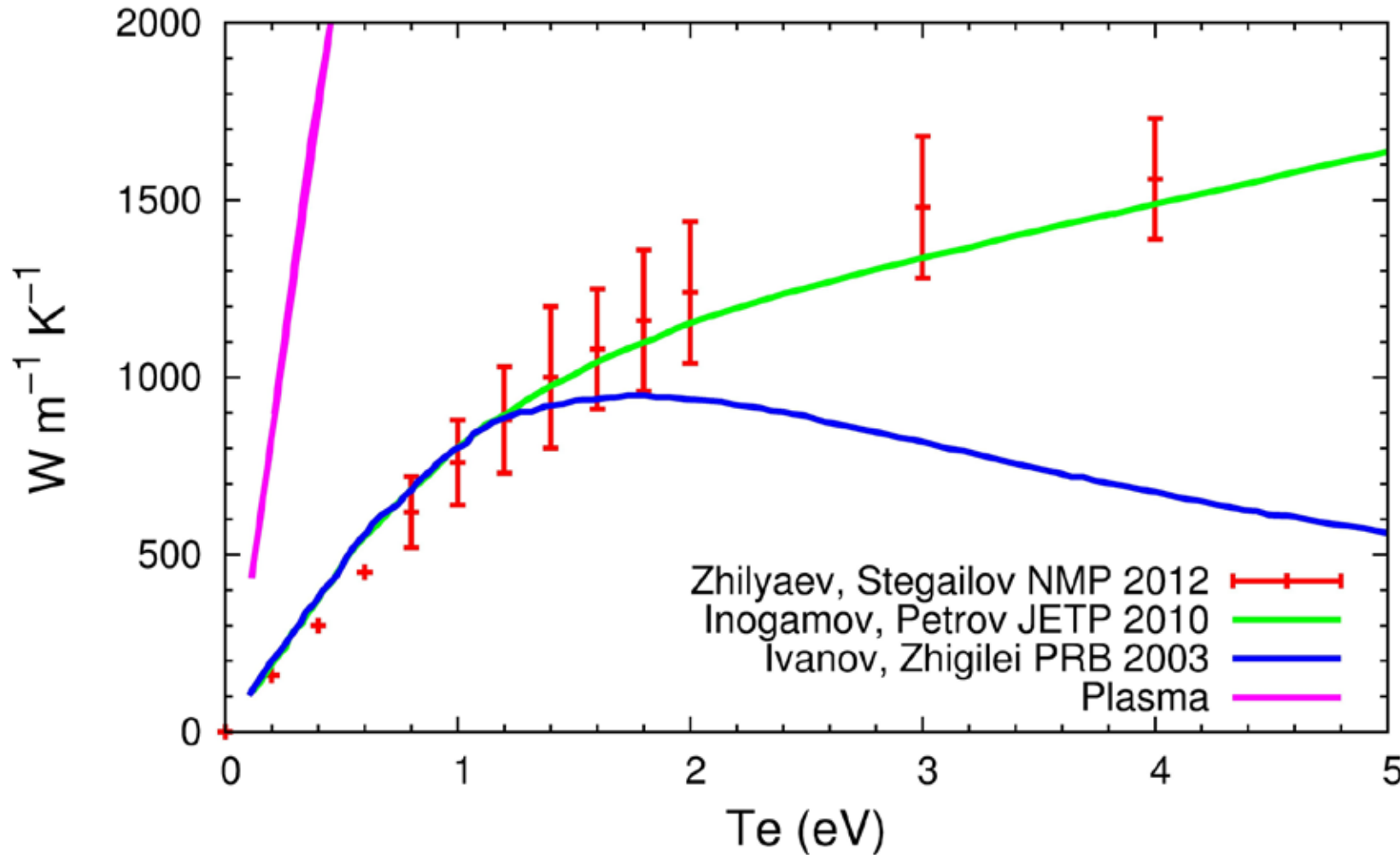
$$\mathcal{L}_{ij} = (-1)^{(i+j)} \frac{he^2}{\Omega} \lim_{\varepsilon \rightarrow 0} \frac{f(\varepsilon'_k) - f(\varepsilon_k)}{\varepsilon} \delta(\varepsilon'_k - \varepsilon_k - \varepsilon) \times \sum_{k', k} \langle \psi_k | \hat{v} | \psi_{k'} \rangle \langle \psi_{k'} | \hat{v} | \psi_k \rangle (\varepsilon'_k - \mu)^{i-1} (\varepsilon_k - \mu)^{j-1}$$

$$K = \frac{1}{eT} \left(\mathcal{L}_{22} - \frac{\mathcal{L}_{12}^2}{\mathcal{L}_{22}} \right); K(\mathbf{0}) = \lim_{\omega \rightarrow 0} K(\omega) \quad \textit{Static heat conductivity}$$

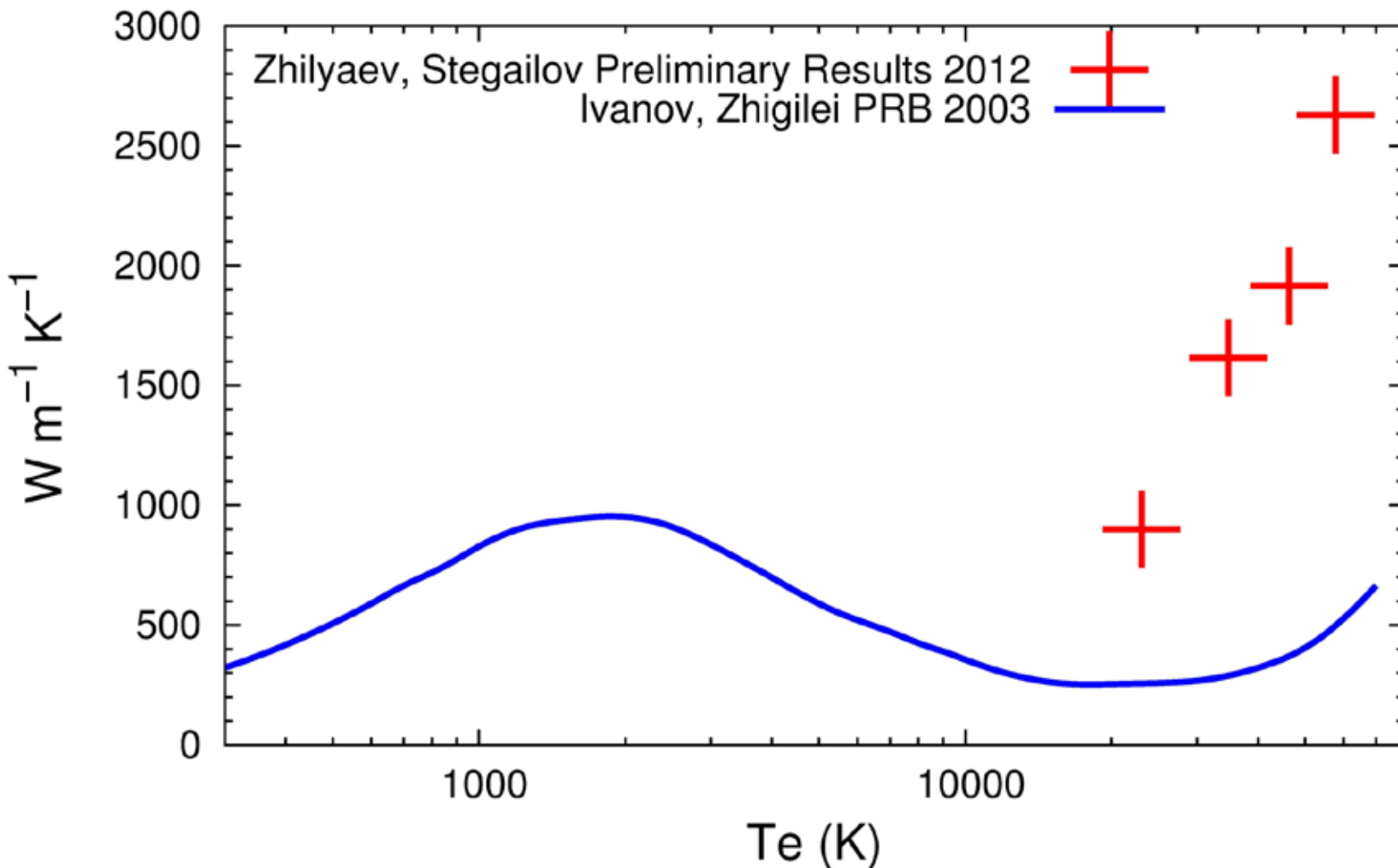
$$\sigma = \mathcal{L}_{11}; \sigma(\mathbf{0}) = \lim_{\omega \rightarrow 0} \sigma(\omega)$$

Static conductivity

Electron heat conductivity of liquid aluminum in two-temperature state

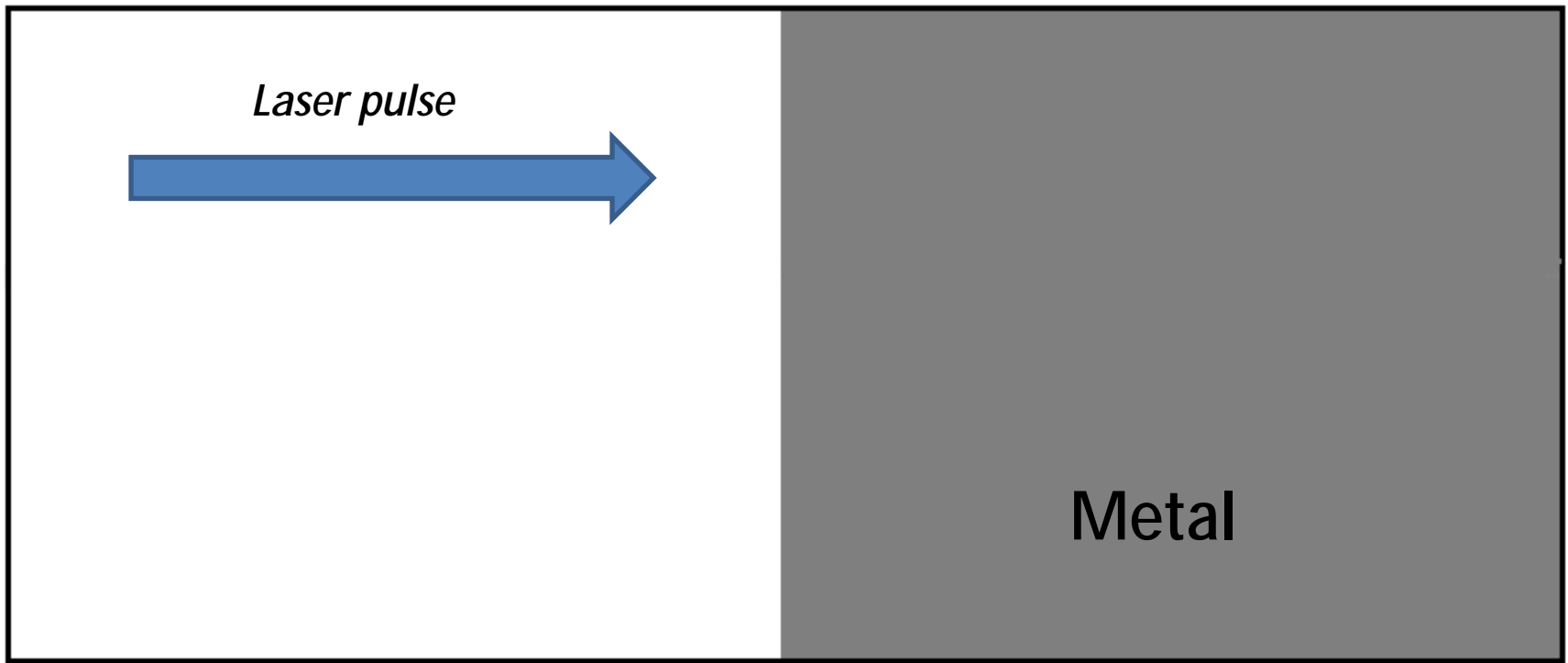


Electron heat conductivity of solid gold in two-temperature state

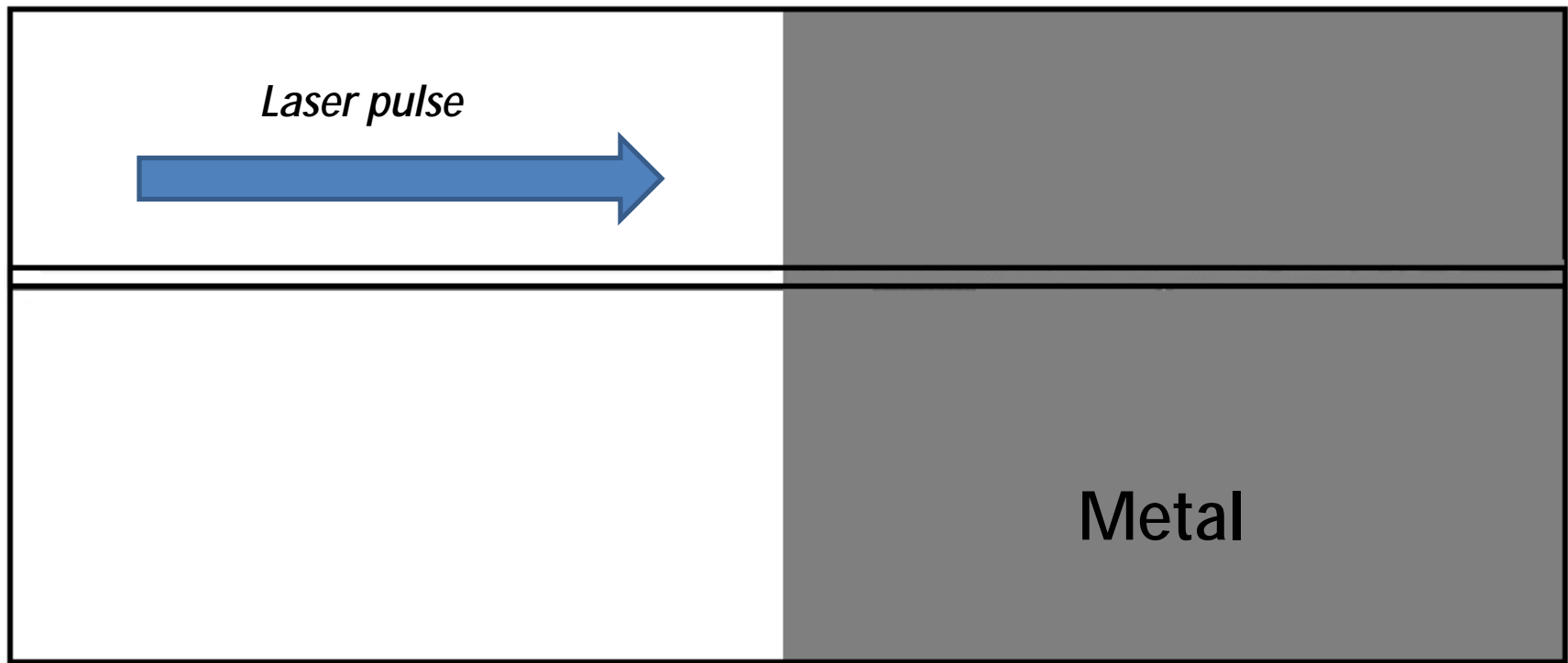


Laser ablation of gold

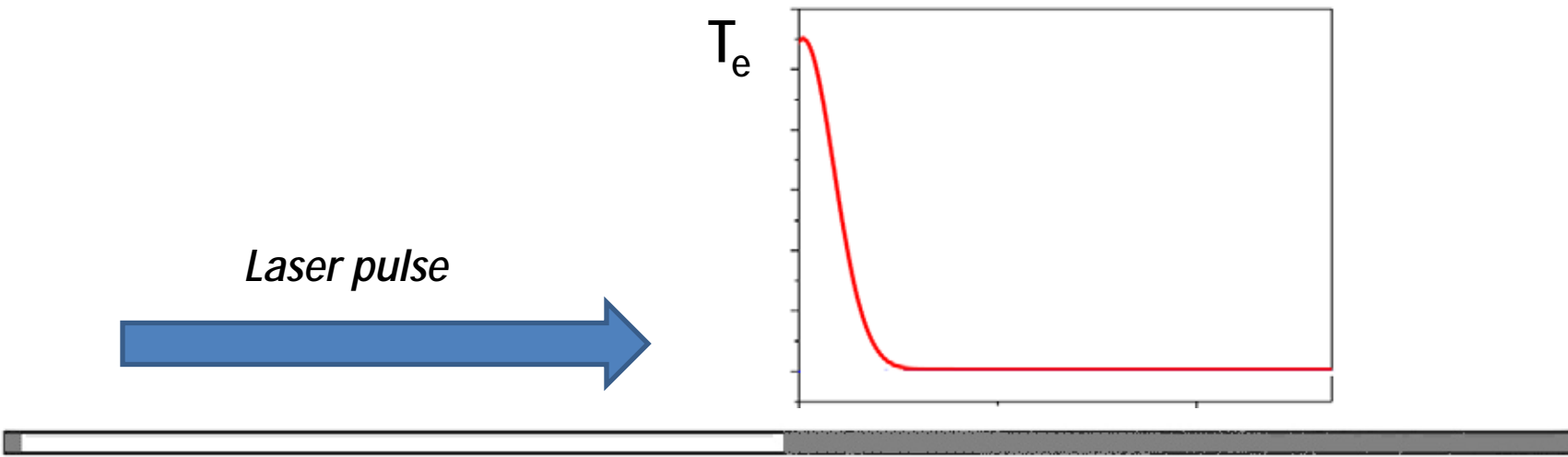
Ion structure in simulation box



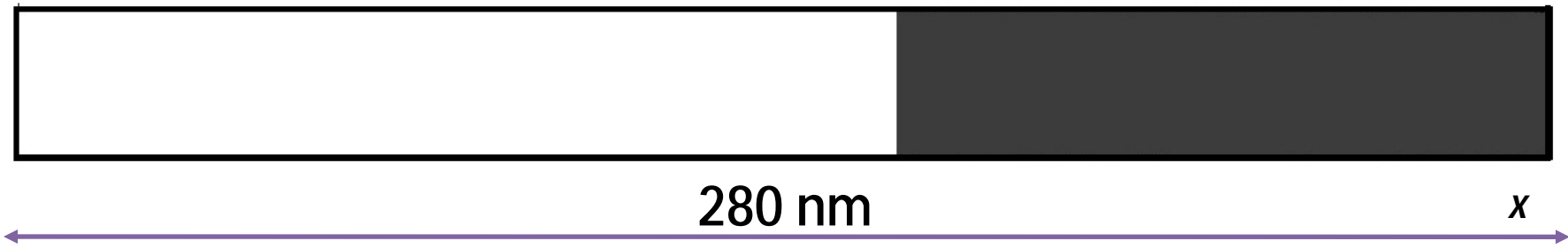
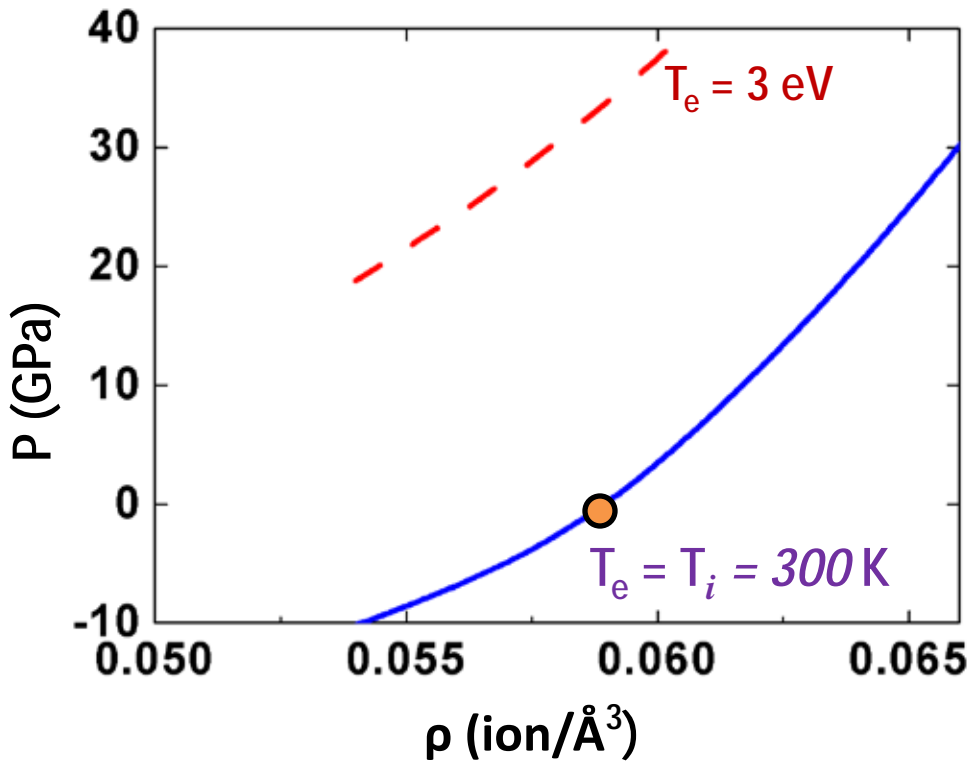
Ion structure in simulation box



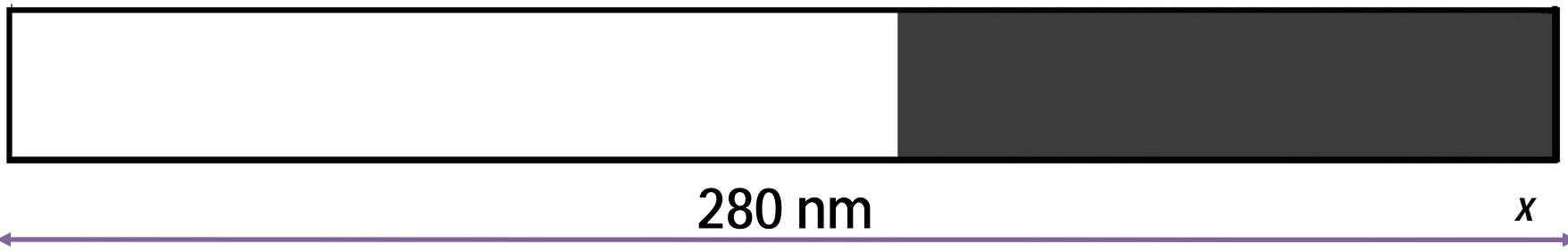
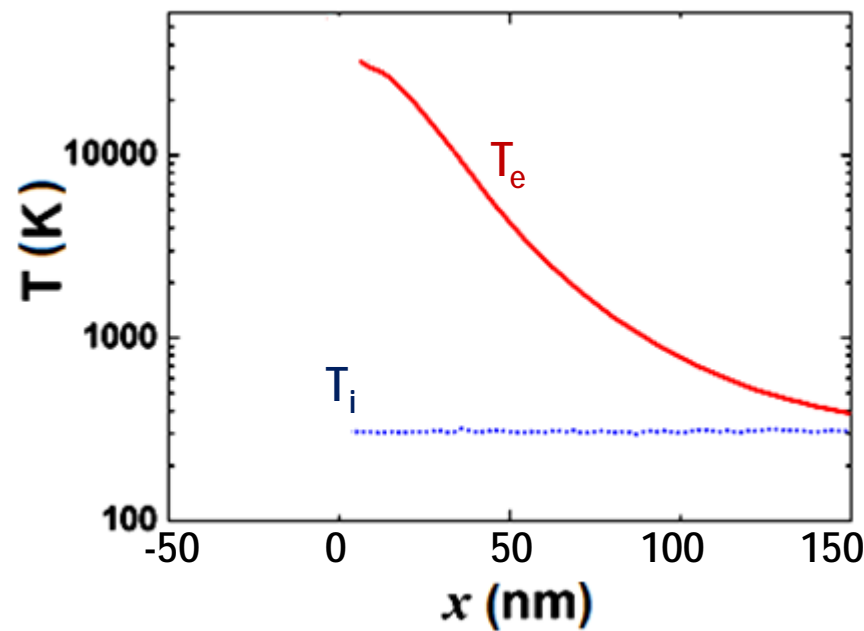
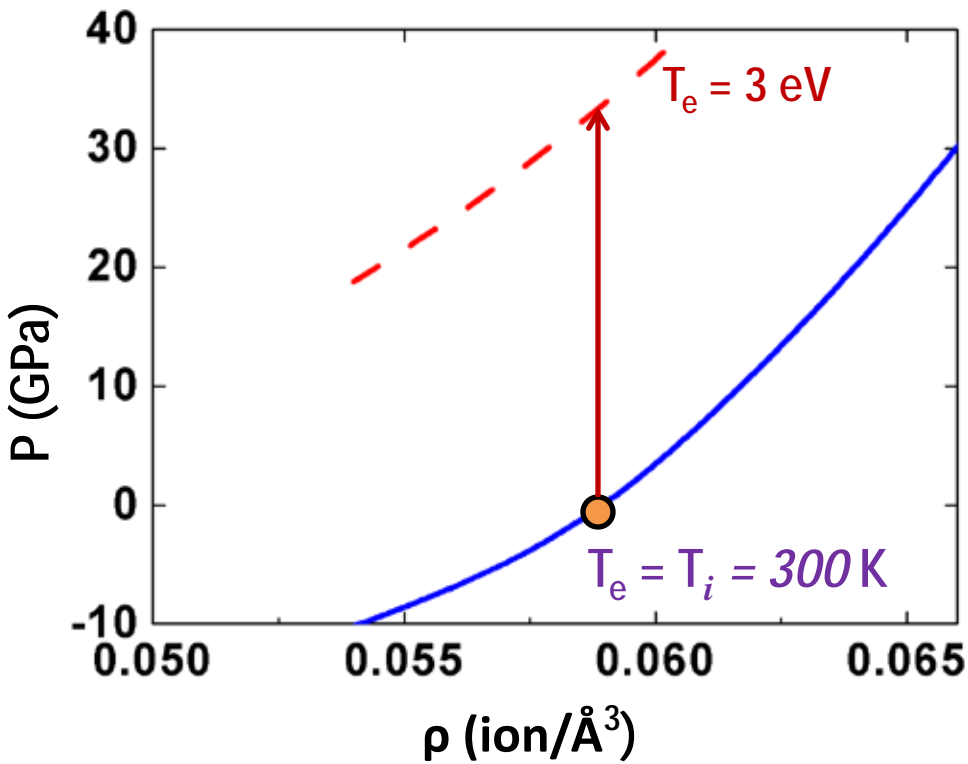
Ion structure in simulation box



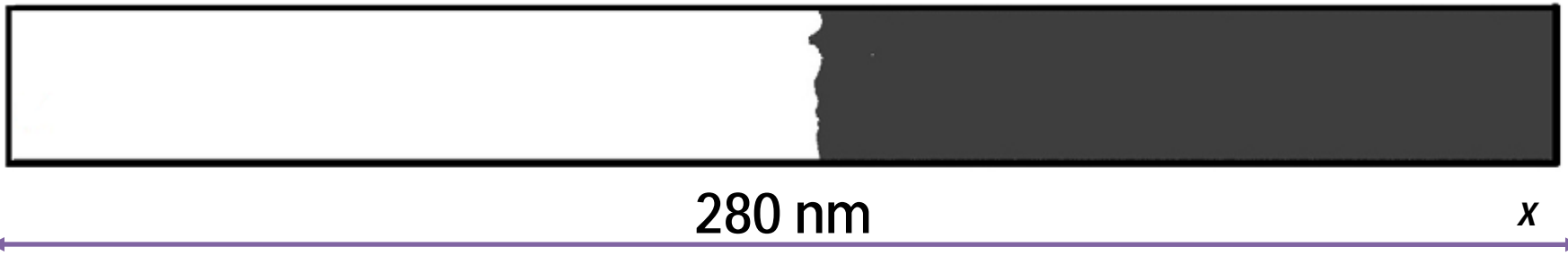
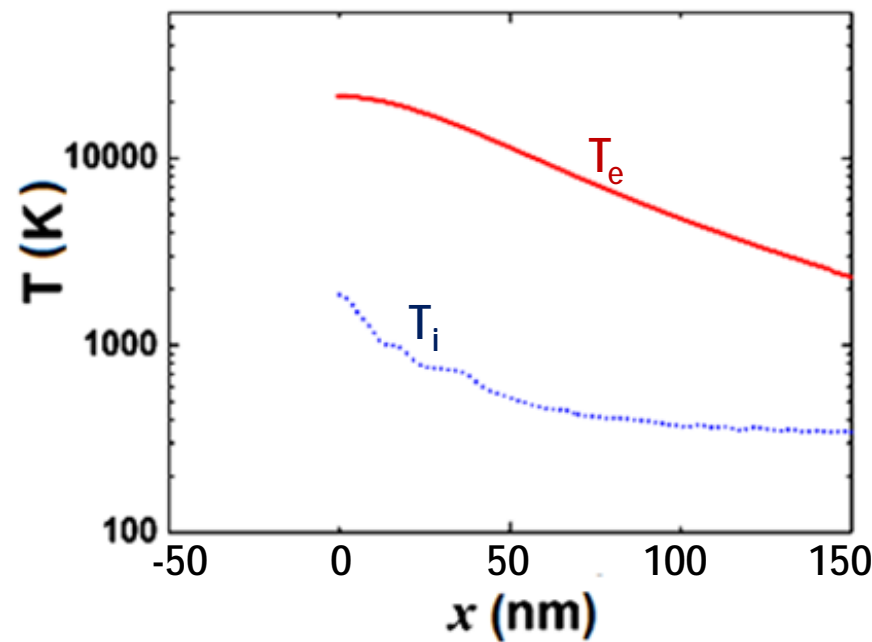
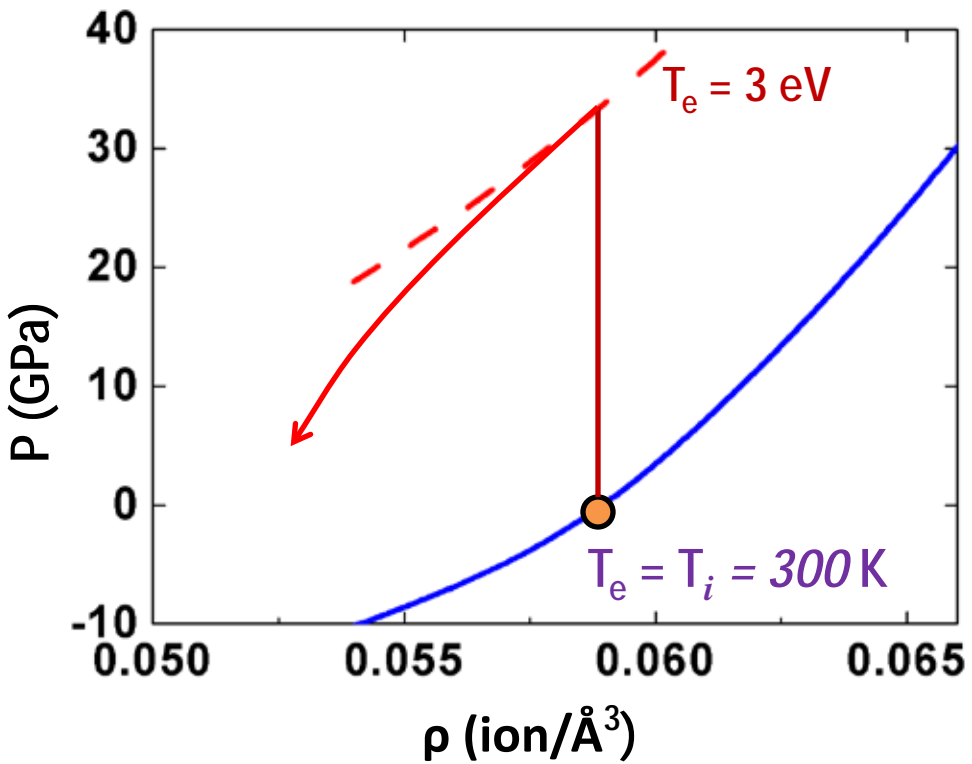
"Short" ablation at sub-ps laser pulse duration



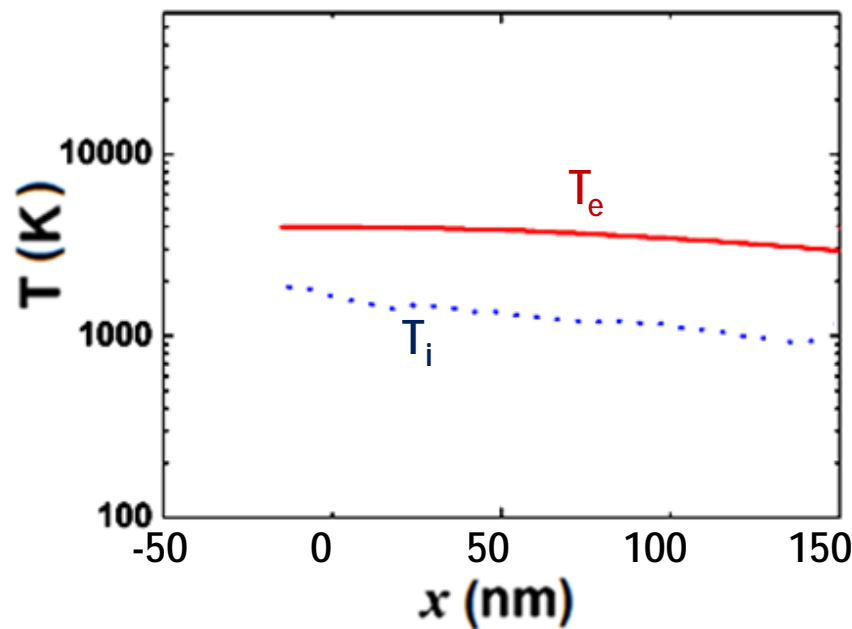
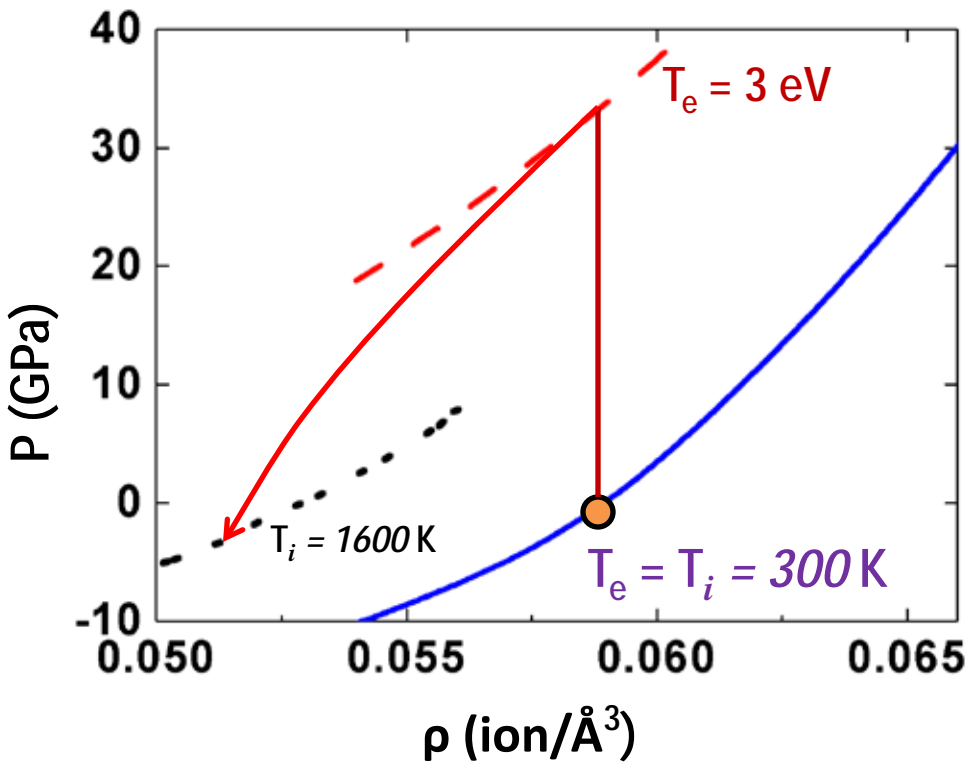
"Short" ablation at sub-ps laser pulse duration



"Short" ablation at sub-ps laser pulse duration



"Short" ablation at sub-ps laser pulse duration



"Short" ablation at sub-ps laser pulse duration

